The Impact of NOD Reaction Kinetics on Treatment Efficiency

by

Laura Jean Jones

A thesis

presented to the University of Waterloo

in fulfilment of the

thesis requirement for the degree of

Master of Applied Science

in

Civil Engineering

Waterloo, Ontario, Canada, 2007

I hereby declare that I am the sole author of this thesis. This is a true copy of this thesis, including any required final revisions, as accepted by my examiners.

I understand that my thesis may be made electronically available to the public.

Abstract

In *situ* chemical oxidation (ISCO) with permanganate is a remedial technology that has been prevalent over the last decade. Permanganate is injected into the subsurface to oxidized reduced organic contaminants with the intent of mineralizing the organics to innocuous compounds such as water, oxygen, and carbon dioxide. However, the demand for permanganate from the naturally occurring reduced components associated with aquifer materials inhibits the ability of permanganate to effectively oxidize the target contaminants. This demand for permanganate is referred to as the Natural Oxidant Demand (NOD) and results from the presence of naturally occurring reduced aquifer species such as inorganic species containing iron, manganese, or sulfur, and natural organic matter. Traditionally, NOD has been considered to be an instantaneous sink for permanganate that required satisfaction before permanganate could propagate through the subsurface. However, recent research has suggested that NOD is kinetically controlled and not instantaneous resulting in the effectiveness of ISCO systems to be underestimated using traditional approaches. The objectives of this research were to develop a comprehensive NOD kinetic model from existing laboratory data of several aquifer materials, and then to use this model to estimate the impact of NOD kinetics on treatment efficiency.

The NOD kinetic model primarily was developed using results of bench-scale experiments performed on four aquifer materials, measuring the reduction of permanganate and oxidizable materials. Data analysis indicated that there are two bulk reactions occurring: a fast reaction and a slow reaction. For both of these reactions a second-order rate law was deemed to be appropriate; first-order with respect to each reactant. The slow reaction was subject to passivation and the reaction rate coefficient decreased hyperbolically as manganese oxide reaction by-products precipitated on grains. The developed NOD kinetic model was incorporated into a 1-dimensional transport model and was used to successfully simulate the results of NOD column studies.

Experimental efforts were completed to validate the 1-dimensional reactive transport model with data for organic contamination. A column study was completed to characterize the oxidation of an isolated trichloroethylene residual source zone. The chloride breakthrough

data were used to represent the rate of TCE oxidation and a bromide tracer test was used as a conservative tracer to determine the dispersivity and porosity of the column. Both the simulated bromide and chloride breakthrough curves fit the experimental data well using published and calculated transport and chemical parameters.

The impact of NOD kinetics on treatment efficiency was evaluated through numerical simulations of four common organic contaminants using two injection schemes: vertical well flushing and inject-and-leave. The treatment efficiency was defined as the fraction of supplied permanganate used to oxidize the organic compound. Two aquifer materials were simulated representing a wide range of NOD characteristics. The results indicated that despite a great difference in the ultimate NOD (order of 15) the treatment efficiency only varied by 0-7% between the materials. In general, the treatment efficiency of the contaminant increased as the solubility and the reaction rate coefficient increased.

For treatment of organic compounds with a low solubility and reaction rate coefficient, the fast and slow NOD reaction kinetics should both be characterized since both exert a strong demand for permanganate in both the vertical flushing and inject-and-leave schemes. For organic compounds having moderate solubility and reaction rate coefficient the NOD species that require kinetic characterization depends on the injection scheme used: for a vertical well flushing scheme only the fast NOD requires characterization, whereas for the inject-and-leave scheme both the fast and slow NOD require characterization. For treatment of organic compounds with high solubility and reaction rate coefficient only the fast NOD requires characterization since the organic and fast NOD are depleted at the same time and the slow NOD does not play a significant role in permanganate consumption while free phase organic and fast NOD remain.

Traditional modelling approaches were compared, using the vertical well flushing scheme, to compare the treatment efficiency with the NOD kinetic model to past methods. The model was used to simulate ISCO treatment when NOD kinetics were not included and when the ultimate NOD was assumed. The simulations with no NOD term overestimated the treatment efficiency whereas the simulations with the ultimate NOD model underestimated efficiency. These findings further stressed the importance of the NOD kinetics on treatment efficiency.

The kinetics of the NOD kinetics must be characterized to determine if ISCO is a viable, cost-effective treatment option when considering ISCO as a redial strategy. Mischaracterization of these reactions could result in either over or underestimation of the treatment efficiency and poor design of pilot and full-scale treatment systems.

Acknowledgements

Table of Contents

List of Figures

List of Tables

CHAPTER 1: INTRODUCTION

1.1 *Background*

In Situ Chemical Oxidation (ISCO) is a remedial technology that has been proven effective at treating residual source zones of contamination (USEPA, 2006; ITRC, 2005). ISCO involves the injection of a chemical oxidant into the subsurface to treat contaminated soils and groundwater, producing potentially innocuous by-products such as carbon dioxide, oxygen, and water (ITRC, 2005). ISCO source zone treatment, as well as other *in situ* techniques, is an appealing remediation technology since it eliminates the need to handle wastes above ground surface or offsite. ISCO reduces the source zone contaminant mass by lowering the concentration of aqueous phase contaminants which increases the concentration gradient, thereby increasing the rate of mass transfer (Schnarr et al., 1998). Four oxidants have been used with success in ISCO: permanganate, persulfate, Fenton's reagent (i.e., iron catalyzed hydrogen peroxide), and ozone (ITRC, 2005; Siegrist et al., 2001; Schnarr et al., 1998). One of these four oxidants, permanganate, is often chosen due to its stability, ability to react with a wide range of contaminants, and relatively low cost.

Permanganate (MnO_4^-) is a common oxidant that has been used in the waste water industry for several decades (Weber, 1972), and the overall reaction with an organic compound can be expressed as

$$R + MnO_4^- \xrightarrow{\ k\ } MnO_2 + CO_2 + R_{OX} \tag{1-1}$$

where R is the organic compound, k is the reaction rate, MnO_2 is manganese dioxide – a reaction by-product, and R_{ox} is an intermediate organic by-product that maybe further oxidized in the presence of permanganate (Stewart, 1965). In some cases, the intermediate organic by-products may not reach full mineralization; the possibility of toxic by-products being formed is possible (ITRC, 2005). Waldemer and Tratnyek (2006) studied the permanganate oxidation kinetics of 24 common groundwater organic contaminants in the aqueous phase, covering three classes of contaminants, and found

that the reactions were first-order with respect to both permanganate and the contaminant. These findings supported results from other researchers who found that the reaction between permanganate and aqueous phase organics was first-order with respect to both reactants (Forsey 2004; Hunkler et al., 2003; Poulson and Naraoka, 2002; Hood et al., 2000; Huang et al., 2001; Siegrist et al., 2001; Yan and Schwartz, 2000; Yan and Schwartz, 1999; Huang et al., 1999). The reaction rate coefficients for contaminants range from $7.00E-06$ $M^{-1}s^{-1}$ for stable contaminants that resist reaction with permanganate such as benzene, to $2.37E+02$ $M^{-1}s^{-1}$ for highly reactive contaminants like p-cresol (Waldemer and Tratnyek, 2006). If a constant concentration of 5 g/L $KMnO_4$ is assumed, these rates correspond to a half-life that ranges from less than 0.1 seconds for p-cresol to over 3.5 days for benzene.

While reaction rate coefficients and half lives are important factors in determining whether permanganate ISCO will be effective at a site, there are other concerns that must be addressed. Two main concerns that may limit the effectiveness of permanganate ISCO at some contaminated sites are: the formation of manganese oxide precipitates as a reaction by-product (Crimi and Siegrist, 2004; Li and Schwartz, 2004; Conrad et al., 2002; Huang et al., 2002; Lamarche, 2002; Reitsma and Randhawa, 2002; Siegrist et al., 2002; Li and Schwartz, 2000), and the interaction of permanganate with the natural aquifer material (Mumford et al., 2005; Hood, 2000; Schnarr et al., 1998; Barcelona and Holm, 1991).

1.1.1 Precipitate Formation

As illustrated in equation 1-1, the oxidation of reduced species by permanganate results in the formation of manganese oxides, commonly assumed to be manganese dioxide (MnO_2) (Stewart, 1965). Li and Schwartz (2004) investigated the nature of the oxidation by- products formed during TCE oxidation in a batch reactor (with no aquifer material) using X-ray diffraction. They discovered that minerals other than MnO_2 were formed during the oxidation; however, all manganese by-products formed were insoluble and therefore could cause reduced porosity and inhibit mass transfer.

The impacts of by-product solids being formed during permanganate ISCO has been noted in studies involving 1-D column tests, 2-D sandbox studies, and field sites which have encountered resistance, due to reduced porosity, during permanganate injection (i.e., experiencing increased headloss or requiring a greater head to be able to supply permanganate to the source zone) (Crimi and Siegrist, 2004; Li and Schwartz, 2004; Conrad et al., 2002; Huang et al., 2002; Lamarche, 2002; Reitsma and Randhawa, 2002; Siegrist et al., 2002; Li and Schwartz, 2000). This phenomenon has been attributed to clogging of the pore space and well screens by manganese oxides.

Huang et al. (2002) used tracer tests before and after permanganate treatment in columns to estimate a porosity reduction of 20%. Reitsma and Randhawa (2002) conducted several column studies, in which, hydraulic conductivity was measured over time as each column was flushed with PCE (20 mg/L) and permanganate (4 g/L $KMnO_4$). The authors found that the hydraulic conductivity of the aquifer material decreased by a factor of 5-10 over 48 hours and eventually encountered complete plugging after 120-150 hours. Conrad et al. (2002) used a 2-D sandbox to visualize the formation of manganese oxides during permanganate oxidation of TCE. Their results indicated that formation of manganese oxides may not inhibit the ISCO processes during treatment of a residual source zone; however, they observed the formation of a "rind" surrounding TCE pool source zones resulting in incomplete oxidation of TCE. This finding is supported by MacKinnon and Thomson (2002) who completed a 2-D MnO_4^- treatment of a PCE pool. They found that although a mass flux of PCE leaving the system decreased over time, there was still some pooled PCE present. They further suggested that MnO_2 deposition at the PCE interface resulted in a decrease in mass transfer and lower concentrations of PCE. However, MacKinnon and Thomson (2002) did demonstrate that over all, ISCO significantly enhanced the mass transfer rate from a pooled source zone relative to a water flush.

Further to the physical effects of precipitates on the source zone (i.e., plugging and pore space reduction and mass transfer impacts), some studies have also suggested that MnO_2

precipitates will act as a catalyst for the auto decomposition of permanganate (Huang et al., 1999) which can lead to a small long-term demand for permanganate.

Attempts are currently underway to model the mass transfer of contaminants from the pure phase to the aqueous phase in the presence of permanganate (Brown and Gupta, submitted; Urynowicz and Siegrist, 2005). Urynowicz and Siegrist used micro-extraction/reaction vessels with TCE to measure the rate of dissolution of TCE in the presence of permanganate under static and mixed conditions. They found that dissolution was greater in the static reactor than in the mixed reactor and presented a simple model for the dissolution of TCE. However, it is unclear how this dissolution model would perform when adapted into a reactive transport model. Brown and Gupta (submitted) investigated the mass transfer of BTEX and naphthalene from coal tar into an aqueous solution containing permanganate. At a concentration of 0.5 g/L $KMnO_4$, the mass transfer coefficients were unchanged from reactors containing no permanganate; however, when the concentration of permanganate was increased to 1.0 g/L $KMnO_4$, significant reductions in mass transfer were observed. The reduction in mass transfer with 1.0 g/L $KMnO_4$ could not be quantified due to experimental complications.

The presence of manganese oxide by-products has been shown to limit mass transfer of free phase contaminants, particularly when NAPL pools are present; however, this phenomenon could have a positive side. Adventus Group of Freeport, Illinois, is marketing the reduced mass transfer and porosity as a treatment option they have named *In Situ* Biogeochemical Stabilization (ISBS) (www.adventusgroup.com/products/isbs.shtml, 2007). ISBS involves the injection of permanganate at high concentrations to build a rind of manganese oxides surrounding a pooled NAPL source zone slowing and eventually preventing mass transfer of contaminants. To date there is no evidence to support that this process is possible to achieve at the field scale.

1.1.2 Natural Oxidant Demand

Early ISCO experiments by Schnarr et al. (1998) observed that more permanganate was required to fully oxidize an emplaced TCE source zone than was required based on the stochiometry of the redox reaction. This finding resulted in the hypothesis that the aquifer material was being oxidized in conjunction with the contaminant. Barcelona and Holm (1991) also reported that "the oxidation-reduction capacities of aquifer solids represent(ed) obstacles to effective in situ treatment of subsurface contamination by chemical or microbial means".

Permanganate consumption by uncontaminated aquifer solids is called the natural oxidant demand (NOD) and is defined as the unwanted consumption of permanganate by naturally occurring organic material and reduced minerals associated with aquifer solids. The additional demand results in a competition for the injected permanganate between the aquifer solids and the target contaminants. To estimate NOD consumption, Hood (2000) performed column experiments on several sandy aquifer materials and used mass balance considerations to determine the mass of permanganate consumed by each material. His results showed that there was a poor correlation between the permanganate demand of an aquifer material and the natural organic matter present. Hood's results may have been compromised by one material with a mid-range organic matter content exhibiting a high oxidant demand that appears to be an outlier. Xu (2006) estimated the NOD of several aquifer materials and found that the NOD was highly correlated to the natural organic matter (NOM).

NOD is typically determined though batch experiments measuring the reduction in permanganate over time and mimics the experimental method of typical biochemical oxygen demand tests (BOD – measures the total reductive capacity of waste waters) (Mumford et al., 2004; Mumford et al., 2002; Xu et al., 2004). Long-term batch experiments are used to determine an ultimate NOD; however, they fail to fully characterize the reaction kinetics.

The traditional conceptual model for the NOD reaction is to assume a simple reaction between the aquifer solids and permanganate which is represented by an instantaneous sink of permanganate equal to the ultimate NOD (Zhang and Schwartz, 2000). Recent work by Xu et al. (2004) and Mumford et al. (2005) have indicated that NOD is kinetically controlled and the NOD properties (i.e., reaction rates and concentration of the reduced species) vary widely between aquifer materials.

Xu (2006) conducted a series of bench-scale column experiments focusing on NOD reactions of uncontaminated materials from several sandy aquifers across North America. The column breakthrough curves showed evidence of multiple reactions. Initially permanganate breakthrough was delayed by 0.26 to 1.19 pore volumes relative to a conservative tracer; the delay was deemed to represent a fast reaction. The tail of the permanganate breakthrough curve failed to reach the inlet concentration after several pore volumes of permanganate were flushed through the column indicating the presence of a slow reacting species. Other researchers have also made similar hypotheses about multiple reactions contributing to NOD (Mumford et al., 2005).

1.1.2.1 Nature of Reductive Species

Barcelona and Holm (1991) attributed the reduction capacity of sandy aquifer material to two main components, NOM and reduced inorganic species containing manganese, sulphur, and iron. Other researchers have compared the reduction capacity to the aquifer material geochemistry and reached similar conclusions with regard to which reduced species contributed to high reduction capacities (Hartog et al., 2002; Christensen et al., 2000; Appelo and Postma, 1996; Heron et al., 1994). Xu et al. (2004) studied the geochemistry of 10 sandy aquifer materials and determined that the main reduced components in the aquifers were organic carbon and inorganic species containing reduced iron, indicating that manganese and sulphur did not play a large role in the oxidant demand. Mumford (2002) suggested that the inorganic species associated with aquifer solids would react quickly with permanganate while the organic matter would react at a much slower rate; these findings were supported by the results observed by Xu et al. (2004). Results from Barcelona and Holm (1991) indicate that organic carbon in the

aquifer solids represents a significant percent of the reduced species in the aquifer. Xu et al. (2004) also found significant fractions of organic carbon in several aquifer materials exhibiting high NOD.

Organic carbon can be present in aquifers in several forms: biogenic carbon (undecomposed plant matter), humic substances (altered/decomposed plant matter), bitumen/kerogen (geologically aged organics), and black carbon (combustion by-products) (Allen-King et al., 2002; Gustafsson et al., 2001). Biogenic carbon, such as plant roots, represents only a small faction of the total organic matter in aquifers. An example cited by Allen-King et al. (2002) stated that biogenic carbon in grassland soil was roughly 20 times less than the humic carbon present. Humic substance/humus is defined by Sposito (1989) as the organic matter that is not identified as unaltered/partially altered biomass (such as plant parts or identified biochemicals). Allen King et al. (2002) stated that humic substances are polymeric compounds that are produced from biogenic compounds which have been microbial degraded. Swift (1996) presented three main fractions in humic substances: fulvic acids, humic acids and humins. These fractions vary based on their ability to precipitate in acids/dissolve in bases, molecular weight, and structure. Humic substances have been identified as the most prevalent form of organic matter in surface soils (Sposito, 1989). Kerogen/bitumen are organic geopolymers that result from changes to biogenic material over a long period of time when exposed to high temperatures and pressures (Allen-King et al. 2002). Kerogen and bitumen are frequently not included when considering the Normal Soil Organic Matter (NSOM) which generally includes only bitumen and humus (Allen-King et al., 2002). Black carbon is the term that includes combustion by-products such as soot and chars (Gustafsson et al., 2001). Black carbon is not always considered to be organic matter, but is included in measurement of the fraction of organic carbon (f_{oc}) in aquifer materials (Allen-King et al., 2002). The composition of the organic matter in soils varies significantly from site to site; however, Allen-King et al. (2002) suggested that humic substances make up the majority of organic carbon in most aquifers with possibly large fractions of black carbon or kerogen and bitumen depending on the site.

Several reactions have been proposed as surrogate reactions for the organic portion of NOD. Barcelona and Holm (1991) proposed using phthalic acid as a surrogate for the organic carbon present in the aquifer. Phthalic acid contains carbon and oxygen in the aromatic ring structure and closely matches the structure of many humics found in the subsurface (Barcelona and Holm, 1991). The reaction between phthalic acid and permanganate is

$$C_8H_6O_4 + 10MnO_4^- + 10H^+ \rightarrow 8H_2O + 8CO_2 + 10MnO_2(s) \qquad \text{(1-2)}$$

Mumford et al. (2005) proposed the use of a simple carbohydrate to obtain the stochiometry between organic carbon and permanganate, as given by

$$3CH_2O + 4MnO_4^- \rightarrow H_2O + 4OH^- + 3CO_2 + 4MnO_2(s) \qquad \text{(1-3)}$$
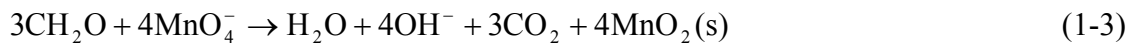
However, at the end of the 14-week batch experiments exposing aquifer material from CFB Borden to permanganate, only 60-90% of the organic carbon remained (Mumford et al., 2005). Based on these findings, the authors suggested that significant over-estimation of the NOD would occur if it was assumed that all organic carbon in the aquifer material is oxidized by permanganate.

Reduced inorganic minerals, specifically those containing iron, manganese, or sulfur, can also contribute to the NOD of the aquifer materials. The stochiometric ratio between permanganate and reduced minerals varies significantly between different inorganic species. These ratios could be used to estimate the amount of permanganate each mineral would consume during oxidation if the geochemistry of the aquifer material is known. For example, the oxidation of siderite, pyrite, and rhodochrosite by permanganate respectively are given by

$$3Fe(CO_3)(s) + MnO_4^- + 7H_2O \rightarrow 2H^+ + 3Fe(OH)_3(s) + 3HCO_3^- + MnO_2(s) \qquad \text{(1-4)}$$

$$3FeS_2(s) + 14MnO_4^- + 2H_2O + 2H^+ \rightarrow 3Fe(OH)_2(s) + 6SO_4^{2-} + 14MnO_2(s) \qquad \text{(1-5)}$$

$$3MnCO_3 + 2MnO_4^- + 2H_2O \rightarrow H^+ + 3HCO_3^- + 5MnO_2(s) \qquad \text{(1-6)}$$
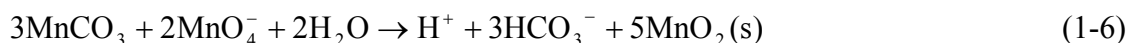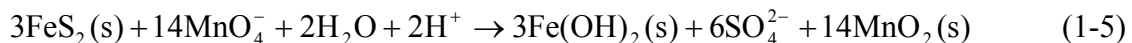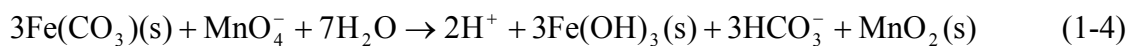
Xu (2006) summarized the inorganic reduced species in aquifer materials and focusing on iron, manganese, and sulfur. Iron is the most abundant transition metal in the earths crust, occurring in two valence states (i.e., ferrous Fe(II) and ferric Fe(III)). Reduced iron (ferrous) minerals are thought to be the most significant inorganic species contributing to NOD. In aquifer systems the most common ferrous minerals are siderite, amorphous ferrous sulphide, mackinawite, and pyrite (ferrous). Several oxidation states exist for manganese; however, of these states, the ones with the most impact on the redox chemistry of aquifer soils are Mn(II), Mn(III) and Mn(IV) (Appelo and Postma, 1996). Mn(IV), the most stable of these oxidation states, is present in aquifer materials as pyrolusite, birnessite, and vernadite (Xu, 2006). Mn(II) commonly exists in carbonates such as rhodochrosite or as an insoluble ion in acidic aquifers (Xu, 2006). Mn(III) is often found in oxides and oxyhydroxides such as manganite, bixbyite, and hausmannite (Xu, 2006). Sulfur also plays an important role in redox chemistry as it exists in aquifers minerals containing sulphate (e.g. gypsum) and sulphide (e.g. mackinawite, pyrite and marcasite) and as elemental sulphur (Xu, 2006). The most common sulphur containing minerals that affect groundwater chemistry are gypsum and pyrite (Hartog, 2003; Christensen et al., 2000; Appelo and Postma, 1996).

1.1.3 Existing NOD Kinetic Models

Various mathematical models have been developed to simulate the subsurface processes occurring during *in situ* chemical oxidation (Mumford, 2002; Reitsma and Dai, 2001; Hood and Thomson, 2000; Zhang and Schwartz, 2000), and could be used during site screening to determine if ISCO is an effective treatment option given the site characteristics and contaminant properties. However, to date, no defendable model has been developed which accurately captures the complex NOD reaction kinetics taking place during ISCO treatment. The kinetics are necessary to determine the impact of NOD on the treatment efficiency during site screening and remedial design. Historical methods of modelling the NOD as an instantaneous sink of permanganate would significantly underestimate the treatment efficiency, since the NOD had to be satisfied before permanganate can be propagated through the domain. However, excluding NOD

from the model would significantly overestimate the efficiency since an important sink for permanganate would not be included.

1.2   Research Objective

The ability of permanganate to treat a contaminant of concern depends on several conditions, most notably whether the permanganate is being used efficiently to reduce the mass of contaminants in the subsurface rather than being consumed by the inherent demand from the aquifer material (NOD). The objective of this research is to determine the role that NOD kinetics play in ISCO treatment efficiency where competition for permanganate arises between the aquifer material and dissolved phase organics.

The research objective was completed by:

1. Developing a defendable NOD kinetic model based on the experimental data compiled by Xu (2006);

2. Developing a one-dimensional multi-component reactive transport model capable of simulating the governing physical and chemical processes (mass transfer, sorption, target contaminant reaction, NOD reaction, and free phase mass destruction);

3. Conducting a representative column experiment so that the data can be used to validate (Schnoor, 1996) the developed model; and

4. Using the NOD kinetic model in conjunction with the reactive transport model to simulate scenarios that examine the treatment efficiency of permanganate during representative *in situ* chemical oxidation applications.

1.3   Thesis Scope

Chapter 2 provides details of batch and column experiments completed by Xu (2006), and develops the NOD kinetic model. Chapter 3 presents the background and findings from the representative column experiments performed on the treatment a TCE source

zone. Generated data is used to benchmark the mathematical model. Chapter 4 examines the implications of NOD kinetics on treatment efficiency by using the one-dimensional transport model to simulate the permanganate treatment of several common contaminants using two common injection schemes. Chapter 5 presents the conclusions and summarizes recommendations for future study.

CHAPTER 2: DEVELOPMENT OF THE NOD KINETIC MODEL

2.1 Theoretical Considerations

As discussed in Chapter 1, organic carbon and inorganic species are the main reducants that contribute to permanganate consumption and therefore the permanganate rate law could be written as

$$\frac{d[C_{MnO_4^-}]}{dt} = -\sum_i k_i^{NOM}[C_i^{NOM}]^{\alpha_i}[C_{MnO_4^-}]^{\beta_i}$$
$$-\sum_j k_j^{inorganic}[C_j^{inorganic}]^{\alpha_j}[C_{MnO_4^-}]^{\beta_j}$$
$$-k_{MnO_2}[C_{MnO_2}]^{\alpha_{MnO_2}}[C_{MnO_4^-}]^{\beta_{MnO_2}}$$

$$(2\text{-}1)$$

where $C_{MnO_4^-}$, C_i^{NOM}, $C_j^{inorganic}$, and C_{MnO_2} represent the concentration of permanganate, the concentration of the ith component of the natural organic matter, the concentration of jth inorganic component, and the concentration of manganese dioxide; k_i^{NOM}, $k_j^{inorganic}$ and k_{MnO_2} are the reaction rate coefficients associated with the NOM, inorganic species, and the manganese dioxide; and α and β are the respective reaction orders. However, for Eq. (2-1) to be useful in a predictive sense, the concentration, rate coefficient, and reaction order for each reductant must be known. An alternative to Eq. (2-1) is to consider the overall heterogeneous reaction between the bulk oxidizable aquifer matter (OAM) and permanganate which may be written as

$$OAM + pMnO_4^- \rightarrow pMnO_2 + q \text{ Oxidized } -OAM \qquad (2\text{-}2)$$
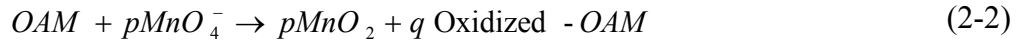
where p and q are stochiometric coefficients. The term "bulk OAM" refers to all significant non-target reductants associated with the aquifer materials as discussed in Section 1.2 and includes organic carbon, and minerals containing S(-II), Mn(+II), and Fe(+II). Associated with Eq. (2-2) are the following general rate law expressions:

$$\frac{d(C_{OAM})}{dt} = -k_{bulk}^{OAM}(C_{OAM})^\beta(C_{MnO_4^-})^\alpha \qquad (2\text{-}3a)$$

and

$$\frac{d(C_{MnO_4^-})}{dt} = -k_{bulk}^{MnO_4^-} (C_{MnO_4^-})^{\alpha} (C_{OAM})^{\beta}$$

(2-3b)

where k_{bulk}^{OAM} and $k_{bulk}^{MnO_4^-}$ is the bulk reaction rate coefficient with respect to the bulk

OAM and permanganate; α and β are the overall reaction order with respect to

permanganate and the OAM; and C_{OAM} and $C_{MnO_4^-}$ are the concentrations of the bulk

OAM (mass/system volume) and permanganate (mass/volume of solution). To evaluate

the reaction kinetics associated with Eq. (2-3) from an experimental perspective, it is

customary to hold one of the reactants constant or in excess to observe changes in the

other reactant (Levenspiel, 1999). Once the experimental program has been executed, the

experimental data are then analysed to determine suitable reaction rate coefficients and

reaction orders that honour the experimental data. The purpose of this chapter is to

present an overview of the experimental findings reported by Xu (2006), and then to use

these data to develop a NOD kinetic model that can be used in groundwater flow and

transport modelling applications to adequately represent the interaction between

permanganate and aquifer materials.

2.2   *Experimental Methods and Results*

Xu (2006) performed short-term batch experiments that were designed to yield kinetic

data that describe the behaviour of permanganate in the presence of various aquifer

materials, and column experiments which were used to investigate permanganate

transport in a system that mimics the subsurface environment.

Aquifer Materials: Xu (2006) obtained nine aquifer materials from eight sites across

North America, but only the following aquifer materials are relevant to this study:

material from the sand pit at Canadian Forces Base (CFB) Borden, material from the East

Gate Disposal Yard (EGDY) in Washington State, and two materials from Launch

Complex 34 in Cape Canaveral Florida (denoted here as the Lower Sand Unit (LC34-

LSU) and the Upper Sand Unit (LC34-USU)) (Table 2.1). Based on a visual inspection

and grain size analysis, these aquifer materials were predominantly sand; however, the EGDY aquifer material was heterogeneous and contained large cobbles. Xu (2006) contains details on material handling and preparation. Relevant physical and chemical properties of these four aquifer materials are summarized in Table 2.2 (Xu, 2006).

To quantify the overall reactivity of the naturally-occurring reductants Xu (2006) used the acidified dichromate chemical oxygen demand method consistent with previous efforts to quantify the reductive capacity of aquifer solids (Lee and Batchelor, 2003; Korom, 1996; Pedersen et al., 1991; Barcelona and Holm, 1991, and Powell et al., 1988). Since a fraction of the complex natural organic matter, and various crystalline and amorphous inorganic components present in aquifer materials may be recalcitrant to permanganate (Christensen et al., 2000; Evanko and Dzomak, 1998; Blair et al., 1995) the use of the dichromate COD test to estimate permanganate consumption will lead to significant overestimation. To overcome this potential overestimation, Xu and Thomson (2007) extended the permanganate COD test used in water and wastewater applications to test aquifer solids since the ultimate permanganate consumption rather than dichromate demand by aquifer materials is of interest in permanganate ISCO applications. Both the dichromate and permanganate COD test results are presented in Table 2.3 and indicate that the permanganate COD values were less than the dichromate COD test results for all aquifer materials except for the LC34-USU solids. This outlier is presumed to be due to experimental variability. Assuming that the difference between the dichromate and permanganate COD test results are reflective of the fraction of the total reductive capacity that is recalcitrant to oxidation by permanganate, then between 35 and 100% of the dichromate COD value can be considered reactive.

2.2.1 Batch Experiments

Following the method of excess, two series of experiments were conducted by Xu (2006): (1) an excess permanganate experiment which allows Eq. (2-3a) to be reduced to

$$\frac{d(C_{OAM})}{dt} = -k_{bulk}^{OAM}(C_{OAM})^{\beta}(C_{MnO_4^-})^{\alpha} = -(k_{bulk}^{OAM})_{obs}(C_{OAM})^{\beta} \qquad (2\text{-}4a)$$

14

and (2) an excess aquifer material experiment which allows Eq. (2.3b) to be replaced by

$$\frac{d(C_{MnO_4^-})}{dt} = -k_{bulk}^{MnO_4^-}(C_{MnO_4^-})^\alpha (C_{OAM})^\beta = -(k_{bulk}^{MnO_4^-})_{obs}(C_{MnO_4^-})^\alpha \qquad (2\text{-}4b)$$

where $(k_{bulk}^{OAM})_{obs}$, and $(k_{bulk}^{MnO_4^-})_{obs}$ are the observed bulk reaction rate coefficient with respect to the OAM and permanganate.

Excess Aquifer Material Mass Kinetic Experiments: The mass of aquifer material used in these experiments was determined so that the permanganate mass employed would be at least ten times less than the ultimate permanganate consumption as estimated from the long-term NOD experiments performed by Xu (2006) and the permanganate COD tests (Table 2.3). Each experimental run consisted of loading ~100 g of aquifer material in the reactor and then adding the permanganate solution (0.06 – 2.5 g/L). Table 2.4 lists the aquifer material mass, solution volume, and permanganate concentration used for each experimental run. All KMnO$_4$ solutions were prepared by heating at 80°C for ~1 hour, and then filtering the cooled solution through a 0.45-μm glass fibre filter (Pall Corp.). A phosphate buffer (sodium phosphate dibasic at 10 mM) was added to the permanganate solution to maintain a neutral pH (~7.2). At specified reaction times (nominally 2, 5, 10, 20, 40, 70, 120, and 180 min) an aliquot (~2 mL) of the permanganate solution was extracted from the reactor with a syringe (LUER-LOK, Becton & Dickinson), and filtered through a 0.45 μm syringe filter (Acradisc, Pall Corp.). The permanganate concentration was quantified with a spectrophotometer (Milton Roy, 20D) at 525 nm. All experiments were performed in duplicate using 300 mL reactor vessels in conjunction with a 3.2 cm stir bar placed on a stir plate. The data collected from these experiments are shown in Figure 2.1 where each data point represents the average from the duplicate experimental runs and hence no error bars are shown. In this figure, the five sets of data represent the five experiments in which different initial concentrations of permanganate were used for each material. These data indicate that permanganate consumption by a given aquifer material is a function of the initial permanganate concentration and that consumption slows significantly over the course of the experiment. This trend is especially evident for

15

the EGDY aquifer material where the initial decrease in permanganate concentration is much higher than that observed later in the experiment.

Excess Permanganate Mass Kinetic Experiments: In these experimental runs two to three masses of aquifer material (10 to 25 g) from each site were loaded into a reactor followed by the addition of a specified volume (between 100 to 150 mL) of a permanganate solution with a concentration of 20 g/L. After a specified reaction duration (nominally 5, 15, 30, and 60 min) the experimental run was quickly terminated by filtering the slurry through a 6-µm filter paper (Whatman, VWR Lab) and rinsing the material retained on the filter with Milli-Q water until only a faint pink color persisted. The solid material remained on the filter paper was then transferred to aluminum trays, dried at $80^{\circ}C$ for 24 hours, and ground in a porcelain mortar to pass through a 150-µm sieve. Aliquots of the ground aquifer material were then submitted for dichromate COD analyses to capture changes in the overall reductive capacity. Table 2.5 lists the aquifer material mass, solution volume, and permanganate concentration used for each experimental run. The results from the COD test were used to represent the concentration of the bulk oxidizable aquifer material (C_{OAM}) as estimated from

$$C_{OAM} = COD \; m_{aq} \, / \, V_{total} \qquad\qquad (2\text{-}5)$$

where *COD* is the dichromate COD test result expressed as *g*-KMnO$_4$/*kg* of dry aquifer material, m_{aq} is the mass of dry aquifer material, and V_{total} is the total system volume (solution and aquifer material); hence the units for C_{OAM} are *g*-KMnO$_4$/L. Data generated from these kinetic experiments indicate that the differing mass of aquifer materials had little impact on the measured COD thus an average value was taken for each time point. Thus, each data point on Figure 2.2 is the average of six or nine COD values and the error bars indicate the standard deviation. All data points in Figure 2.2 cannot be fit using a traditional first-order or second-order fit, since that the COD value dropped quickly during the first 5 min, indicative of a fast reaction, followed by a relatively slow decrease over the next 1 to 2 hours. Unfortunately the first sampling episode was at 5 min and therefore lack of data at a resolution <5 min is a concern.

2.2.2 Column Experiments

Column experiments are generally considered to be more representative of *in-situ* conditions than short-term batch experiments since they provide more realistic aquifer material contact. Thus, a series of permanganate column experiments were designed to complement and expand the findings of the batch experiments.

A typical column was constructed from a 40-cm long section of nominal 3.81 cm (1.5-inch) diameter transparent Plexiglas pipe equipped with four equally spaced sampling ports. Due to the high NOD associated with the EGDY aquifer materials as indicated from the batch test results, columns for this material were constructed from 12-cm long sections of nominal 2.54 cm (1-inch) diameter Schedule 40 PVC pipe to minimize experimental time. Permanganate source solutions were prepared by adding analytical grade $KMnO_4$ (EM Science) to Milli-Q water and boiling for ~1 hour. The cooled solution was filtered (0.45-μm glass fibre, Pall Corporation) and standardized by titration into a sulphuric acid and sodium oxalate solution (APHA, 1998).

To avoid problems associated with dry packing, homogenized aquifer material was wet with Milli-Q water to near saturation before use. Each column was packed in three stages: (1) the bottom 1.0 cm of the column (0.3 cm for the EGDY columns) was filled with 0.59 to 0.84 mm diameter glass beads (Potters Industries Ltd.) on top of which a thin layer of glass wool (Pyrex, VWR) was placed; (2) the next 38 cm (or 10 cm for the EGDY columns) was packed with aquifer material in 1 to 2 cm lifts compacted using a 1 cm diameter glass rod with the column attached to vertical vibrating rod; and (3) the top of the packed aquifer material was fitted with a 500-mm stainless steel screen, then filled with 0.59 to 0.84 mm diameter glass beads (Potters Industries Ltd.) and topped with a thin layer of glass wool (Pyrex, VWR). Both the bottom and top tubing couplers were fitted with a 500-mm stainless steel screen to prevent solids from escaping. Control columns filled exclusively with clean 0.59 to 0.84 mm diameter glass beads (Potters Industries Ltd.) were used to validate the experimental set-up and quantify apparatus/permanganate interactions.

Each column was operated in a continuous up-flow mode using a peristaltic pump (Cole-Parmer Instrument Co., Model No. 7553-80, 1-100 RPM, size 14 tubing) to control the rate of inflow, and a constant hydraulic head applied at the effluent end. Column experiments for each aquifer material were conducted in duplicate.

Table 2.6 summarizes the various column experiments performed. Prior to each experiment, the column was flushed with Milli-Q water until a stable flow rate was achieved (this process took about 1 to 5 hours). For a typical experiment trial the column was flushed with the permanganate source solution until sufficient permanganate breakthrough was observed, then flushed with Milli-Q water until no permanganate was detected (or no pink color appeared) in the effluent, and then flushed again with the same source solution until sufficient permanganate breakthrough was observed. The purpose of the second flush was to investigate the breakthrough behaviour of permanganate in a system that was previously exposed to permanganate. At designed times, samples (with a typical volume of 0.2 to 0.5 mL) were taken and used to quantify permanganate concentration by spectrophotometry (Milton Roy Company, Spectronic 20D) at 525 nm with a method detection limit of 1.3 mg/L.

Tracer tests using sodium bromide solution (Fischer Scientific) at a constant concentration ranging from 50 to 100 mg/L were conducted to compare the tracer and permanganate breakthrough curves, as well as to evaluate hydrodynamic properties (porosity and dispersivity) of each aquifer material packed column. Bromide concentrations were determined by ion chromatography (IC) (Dionex AS4A-SC 4mm x 250 mm column; 1.8 mM sodium carbonate, 1.7 mM sodium bicarbonate eluate; 1.5 mL/min flow rate) with a MDL of 1.2 mg/L.

The breakthrough of permanganate and bromide (Br⁻) obtained from the duplicate columns at identical sampling times were normalized to the source concentration and averaged. The resulting breakthrough curves are shown in Figure 2.3. In general for all cases, the arrival of permanganate was delayed with respect to Br⁻. After breakthrough, the permanganate concentration increased towards the source concentration, but showed extensive tailing and in all aquifer materials never reached the source concentration. This

incomplete breakthrough (C/C_o <1.0) occurred despite several pore volumes (PVs) being flushed through various columns. This observation suggests that a slow reaction between the aquifer material and permanganate was still occurring at the end of each experimental run and is consistent with observations from the long-term batch tests in which measurable permanganate consumption was observed for >200 days for most aquifer materials (Xu, 2006). All column tests showed a delay in permanganate breakthrough relative to Br⁻ indicative of a fast reaction at the time scale of these observations.

2.3 Kinetic Model

Data presented in Figure 2.2 clearly indicate that the COD test value dropped quickly during the first 5 min followed by a relatively slow decrease over the next 1 to 2 hours. For all materials, the decrease in the dichromate COD ranged from 0.98 to 8.4 g KMnO$_4$/kg (10 to 30% of the initial COD value) over the first 5 min, and from 0.84 to 6.8 g KMnO$_4$/kg over the next 55 min, implying some "very fast" and "intensive OAM-consuming" reactions took place over the first 5 minutes. The average observed COD consumption rate decreased by an order of magnitude from the first 5 min (0.5 g KMnO$_4$/kg/min) to the next 55 minutes (0.04 g KMnO$_4$/kg/min). Unfortunately, the elapsed reaction time prior to the first sampling episode was 5 min and therefore the reaction rates occurring over a time frame less than 5 min could not be resolved.

Based on these observations and the data in Table 2.3, it was assumed that the bulk concentration of OAM can be represented by a fast, slow and non-reactive component as expressed by

$$C_{OAM}^{total} = C_{OAM}^{fast} + C_{OAM}^{slow} + C_{OAM}^{non-reactive} \qquad (2\text{-}6)$$

with

$$C_{OAM}^{non-reactive} = (\text{Dichromate COD value} - \text{Permanganate COD value})\rho_b \qquad (2\text{-}7)$$

where C_{OAM}^{total} is the total concentration of OAM as captured by the dichromate COD test on unoxidized aquifer solids (expressed in terms of an equivalent mass of KMnO$_4$ per volume of system), C_{OAM}^{fast} is the fraction of COD attributed to the fast reaction (COD decrease over the first 5 min), C_{OAM}^{slow} is the fraction of the COD attributed to the slow reaction (the remaining COD available for reaction with permanganate), $C_{OAM}^{non-reactive}$ is the fraction of the COD that was non-reactive with permanganate as estimated from the difference between the dichromate and permanganate COD values, and ρ_b is the bulk density. Table 2.7 lists the concentration of each component for the aquifer materials investigated.

Supported by observations from the batch and column experiments, and the clear presence of a fast and slow reacting OAM, the following overall kinetic model was assumed sufficient to capture the observed NOD behaviour

$$\frac{d\,C_{OAM}^{fast}}{dt} = -k_{OAM}^{fast}\,(C_{OAM}^{fast})^{\alpha_{fast}}\,(C_{MnO_4^-})^{\beta_{fast}}$$

$$\frac{d\,C_{OAM}^{slow}}{dt} = -k_{OAM}^{slow}\,(C_{OAM}^{slow})^{\alpha_{slow}}\,(C_{MnO_4^-})^{\beta_{slow}}$$

(2-8)

and,

$$\frac{d\,C_{MnO_4^-}}{dt} = -k_{MnO_4^-}^{fast}\,(C_{OAM}^{fast})^{\alpha_{fast}}\,(C_{MnO_4^-})^{\beta_{fast}} - k_{MnO_4^-}^{slow}\,(C_{OAM}^{slow})^{\alpha_{slow}}\,(C_{MnO_4^-})^{\beta_{slow}}$$

where $C_{MnO_4^-}$ is the permanganate concentration (mass of permanganate per volume of solution); k_{OAM}^{fast} and k_{OAM}^{slow} is the fast and slow OAM reaction rate coefficient (units depend on reaction orders); $k_{MnO_4^-}^{fast}$ and $k_{MnO_4^-}^{slow}$ is the fast and slow permanganate reaction rate coefficient (units depend on reaction orders); α_{fast} and α_{slow} is the reaction order associated with the concentration of the fast and slow reacting OAM; and β_{fast} and β_{slow} is the reaction order associated with the permanganate concentration.

The slow OAM reaction rate coefficient and order where estimated using the integral method (Levenspiel, 1999) with the followed rate expression

$$\frac{d\,C_{OAM}^{slow}}{dt} = -k_{OAM}^{slow}\,(C_{OAM}^{slow})^{\alpha_{slow}}\,(C_{MnO_4^-})^{\beta_{slow}} \approx -(k_{OAM}^{slow})_{obs}\,(C_{OAM}^{slow})^{\alpha_{slow}} \tag{2-9}$$

where $(k_{OAM}^{slow})_{obs}$ is the observed slow OAM reaction rate coefficient. Using the excess permanganate data (Figure 2.2) and ignoring the data at $t = 0$ the remaining data were well represented ($r^2 > 0.86$) by a first-order kinetic model ($\alpha_{slow} = 1$) with the observed rate coefficients $(k_{OAM}^{slow})_{obs}$ for each aquifer material ranging from 0.0016 to 0.0059 min^{-1} (Table 2.8).

Given the presence of a fast reacting OAM component identified above, the inherent assumption in the excess aquifer material experiments is clearly violated and hence the data shown in Figure 2.1 need to be separated into: permanganate consumption associated with the fast reacting OAM, and permanganate consumption associated with the slow reacting OAM. Since there was no clear point (that could be visually observed) where the reaction rate shifted from fast to slow, the data were fit using the polynomial fit method (Folger, 1999) and displayed in terms of permanganate consumption rate as a function of the mass of permanganate consumed. Specifically each experimental series was fit with a least-squares method to the double-exponential function given by

$$C_{MnO_4^-}(t) = Ae^{-at} + Be^{-bt} \tag{2-10}$$

where A, B, a, and b are fitting parameters. Figure 2.4 shows the results of this fitting effort. For each experimental series, Eq. (2-10) was differentiated to estimate the permanganate consumption rate and plotted as a function of cumulative mass consumed (Figure 2.5). The profiles in Figure 2.5 for each aquifer material clearly show a shift in reaction rate (as indicated by the vertical line) after a critical mass of permanganate, denoted as $M_{MnO_4^-}^{crit}$, had been consumed. This critical mass of permanganate consumed which varied between 0.007 and 0.07 g KMnO$_4$/kg is presumed to be related to

21

satisfaction of the fast reacting OAM. Small fluctuations in the timing of the reaction

rate shift between the different experimental series for an aquifer material are assumed to

be the result of experimental variability. For some experimental series the permanganate

mass is completely consumed prior to reaching $M_{MnO_4^-}^{crit}$ (e.g., those experimental series

involving an initial low concentration of permanganate such as the 0.5 g/L series for the

EGDY aquifer material). Additionally, the materials which are completely consumed

before the shift in reaction rate can be discerned have a slower initial reaction rate due to

the rate being limited by the concentration of permanganate available. Assuming that the

experimental data after $M_{MnO_4^-}^{crit}$ are representative of the slow permanganate reaction

where the concentration of the slow reacting OAM (C_{OAM}^{slow}) is in excess, then the

following holds

$$\frac{d\,C_{MnO_4^-}}{dt} = -k_{MnO_4^-}^{slow}\,(C_{OAM}^{slow})^{\alpha_{slow}}\,(C_{MnO_4^-})^{\beta_{slow}} \approx -(k_{MnO_4^-}^{slow})_{obs}\,(C_{MnO_4^-})^{\beta_{slow}} \qquad (2\text{-}11)$$

where $(k_{MnO_4^-}^{slow})_{obs}$ is the observed slow permanganate reaction rate coefficient. The

integral method was used in conjunction with Eq. (2-11) to estimate the observed reaction

rate coefficient and order of the slow permanganate reaction. The slow permanganate

reaction was found to be first-order with respect to permanganate ($\beta_{slow} = 1$), and in

general the coefficient of variation was >0.80 with some notable exceptions. Table 2.7

lists the first-order reaction rate coefficients for each experimental series for the four

aquifer material investigated. Poor goodness-of-fit was obtained for 5 of the 20

experimental series and was presumed to be due to few (three) data points used. In

general the reaction rate coefficients consistently decreased as the initial permanganate

concentration for each experimental series increased (e.g., $(k_{MnO_4^-}^{slow})_{obs}$ deceased from

2.11E-01 to 1.04E-02 min^{-1} as the permanganate concentration increased from 0.06 to 0.6

g/L for the LC34-USU aquifer material). The one exception to this observation was the

0.4 and 0.5 g/L experiment series for the Borden material which, for unknown reasons,

had essentially the same reaction rate coefficient.

Since there was insufficient data <5 min to determine the fast OAM reaction from the excess permanganate data and the initial portion of the excess aquifer material data are compromised due to the depletion of the fast OAM it was assumed that the reaction order associated with the fast reactions was second-order overall (i.e., first-order with respect to each reactant and hence $\alpha_{fast} = 1$ and $\beta_{fast} = 1$). Other models may have fit the data equally; however, they were not investigated during this research. This assumption yields the following modified NOD kinetic model

$$\frac{d\,C_{OAM}^{fast}}{dt} = -k_{OAM}^{fast}\,C_{OAM}^{fast}\,C_{MnO_4^-}$$

$$\frac{d\,C_{OAM}^{slow}}{dt} = -k_{OAM}^{slow}\,C_{OAM}^{slow}\,C_{MnO_4^-}$$

and,

$$\frac{d\,C_{MnO_4^-}}{dt} = -k_{MnO_4^-}^{fast}\,C_{OAM}^{fast}\,C_{MnO_4^-} - k_{MnO_4^-}^{slow}\,C_{OAM}^{slow}\,C_{MnO_4^-} \tag{2-12}$$

with
$$\gamma_{fast} = k_{MnO_4^-}^{fast} / k_{OAM}^{fast}$$

and

$$\gamma_{slow} = k_{MnO_4^-}^{slow} / k_{OAM}^{slow}$$

and γ_{fast} and γ_{slow} is the stochiometric mass ratio between permanganate and the fast and slow OAM (mass OAM/mass KMnO$_4$).

To estimate the remaining kinetic parameters (k_{OAM}^{fast}, $k_{MnO_4^-}^{fast}$, γ_{fast} and γ_{slow}) for each aquifer material the kinetic model Eq. (2-12) was solved using a fourth-order Runge-Kutta integration scheme coupled with a least-squares parameter estimation algorithm.

Table 2.10 lists the optimal fast reaction rate coefficients along with their respective confidence intervals and Figure 2.6 and 2.7 show the model comparison to the observed data. The fit on these figures is excellent in almost all scenarios. In Figure 2.6 the fast OAM depletes in much less than 5 minutes for all materials. Since the reaction rate coefficient was similar for the 0.4 g/L and 0.5 g/L batch reactors in the Borden excess aquifer material experiments, only one reactor was included in the model. The 0.3 g/L fit of the Borden material deviates slightly from the experimental results for the last two data points. The stochiometric mass ratio for the fast reacting components are < 1 for all materials and are lower than the typical range of 6 to 20 cited in the literature (Mumford et al., 2005). It is presumed that these low mass ratios are due to the fast reactions which have not been adequately characterized previously. The mass ratio for the slow reaction γ_{slow} varies between individual experimental series for each aquifer material since a different $k_{MnO_4^-}^{slow}$ was determined for each permanganate concentration. The use of the slow permanganate reaction rate coefficients (Tables 2.8 and 2.9) to determine these remaining kinetic parameters ensured that they were optimal; however, this limits the portability of this developed model since a different slow permanganate reaction rate coefficient is required for each experiment series or initial concentration. While a kinetic model like this is suitable for the analysis of batch reactor data, its utility for use in transport modelling is severely restricted. As previously mentioned the slow permanganate reaction rate coefficients for each aquifer material decreased as the initial permanganate concentration was increased, and supported by experimental evidence (Xu, 2006) this decrease was hypothesized to be due to precipitation of manganese oxides. These oxides have been shown to cover individual grains presumably associated with reaction sites and this solid phase will negatively affect the rate of reaction between the solids and permanganate due to increased diffusional resistance.

This hypothesis is similar to the catalyst deactivation process due to aging, fouling or poisoning observed in chemical engineered packed-bed reactors, and as catalysts are deactivated the rate of the reaction decreases (Folger, 1999). Similarly, this implies that the slow reaction coefficient decreases as manganese oxide by-products are formed, and hence we assumed that

$$k_{MnO_4^-}^{slow} = f\left(MnO_2_{24}^{formed}\right)$$

where f is some decay function and MnO_2^{formed} is the mass of permanganate consumed per mass of aquifer material. To determine if there was quantitative evidence of passivation, the following four functional decay relationships (linear, exponential, hyperbolic and a modified hyperbolic) were explored:

$$k_{MnnO_4^-}^{slow} = a - bMnO_2^{formed} \qquad (2\text{-}14a)$$

$$k_{MnnO_4^-}^{slow} = a \exp\left(-bMnO_2^{formed}\right) \qquad (2\text{-}14b)$$

$$k_{MnnO_4^-}^{slow} = \frac{a}{1 + bMnO_2^{formed}} \qquad (2\text{-}14c)$$

$$k_{MnnO_4^-}^{slow} = \frac{a}{1 + b\left(MnO_2^{formed}\right)^c} \qquad (2\text{-}14d)$$

where a, b, and/or c are fitting parameters. Using the fast reaction rate coefficients and stochiometric mass ratio ratios for each aquifer material (Table 2.10), each functional decay relationship was implemented and the overall least-squares best fit value (for all four aquifer material) was determined. The best fit was obtained with the hyperbolic decay function (Eq.2.14c), and the optimal values and confidence intervals for a and b are listed in Table 2.11. Figures 2.8 and 2.9 illustrate the kinetic model fits for each aquifer material. The fits obtained in Figures 2.8 and 2.9 do not fit the data as well as those previously given in Figure 2.6 and 2.7, however, the changes to the model reflect the fouling of the reaction surface and allow it to be used for simulating column experiments. These changes also make the model more robust as the reaction rate coefficient is not dependent on the initial mass of permanganate in the system.

The resulting two component kinetic model with passivation was adapted into the one-dimensional reactive transport model developed to simulate the *in situ* oxidation of a contaminant source zone (Appendix B). This model was used to simulate the column

experiments described in Section 2.2.2. The bromide tracer curve was used to determine the dispersivity and porosity of each aquifer material packed column. The porosity was determined by the time at which 50% of the bromide broke through in the column effluent. After the porosity was known, the dispersivity was estimated by altering the dispersivity in the transport model until a good fit to the experimental data was obtained. The porosity and dispersivity results are presented in Table 2.12.

The first attempt to fit the permanganate breakthrough showed that the curve obtained by the proposed batch model was the correct shape, but did not perfectly match the laboratory data (overestimated permanganate consumption in the column). Subsequently, the model was adjusted by making small changes to the a and b parameters until a good fit to the permanganate breakthrough data was obtained (Figure 2.9). The model fit the data fairly well for materials with a high NOD (i.e., EGDY and LC34-LSU); however, the tail was not perfectly captured in the materials with a lower oxidant demand (i.e., Borden and LC34-USU). For both of these materials, the tail in the model fit is slightly lower than the experimental data and represents more permanganate reacting with the aquifer material than is actually occurring. Table 2.13 contains a summary of the kinetic parameters used for each aquifer material.

Table 2.1: General site information.

Sample ID	Sample Location	Soil Texture	Depositional Environment	Depth to Water (m bgs)	K (cm/s)	Sample Depth (m bgs)
Borden	Grownwater Field Laboratory, CFB Borden Ontario	fine/medium sand	Late Wisconsinian Period/ deposited in a prograded beach environment/ glaciolacustrine sand/ unconfined aquifer	0.9	4.21E-04	3.0-4.5
EDGY	East Gate Disposal Yard, Fort Lewis, WA	loamy sand, gravel cobbles	Vashon glacial drift deposit/ recessional outwash	5.5	2.24E-03 - 1.6E-01	5.5-7.6
LC34-LSU	Launch Complex 34, Cape Canaveral AFS, FL	loamy coarse/ medium sand	Pleistocene and recent seashore erosional deposits	1.8	1.82E-04 - 8.97E-04	9.7-13.6
LC34-USU	Launch Complex 34, Cape Canaveral AFS, FL	loamy coarse/ medium sand	Pleistocene and recent seashore erosional deposits	1.8	1.82E-04 - 8.97E-04	3.0-8.2

Table 2.2: Relevant physical and chemical characteristics of aquifer materials.

Characteristic	Borden	EDGY	LC34-LSU	LC34-USU
grain size:				
% gravel	0.2	73.62	4.01	0.9
% sand	89.7	21.22	83.84	91.96
% clay & silt	10.1	5.16	12.16	7.15
% < 2 mm	99.4	18.3	86.55	95.25
d60 (mm)	0.2	22.75	0.49	0.25
d30 (mm)	0.15	6.3	0.13	0.15
d10 (mm)	0.075	0.45	0.065	0.085
hydraulic conductivity (cm/s)[1]	0.0056	0.203	0.004	0.007
coefficient of uniformity	2.67	50.56	7.54	2.94
coefficient of gradation	1.5	3.88	0.53	1.06
specific gravity (g/mL)	2.71	2.67	2.71	2.69
pH (-)	8.4	7.2	8.6	8.8
bulk surface area (m^2/g)	4.155	3.121	2.16	1.919
cation exchange capacity (cmol(+)/kg)	3.5	8.4	12.8	8.3
% total carbon (g/g)	1.58	0.3	4.15	3.15
total organic carbon (g/g): < 2 mm	-	0.228	0.184	0.0878
% total organic carbon (g/g): bulk	0.024	0.17	0.074	0.039
Fe (amorphous) (mg/g)	0.297	1.189	0.504	0.407
% total sulphur (g/g)[2]	0.02	-[4]	-[4]	-[4]
bulk mineralology[3]	quartz plagioclase calcite trace magnetite & ilmenite	quartz feldspar (plagioclase)	quartz calcite aragonite trace feldspars	quartz calcite aragonite trace feldspars

notes:

1. Estimated by the Hazen Equation

2. MDL 0.01%

3. No Fe or Mn minerals detected

4. Data not collected

Table 2.3: Dichromate and permanganate COD tests from Xu (2006).

Site ID	Dichromate-COD[1,2]		Permanganate COD[1,2]	
	Avg	Stdev	Avg	Stdev
Borden	10.21 ± 0.43		3.52 ± 0.85	
EGDY	54.48 ± 1.25		32.58 ± 0.69	
LC34 LSU	30.19 ± 0.41		13.36 ± 0.48	
LC34 USU	11.09 ± 0.32		11.32 ± 1.32	

1) Average and standard deviation based on data from 5 tests of each aquifer material.
2) Units of g $KMnO_4$/kg dry aquifer material

Table 2.4: Excess aquifer material experimental parameters from Xu(2006).

Site ID	Aquifer Material Mass (g)	Solution Volume (mL)	Concentration (g $KMnO_4$/L)
Borden	100	100	0.1, 0.2, 0.3, 0.4, 0.5
EDGY	80	100	0.5, 1.0, 1.5, 2.0, 2.5
LC34-LSU	100	100	0.4, 0.6, 0.8, 1.0, 1.2
LC34-USU	100	100	0.06, 0.2, 0.4, 0.6, 0.8

Table 2.5: Excess oxidant experimental parameters from Xu(2006).

Site ID	Concentration (g $KMnO_4$/L)	Solution Volume (mL)	Aquifer Mass (g)
Borden	20	130	15, 20
EDGY	20	150	15, 20, 25
LC34-LSU	20	150	15, 25
LC34-USU	20	150	10, 20

Table 2.6: Relevant column parameters from Xu(2006).

Site ID	K (g/L)	Flow Rate (mL/min)	Mass of Material (g)	Flush Duration (hrs)	Sampling location - distance from inlet (cm)
Borden	5.17	0.84	710	8.6	20, 38
EDGY	4.94	0.3	100	23.5	10
LC34-LSU	4.93	0.83	620	36	20, 38
LC34-USU	4.95	0.77	720	10	20, 38

Table 2.7: Fractionation of COD

Site ID	COD_{fast}	COD_{slow}	$COD_{non-reactive}$
	(g $KMnO_4$/kg dry aquifer material)		
Borden	0.98	0.84	6.69
EDGY	8.43	6.82	21.90
LC34-LSU	3.02	4	16.83
LC34-USU	1.22	0.89	0[1]

1) LC34-USU Permanganate COD> Dichromate COD therefore non-reactive fraction assumed to be zero

Table 2.8: OAM slow reaction rates.

Site ID	k_{obs} (min^{-1})		r^2	k_{OAM}^{slow} (L g $KMnO_4^{-1}$ min^{-1})	
Borden	1.6E-03 ±	1.9E-03	0.86	7.8E-05 ±	9.4E-05
EDGY	3.2E-03 ±	5.3E-04	0.99	1.6E-04 ±	2.7E-05
LC34-LSU	2.8E-03 ±	1.7E-03	0.96	1.4E-04 ±	8.3E-05
LC34-USU	1.8E-03 ±	1.9E-03	0.89	9.0E-05 ±	9.6E-05

Table 2.9: MnO_4^- slow reaction rate coefficients.

Site ID	Concentration (g $KMnO_4$/L)	k_{obs} (min^{-1})		r^2	$k_{MnO_4^-}^{slow}$ (L g OAM^{-1} min^{-1})
Borden	0.1	1.35E-01 ±	1.12E-02	0.91	3.01E-02 ± 7.56E-02
	0.2	8.72E-02 ±	3.51E-03	0.59	7.54E-03 ± 2.37E-02
	0.3	1.18E-01 ±	2.67E-04	0.79	3.22E-03 ± 1.80E-03
	0.4	1.29E-01 ±	6.35E-05	0.87	1.59E-03 ± 4.29E-04
	0.5	9.75E-02 ±	2.58E-04	0.66	2.24E-03 ± 1.74E-03
EDGY	0.5	3.21E-04 ±	1.23E-03	0.78	9.13E-03 ± 3.50E-02
	1.0	1.96E-04 ±	4.90E-04	0.80	5.57E-03 ± 1.39E-02
	1.5	9.35E-05 ±	5.62E-05	0.93	2.66E-03 ± 1.60E-03
	2.0	6.20E-05 ±	1.64E-05	0.98	1.76E-03 ± 4.67E-04
	2.5	4.48E-05 ±	4.59E-06	0.99	1.28E-03 ± 1.31E-04
LC34-LSU	0.4	2.37E-04	1.88E-04	0.84	6.74E-03 ± 5.34E-03
	0.6	1.14E-04 ±	3.71E-04	0.73	3.26E-03 ± 1.06E-02
	0.8	6.08E-05 ±	6.16E-05	0.53	1.73E-03 ± 1.75E-03
	1.0	3.58E-05 ±	1.06E-05	0.96	1.02E-03 ± 3.02E-04
	1.2	2.16E-05 ±	9.27E-06	0.87	6.15E-04 ± 2.64E-04
LC34-USU	0.06	3.89E-03 ±	2.73E-03	0.84	2.87E-02 ± 2.01E-02
	0.2	6.84E-04 ±	7.54E-04	0.70	5.04E-03 ± 5.56E-03
	0.4	2.45E-04 ±	1.11E-04	0.81	1.81E-03 ± 8.18E-04
	0.6	1.92E-04 ±	8.40E-05	0.81	1.41E-03 ± 6.19E-04
	0.8	9.27E-05 ±	8.40E-05	0.87	6.83E-04 ± 6.19E-04

Table 2.10: Fast reaction rate coefficients for the OAM and permanganate.

Site ID	k_{OAM}^{fast} (L g KMnO$_4^{-1}$ min^{-1})		$k_{MnO_4^-}^{fast}$ (L g OAM^{-1} min^{-1})		γ_{fast} g MnO$_4^-$/g OAM
Borden	2.24E-01 ±	6.00E-02	2.04E+00 ±	6.93E-01	0.15 ± 0.12
EDGY	2.02E-02 ±	4.91E-03	1.94E-01 ±	6.01E-02	0.14 ± 0.11
LC34-LSU	6.27E-02 ±	2.66E-02	3.76E-01 ±	1.97E-01	0.22 ± 0.18
LC34-USU	4.39E-02 ±	1.17E-02	2.83E-01 ±	9.42E-02	0.21 ± 0.16

Table 2.11: Hyperbolic decay fitting parameters and stochiometric ratio of the slow OAM reaction.

Site ID	a (L g OAM^{-1} min^{-1})	b (g MnO$_2^{-1}$)	γ_{slow} g MnO$_4^-$/g OAM
Borden	0.0653 ± 0.0953	57700 ± 6300	7.15 ± 0.32
EDGY	0.0036 ± 0.0010	23 ± 9	3.87 ± 0.85
LC34-LSU	0.0056 ± 0.0025	10100 ± 1500	6.40 ± 0.52
LC34-USU	0.0046 ± 0.0012	11000 ± 1300	8.50 ± 0.31

Table 2.12: Physical properties of the aquifer packed columns.

Site ID	porosity (-)	dispersivity (m)
Borden	0.39	0.0010
EDGY	0.33	0.0077
LC34-LSU	0.34	0.0020
LC34-USU	0.35	0.0003

Table 2.13: Final kinetic parameters derived for each aquifer material.

Site ID	k_{OAM}^{fast} (L g KMnO$_4^{-1}$ min^{-1})	$k_{MnO_4^-}^{fast}$ (L g OAM^{-1} min^{-1})	a (L g OAM^{-1} min^{-1})	b (g MnO$_2^{-1}$)	γ_{slow} g MnO$_4^-$/g OAM
Borden	2.24E-01	2.04E+00	0.0100	60000	7.15
EDGY	2.02E-02	1.94E-01	0.0080	100	3.87
LC34-LSU	6.27E-02	3.76E-01	0.0006	12000	6.40
LC34-USU	4.39E-02	2.83E-01	0.0040	12500	8.50
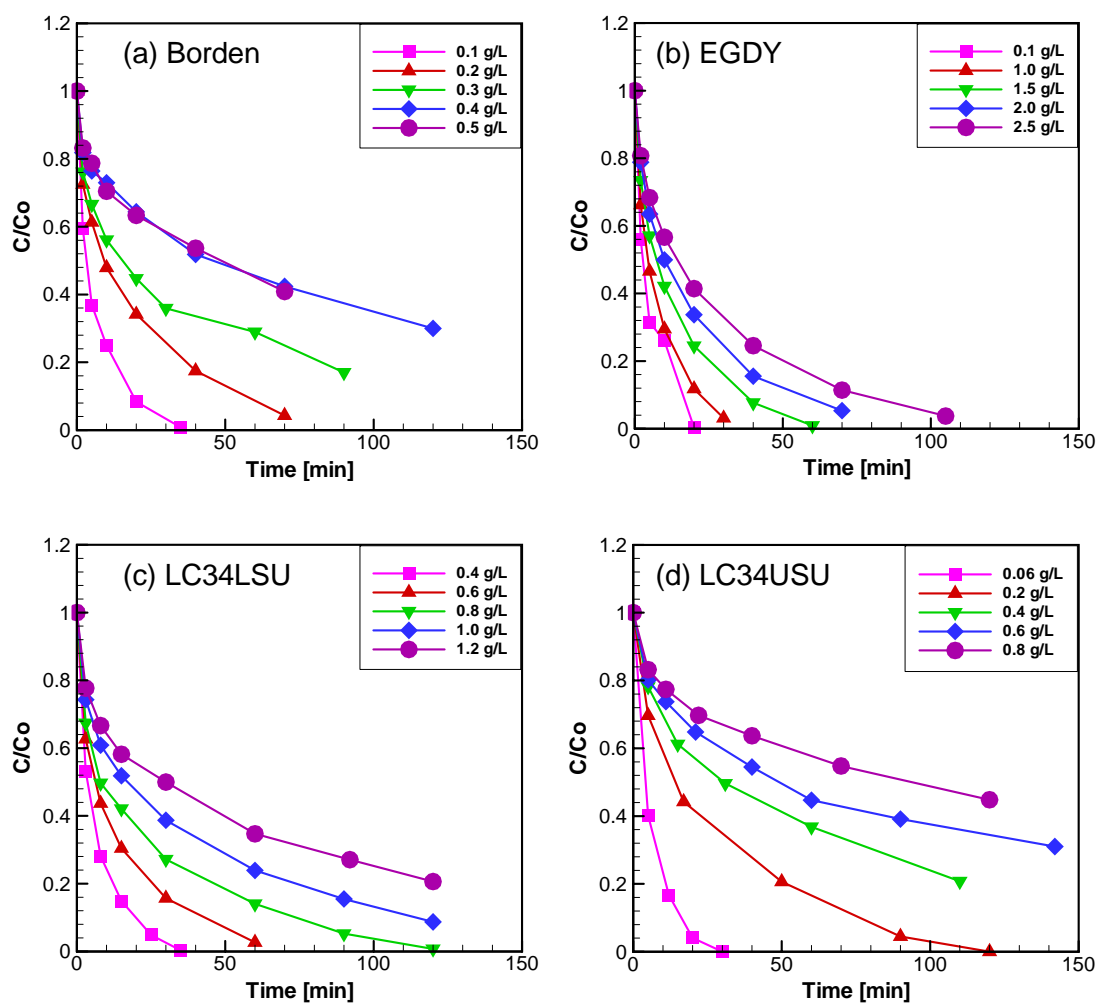
Figure 2.1: Results of the excess aquifer materials experiment in which the degradation of permanganate was measured over time in batch reactors. (a) CFB Borden, (b) EGDY, (c) LC34 LSU, and (d) LC34 USU.
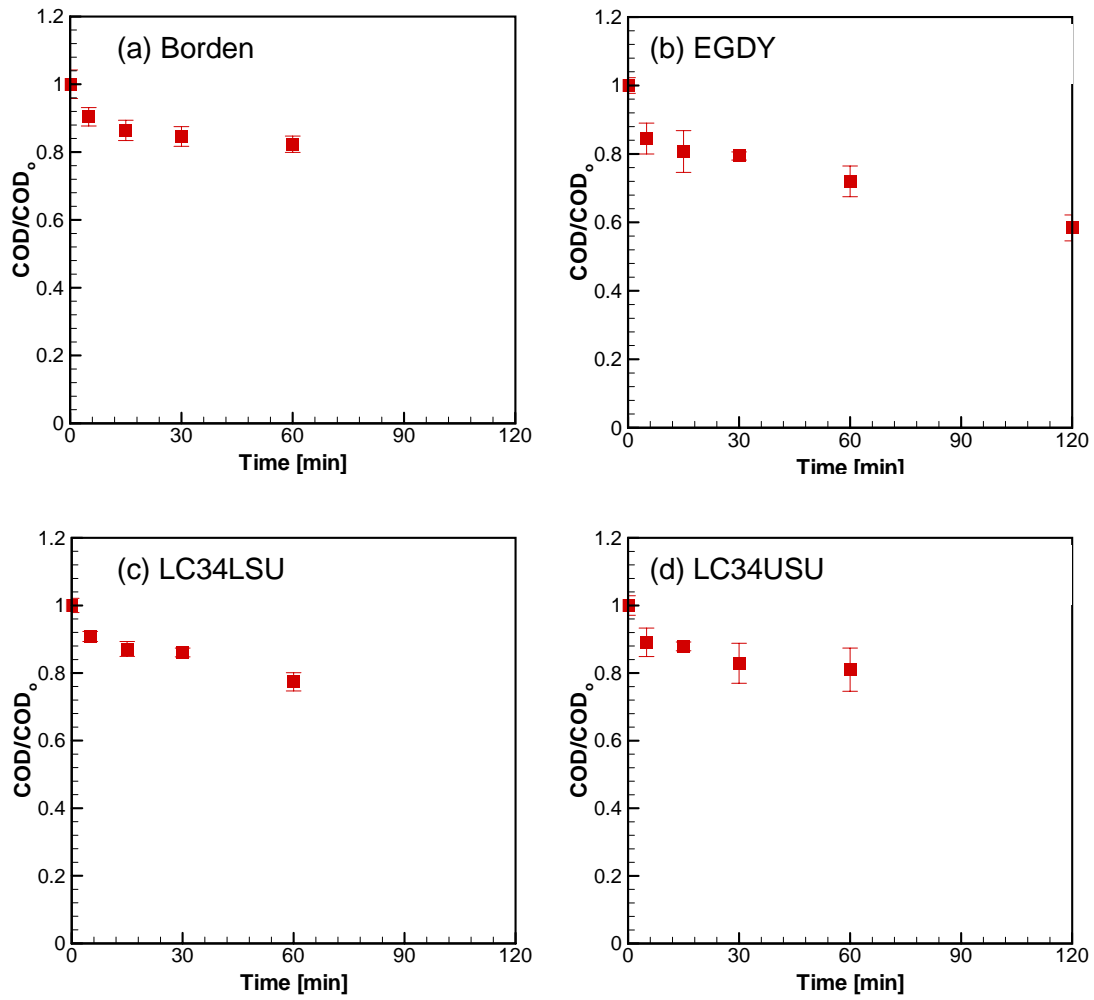
Figure 2.2: Results from the excess oxidant short term batch experiment for (a) CFB Borden, (b) EGDY, (c) LC34 LSU, and (d) LC34 USU.
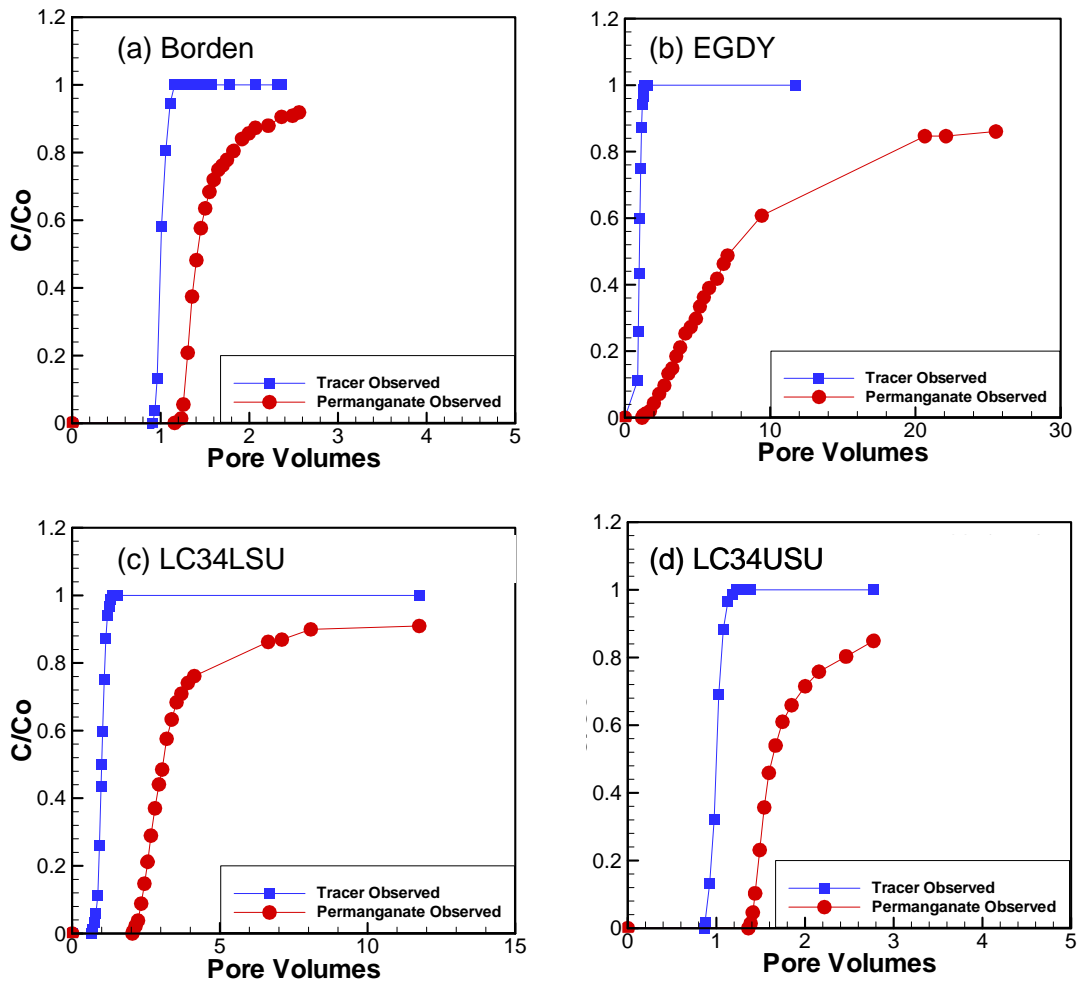
Figure 2.3: Results of the column breakthrough experiments for (a) CFB Borden, (b) EGDY, (c) LC34 LSU, and (d) LC34 USU.
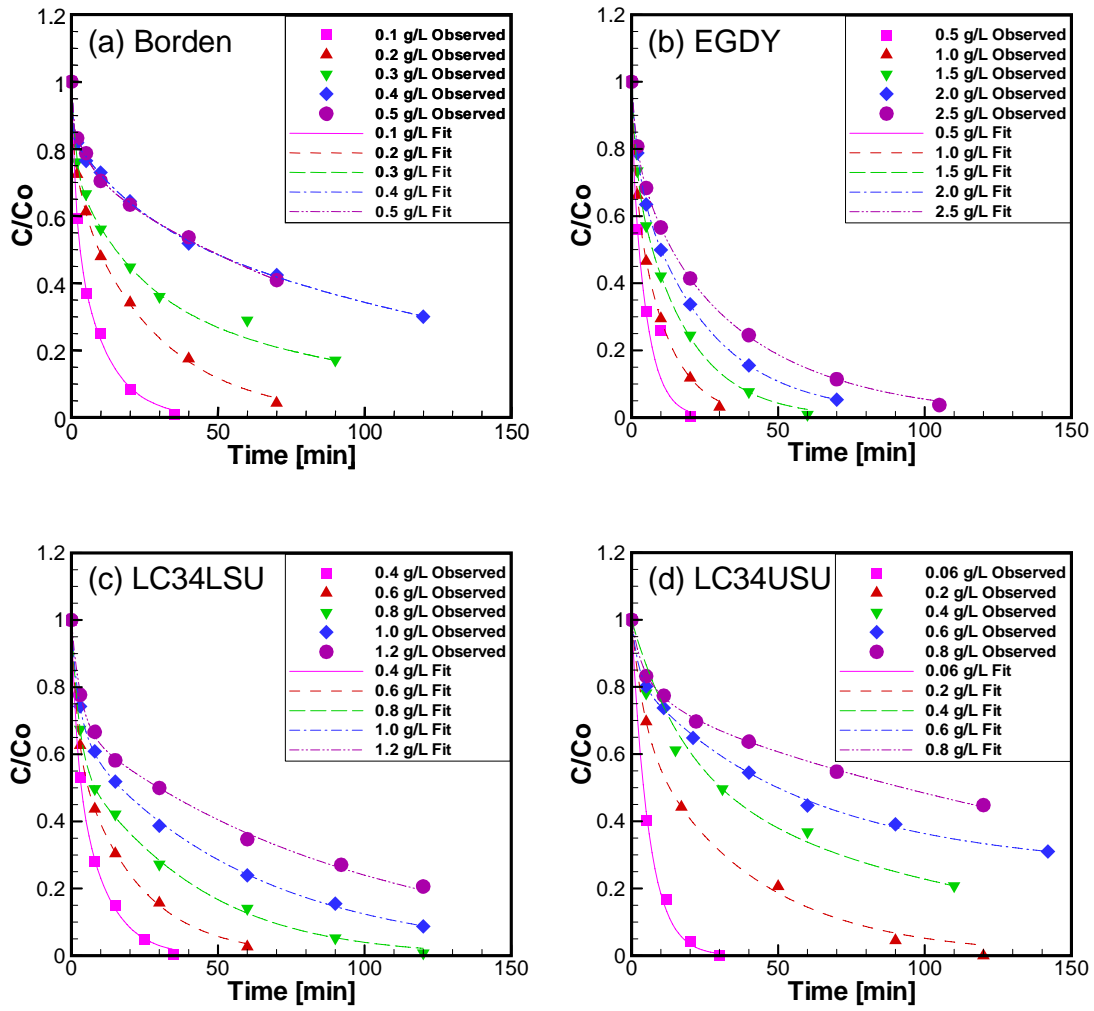
Figure 2.4: Results from the excess aquifer material with and fit with Eq. (2-10) (a) Borden, (b) EGDY, (c) LC34 LSU, and (d) LC34 USU.
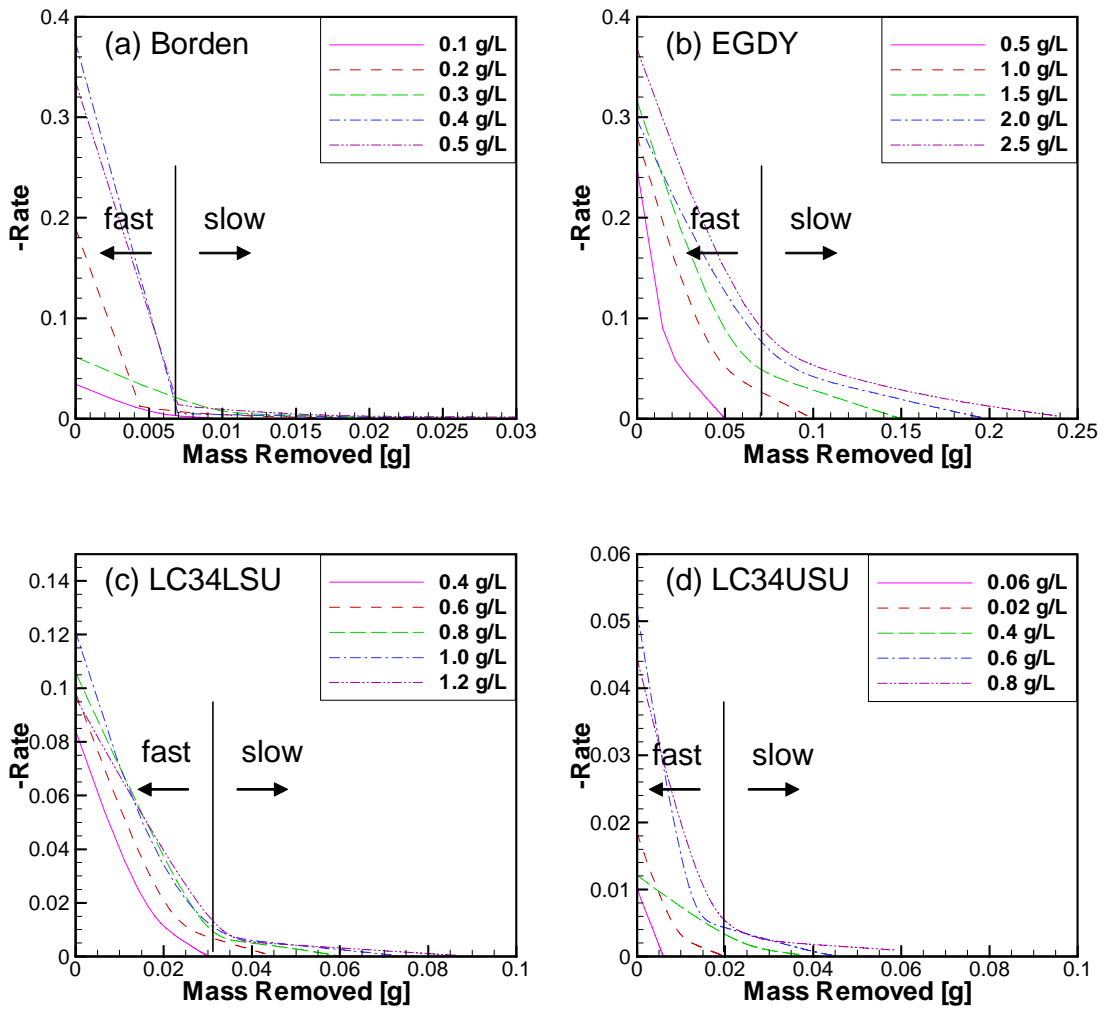
Figure 2.5: Illustration in the change in reaction rate after a set mass of permanganate had been removed from the system for (a) CFB Borden, (b) EGDY, (c) LC34 LSU, and (d) LC34 USU.
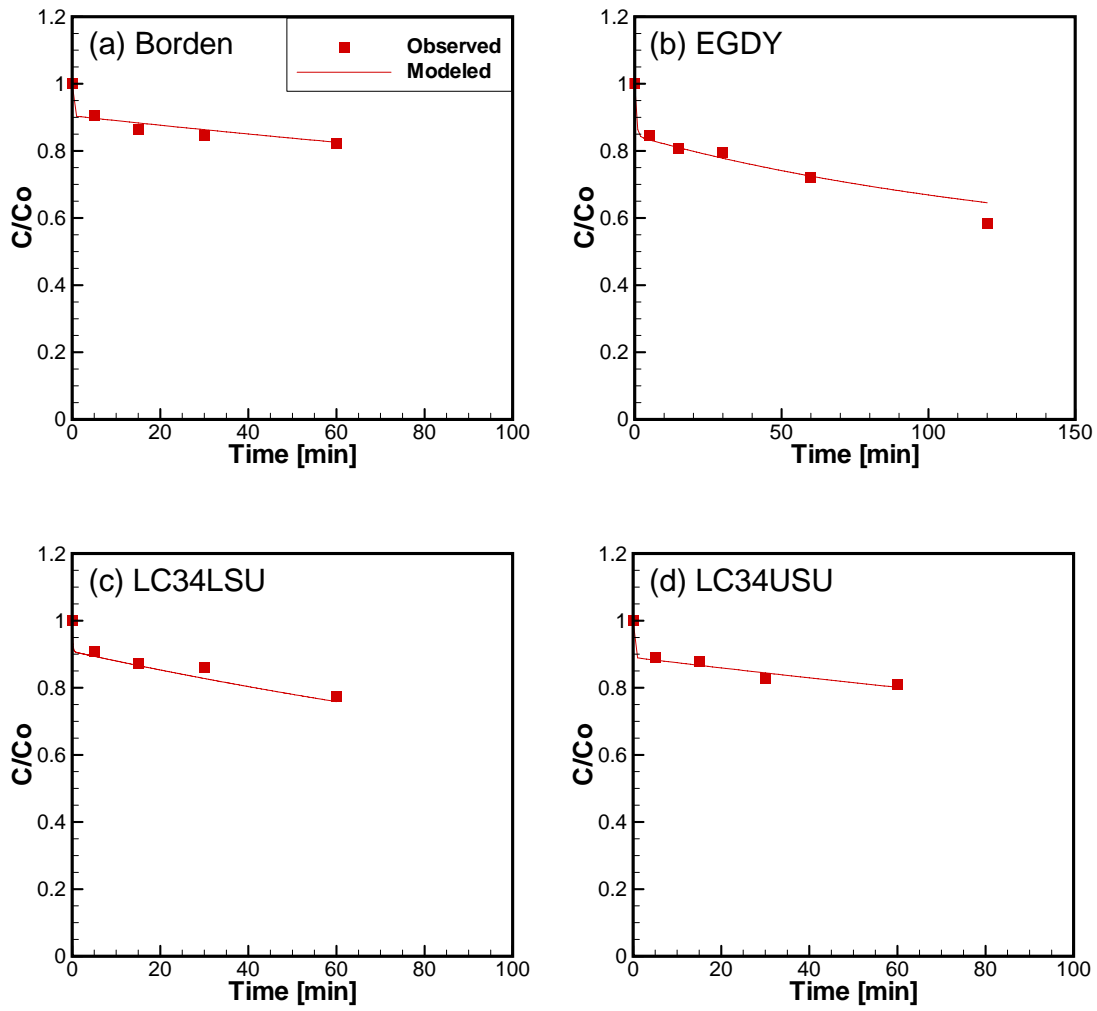
Figure 2.6: Kinetic model fit to observed excess oxidant data (a) CFB Borden, (b) EGDY, (c) LC34-LSU, and (d) LC34-USU.
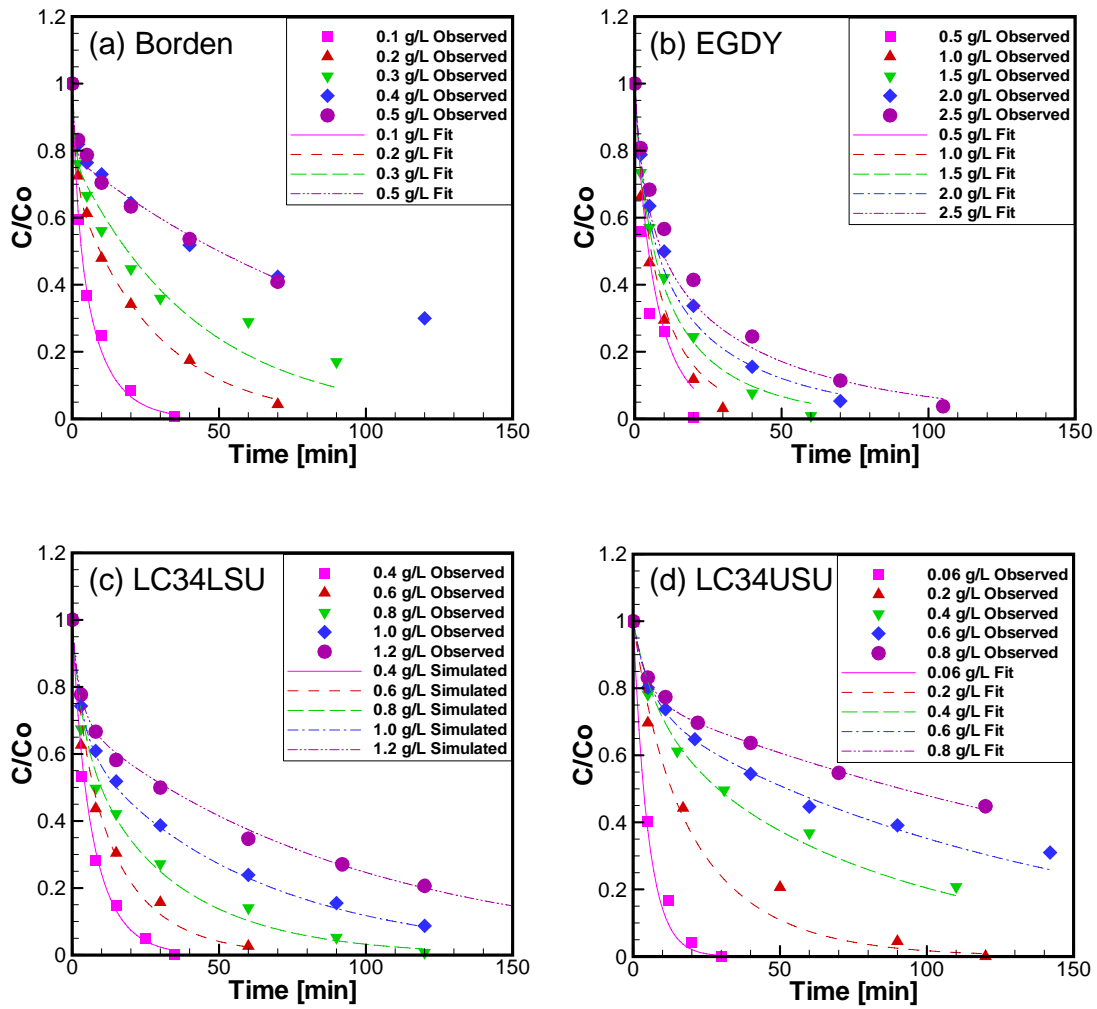
Figure 2.7: Kinetic model fit to observed excess OAM data (a) Borden (b) EGDY, (c) LC34-LSU, and (d) LC34-USU.
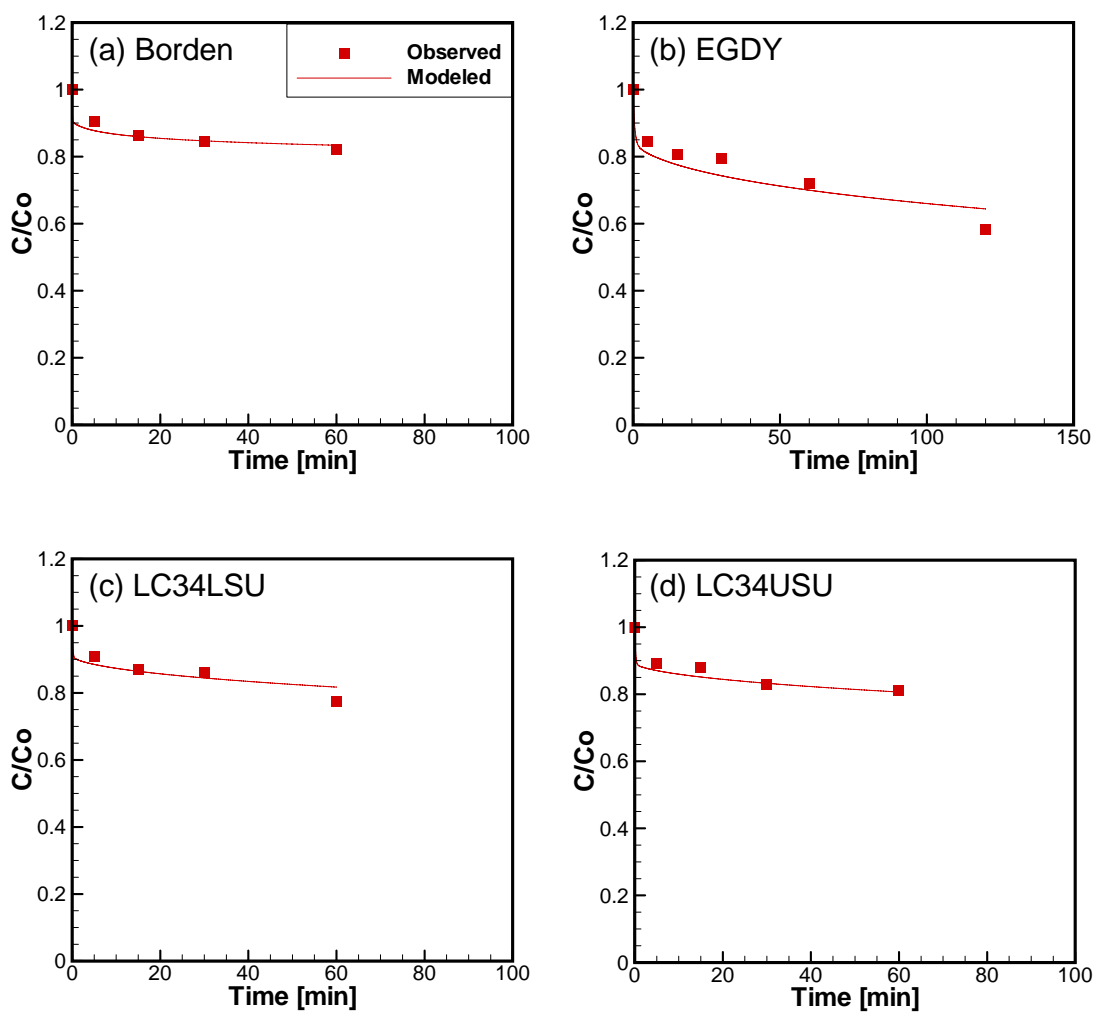
Figure 2.8: Kinetic model fit to observed excess oxidant data incorporating passivation (a) CFB Borden, (b) EGDY, (c) LC34-LSU, and (d) LC34-USU.
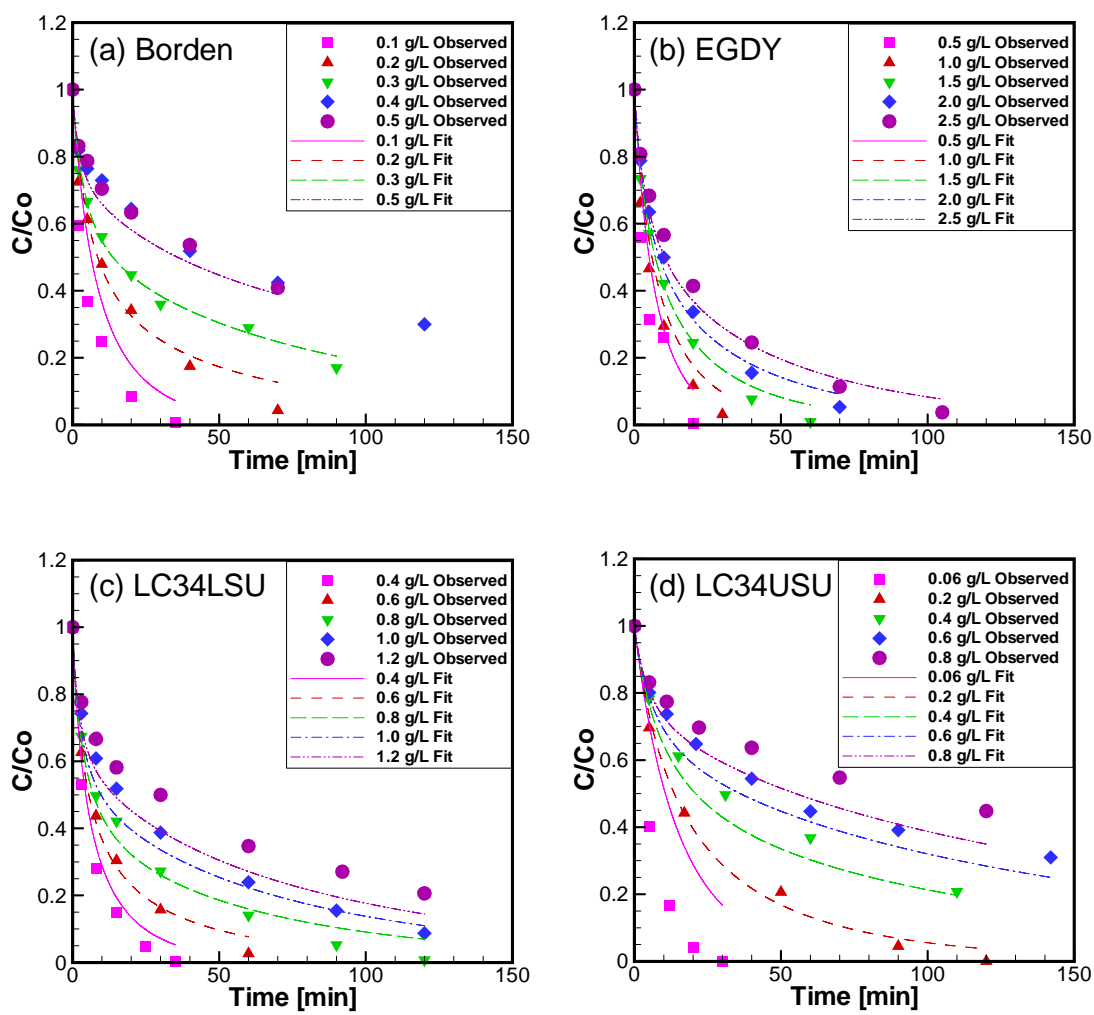
Figure 2.9: Kinetic model fit to observed excess OAM data incorporating passivation (a) CFB Borden, (b) EGDY, (c) LC34-LSU, and (d) LC34-USU.
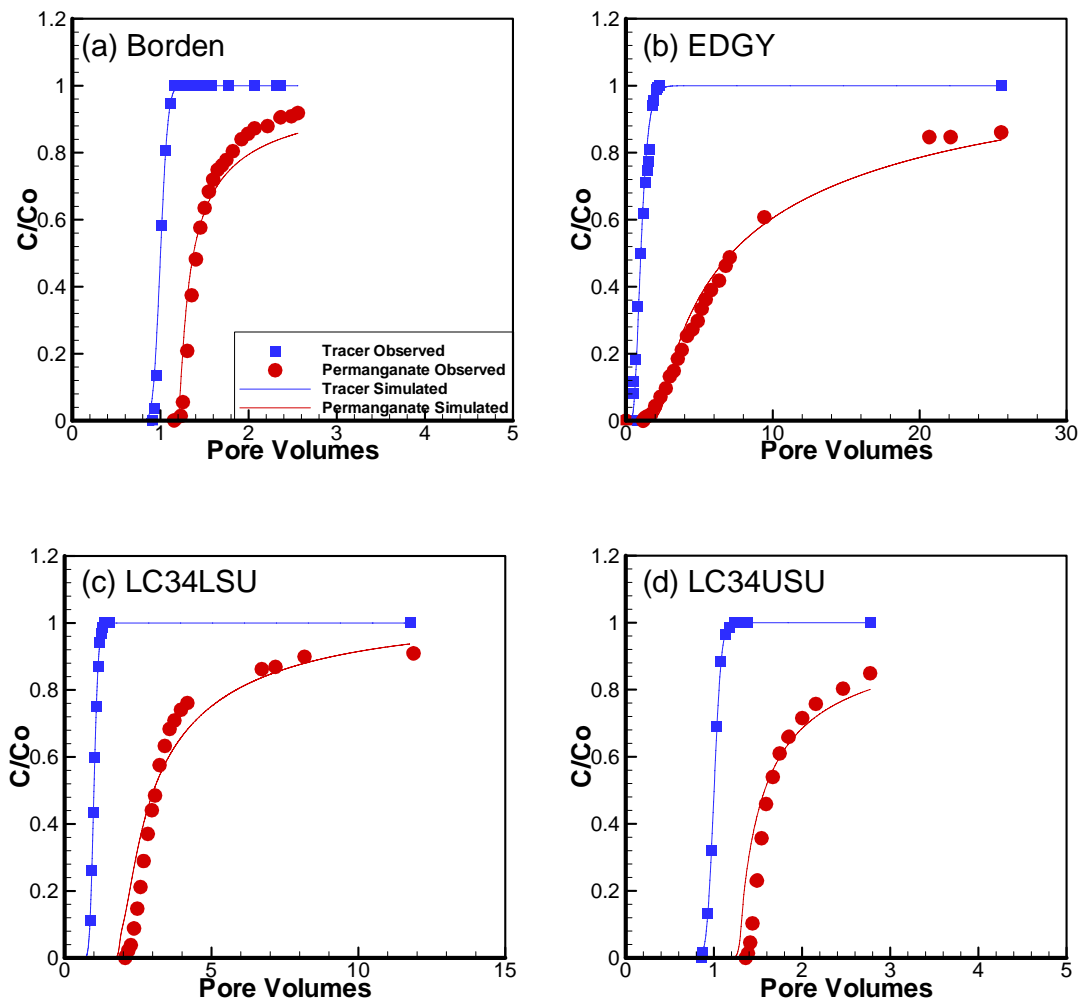
Figure 2.10: Kinetic model fit to column experiment data incorporating passivation (a) CFB Borden, (b) EGDY, (c) LC34 LSU, and (d) LC34 USU.

CHAPTER 3: COLUMN EXPERIMENT

Column experiments were completed to generate data to validate the performance of the one-dimensional model that has been developed (Appendix A) to simulate the competition for permanganate between a contaminant (target reductant) and aquifer material (non-target reductants).

3.1   Experimental Design and Objectives

The objective of these column experiments was to represent an aquifer system where a residual source zone, contained in a high NOD material, is being actively flushed with permanganate. The permanganate migrates through the system from the down-gradient side of the source; thus, permanganate has to migrate through uncontaminated aquifer material prior to contact with the source zone. To represent this system physically each column was designed to contain an isolated residual zone of TCE-contaminated material in the middle of the column and was flushed in three stages: first the column was flushed with Milli-Q water until steady-flow was achieved, then the column was flushed with permanganate (at one of two concentrations) until significant breakthrough of permanganate was achieved, and finally the column was flushed again with Milli-Q water until permanganate was no longer detected in the effluent. Effluent samples were taken throughout all flushing stages and used to determine the concentration of permanganate, chloride, bromide, and TCE.

At the termination of each column experiment, the column was cut open lengthwise and the aquifer materials were sub-sampled to determine the mass of manganese by-products deposited and TCE mass remaining in the column.

To investigate the impact of different permanganate concentrations, two column experiments were performed: one using a solution of 5 g/L $KMnO_4$ (denoted as the 5 g/L column) and the other using a solution of 10 g/L (denoted as the 10 g/L column).

3.2 *Materials and methods*

EGDY aquifer material was chosen for these column experiments because it exhibited significant permanganate consumption. A material with significant permanganate consumption was preferred to ensure that these experiments were able to capture the competition for permanganate between the aquifer material and contaminant.

Each column was constructed from a 10 cm long section of 2.54 cm schedule 40 PVC pipe, with end caps constructed of PVC fittings and sealed with PVC cement and silicone. The bottom end cap was drilled and affixed with 1.11 cm stainless steel tube couplers (Swagelok) and the top end cap was tapped with tubing to allow for outflow.

The bottom of the column was fit with a 500 μm stainless steel screen to prevent aquifer material in the column from escaping. Each column was packed in 1 to 2 cm lifts; the lifts were each compacted using a 1 cm diameter glass rod. The first 3 cm was packed with uncontaminated material and was then allowed to saturate with Milli-Q water which was gravity fed into the column from the bottom. This uncontaminated zone was followed by a 2 to 3 cm of material spiked with TCE (BDH reagent grade) at approximately 2% NAPL saturation. The pore space was again allowed to fully saturate under a gravity feed. The top 4 to 5 cm of the column was packed with additional uncontaminated material and the pore space was allowed to saturate. Figure 3.1 illustrates the experimental design for the columns and Figure 3.2 is a photograph of the experimental set-up. The top of the column was also fit with a 500 μm stainless screen and filled with clean size A 20/30 glass beads (Potters Industries Ltd.) to occupy the void space at the top of the column and glass wool was used to protect the exit tubing from being blocked by the glass beads. The columns were then sealed with Teflon tape.

The TCE spiked aquifer material was prepared by combining 60 g of aquifer solids with 7.0 mL of water and 1.7 mL of TCE in a batch reactor and allowing the material to equilibrate for 24 hours before being packed into the columns. The bulk TCE concentration of this material was 46000 mg/kg and accounts for sorption of TCE to the

aquifer material. Appendix B contains theoretical calculations used to determine the mass of TCE added to the aquifer material.

The columns were flushed in upflow mode using a triple head peristaltic pump (Cole-Parmer Instrument Co., Model No. 7553-80, 1-100 RPM, size 14 tubing), at a designed flow rate of 0.2 mL/min (Darcy flux of 172 cm/day). A free exit condition was used at the outlet. Initially each column was flushed with Milli-Q water until steady outflow was achieved and no air bubbles were observed in the effluent. The column feed was then switched to a permanganate solution of either 5 or 10 g/L $KMnO_4$ (Analytic Grade, EM Science) and 100 mg/L bromide (Br^-, Fisher Scientific). Bromide was used as a conservative tracer to determine the porosity and dispersivity of the aquifer material. When a significant concentration of permanganate was observed in the column effluent, the treatment in of the column was ceased and the column was flushed once again with Milli-Q water until no permanganate was observed in the effluent.

The column effluent was collected frequently (every 15 to 30 minutes during the initial 10 hours and then every hour during daytime over the following days) and used to quantify TCE, $KMnO_4$, chloride (Cl^-, is an oxidation by-product of TCE), and Br^-. Due to the low flow rate, duplicate samples were not collected. Exactly 0.8 mL of effluent from each column was decanted into a Hewlett-Packard glass 2 mL auto-sampler vial. The exact volume of sample in the auto-sampler vial was important due to the method of TCE analysis. If permanganate was visually detected in the effluent, the sample was quenched in the 2 mL auto-sampler vial using a sufficient volume of sodium thiosulphate ($Na_2S_2O_3$, EMD Chemicals Inc.) to ensure the all permanganate was reduced to protect the analytical equipment. TCE and ion concentrations were quantified throughout the experiment; however, the concentration of permanganate was only measured when it was visually observed in the effluent.

Manganese oxides (reaction by-products) were extracted from a sub-sample of the aquifer material at the end of the experiment in three segments – pre source zone (0-3 cm), source zone (3-6 cm), and post source zone (6-10 cm). The material from the source

zone was further sub-sampled into three 1-cm long intervals (3-4, 4-5, and 5-6 cm) to determine the mass of TCE remaining at the end of the experiment.

3.3   *Analytical Methods*

3.3.1   TCE Concentration

The TCE concentration was determined using solid phase micro extraction (SPME) with gas chromatography according to ASTM Standard Practice D6520-00 (ASTM, 2003). Since the SPME method samples the vial headspace, each sample vial can only be used once and hence duplicate measurements were not possible.

For measurement purposes, 0.8 mL of each sample was placed into a 2 mL septum-sealed auto-sampler vial and allowed to equilibrate into the headspace for a minimum of two hours. The vials were then placed into the auto-sampler (Varian 8200) of the gas chromatographer (GC; Hewlett Packard 6890). The SPME fibre (Supelco 100 mm polydimethylsiloxane) was exposed to the headspace of the auto-sampler vials for 4 minutes for adsorption and was then injected into the injector port of the GC at 250°C for two minutes of desorption. The GC was operated in splitless mode and vented to split mode at 15 seconds with a constant septum purge of 2 mL/min. Helium was used as the carrier gas with an oven temperature of 50°C and a flame ionization detector (FID) temperature of 280°C. The column used was a Hewlett Packard HP5 with a length of 30 m, a diameter of 0.32mm, and a film thickness of 0.25 μm.

Standards were prepared to create an 11 point calibration curve ranging in concentration from 0.1 to 800 mg/L. The method detection limit (MDL) was estimated to be 0.05 mg/L (USEPA MDL Procedure – CFR, 1986), the standard deviation of 7 duplicate samples of the 0.1 mg/L standard multiplied by 3.14. Repeat measurements of the 10 mg/L calibration standard were used throughout all GC runs to ensure accurate TCE measurements.

3.3.2 Ion Concentrations

The concentration of Cl⁻ and Br⁻ was measured by ion chromatography using a Dionex AI-450 ion chromatographer with a Dionex AS4A 4x250 anion analytical column and a Dionex ASRS anion chemical suppressor. The eluent was a solution containing 1.8 mM sodium carbonate (Na_2CO_3) and 1.7 mM sodium bicarbonate ($NaHCO_3$) and the regenerant was a solution of 25 mM sulphuric acid (H_2SO_4). For each sample, 50 μL was injected into the sample loop, at a flow rate of 2 mL/min. The chromatograph was run for 20 minutes to allow for the conductivity to return to the baseline. The vials from the TCE analysis were used for ion analysis and were diluted with 0.8 mL of Milli-Q water to ensure sufficient supernatant was available for analysis. Each sample was analyzed in duplicate. Standards for chloride and bromide were prepared according to Standard Method 4110 (APHA, 1998). The MDL for Cl⁻ and Br⁻ analysis was 0.5 mg/L.

3.3.3 Permanganate Concentration

The concentration of permanganate in the effluent was measured using a combination of titration and spectrophotometry. The concentration of permanganate was determined by titration of the 5 g/L feed solution with sodium oxalate (($COONa)_2$, BDH Laboratories) using Method 4500 for $KMnO_4$ (APHA, 1998). The 5 g/L feed solution was then used to calibrate the spectrophotometer (Milton Roy Company Spectronic 20D) to 525 nm. When permanganate was visually observed in the effluent, frequent samples of effluent were collected and diluted with a known volume of Milli-Q water to obtain a sufficient sample size and concentration, and analyzed using the spectrophotometer with an MDL of 1.3 mg/L.

3.3.4 MnO$_x$ and TCE Bulk Soil Concentrations

The bulk concentration of manganese in the aquifer materials following the column experiment was determined by using the modified Chao's method (Chao, 1972) proposed by Neamana et al. (2004).   Manganese precipitates were extracted from a small mass (< 10 g) of oven dried (50^oC over night) aquifer solids from the three zones of each column. The material from both columns was extracted for two hours using an acidified 1.0 M

hydroxylamine hydrochloride (NH_2OH-HCl) at pH 2.0 and adjusted by a 2% nitric acid (HNO_3) solution. The manganese content was determined using an inductively coupled plasma (ICP) emission spectroscopy with a Spectro Flame instrument (Spectro Analytica). The MDL of this method is 0.01 mg/L

Bulk TCE concentration for the aquifer material from the TCE spiked zone, was determined by a methanol extraction procedure (Sawhney et al., 1988). The TCE was extracted by placing a small amount of aquifer material (< 5 g) into a 25 mL vial with 5 mL of methanol (Burdick and Jackson, Analytic Grade). The vials were continuously inverted end-over-end for 12 hours to ensure adequate contact between the methanol and aquifer material. The methanol was then diluted into Milli-Q water (dilution factor 10-100 Milli-Q water : 1 methanol) and anaylzed using the SPME method described in Section 3.3.1. The bulk TCE concentration was calculated based on the mass of aquifer material used in the extraction, the volume of methanol added, and the dilution factor.

Since there was only a small mass of aquifer materials within the columns, and samples were required for both Mn and TCE extractions, only one extraction for each interval was completed. The extraction samples were measured once.

3.4   *Results and Analysis*

Instead of a 3 cm thick TCE spiked zone, the source zone in the 5 and 10 g/L columns had a thicknesses of 2.8 and 2.5 cm respectively. Based on bulk TCE analysis, the concentration of TCE in the source zone was 45800 mg/kg, which corresponds to masses of 1.27 and 1.13 g in the 5 and 10 g/L columns respectively.

The actual flow rates measured in the columns deviated from the design flow of 0.2 mL/min; the 5 g/L column was much lower at 0.060±0.005 mL/min or 52 cm/day, while the 10 g/L column achieved an average flow rate of 0.174±0.006 mL/min or 150 cm/day. The lower flow rate for the 5 g/L column was attributed to fouling of the tubing within the pump and resulted in a much longer duration of treatment for the 5 g/L column as compared to the 10 g/L column.

The concentration of permanganate in the nominal 5 g/L solution was determined to be 4.93 g/L and the nominal 10 g/L solution was 9.92 g/L. The concentration of Br⁻ was 147 mg/L in the 5 g/L permanganate solution, and 134 mg/L in the 10 g/L permanganate solution.

The 5 g/L column was flushed with permanganate for ~ 70 hours before the column became completely blocked with manganese oxide particles so that the column was unable to conduct fluid. Consequently, the 5 g/L column was not flushed with Milli-Q water following treatment. At the end of the 70 hours, the effluent permanganate concentration reached only ~ 25% of the inlet concentration. The 10 g/L column was flushed with permanganate for ~ 8 hours before the inlet solution was switched to Milli-Q water. The 10 g/L column was then flushed for an additional 44 hours with Milli-Q water before the final flushing phase was terminated.

3.4.1 Breakthrough Data

Breakthrough curves (BTCs) for bromide, TCE, permanganate, and chloride for the 5 and 10 g/L columns are shown in Figures 3.3 and 3.4 respectively. The Br⁻ and MnO_4^- BTCs were normalized to the influent concentration. Time zero is defined as the point when permanganate was visually observed to enter each column and therefore chloride and TCE concentrations detected prior to the start of the permanganate flush occur before time zero on the Cl⁻ and TCE BTCs.

3.4.1.1 Bromide

The breakthrough for bromide (Figures 3.3(a) and 3.4(a)) was analyzed to determine the porosity and dispersivity of the columns. The porosity was calculated from the time when the bromide effluent concentration reached 50% of the source concentration and the volume of the column. The dispersivity was determined by matching the bromide BTC with the results from a 1-D transport model (Appendix A).

The porosity of the 5 g/L column was determined to be 0.59, which is substantially higher than the expected porosity of 0.33 for EGDY aquifer material based on Xu's

47

(2006) column experiments. It was hypothesized that the top of the column had a large amount of void space due to poor column construction which lead to an increase in the volume of solution required for 50% of the bromide to breakthrough. The void space also caused continuous mixing of pooled effluent further delaying bromide breakthrough. The lack of adequate porosity values for the 5 g/L column, along with the plugging that eventually occurred, made it impossible for the results of the 5 g/L column study to be used for validation of the model. It further meant that the dispersivity of the 5 g/L column could not be determined. Due to these reasons, the 5 g/L column cannot be used for modelling purposes, however, the results are nonetheless interesting, so will be further discussed.

The porosity of the 10 g/L column was determined to be 0.28 which is much closer to the previously reported value of 0.33 (Xu, 2006). Due to the experimental data and the calculated porosity values, which do no indicate there were significant experimental errors, it was assumed that the 10 g/L column was packed correctly, with no large void space at the end of the column. The difference between this porosity and the previously reported value is assumed to be due to a combination of the packing of the column, and the presence of DNAPL. Although the design NAPL saturation of 2% would result in minor changes to the porosity (0.007), the actual saturation in the source zone may have been much higher due to the increased mass of TCE present for sorption considerations. Based on the porosity of the column ~ 5.8 PVs of permanganate were supplied to the column. The dispersivity of the 10 g/L column was determined to be 0.01 m which was approximately the value obtained from analysis of Xu's EGDY NOD column results (0.008 m).

3.4.1.2 TCE

The general shape of the TCE BTCs is similar for both columns (Figures 3.3(b) and 3.4(b)). The concentration of TCE generally increases with fluctuations until a maximum concentration was reached after 132 mg of permanganate were delivered to the 5 g/L column, and 185 mg of permanganate to the 10 g/L column. The TCE concentration in the 5 g/L column proceeded to decrease slowly over the following 2 days eventually

reaching non-detect levels near the end of the experiment. The concentration of TCE in the 10 g/L column decreased at a much faster rate, and remained at non-detect levels for the duration of the permanganate flush. During the post-treatment Milli-Q flush, TCE concentrations in the 10 g/L column rebounded to as high as 25 mg/L. The lower concentration of TCE post-treatment, relative to pre-treatment, could be due to manganese precipitates inhibiting mass transfer; however, there is no evidence that supports this hypothesis.

In the 5 and 10 g/L column, the maximum TCE concentration in the effluent pre-oxidation was approximately 160 mg/L, substantially less than the maximum solubility reported in literature (e.g., 1100 mg/L; Merck, 2003. This lower concentration is suspected to be due to a combination of TCE sorption on to the aquifer materials and, incomplete transfer into solution and a lower maximum solubility.

The significant fluctuation in the effluent TCE concentration is suspected to be the result of a number of factors including: sampling error, SPME fibres coming in contact with sample, and the small variations in the darcy flux. Sampling errors could occur due to samples being open to the atmosphere for differing lengths of time before they were transferred to the auto-sampler vials and sealed; thereby allowing for some TCE to be depleted through volatilization. Additionally, the SPME fibre may have been exposed to the aqueous sample during its injection and removal from the vial due to small volumes of sample which were observed to adhere to the vial cap. The consequences of such an occurrence are not known. Small variations in the darcy flux would affect the contact time in the source zone (mass transfer) and down-gradient of the source zone (sorption) and the time available for reactions.

3.4.1.3 Permanganate

The permanganate BTCs for the 5 and 10 g/L columns (Figures 3.3(c) and 3.4(c) respectively) were investigated to understand the timing of the permanganate breakthrough. For the 5 g/L column, the permanganate first appeared after ~ 0.44 g of permanganate had been supplied to the column, due to the extremely slow flow rate of

the 5 g/L column, this mass corresponded to approximately 1 day into the permanganate flush. By the time a measurable concentration of permanganate was detected in the effluent of the 5 g/L column, the concentration of TCE in the effluent had dropped significantly to below 20 mg/L. Eventually, when the effluent concentration of permanganate reached a maximum concentration of 1.15 g/L, the concentration of TCE in the effluent had dropped to less than 2 mg/L. These concentrations are significantly higher than the MOE standard of 5 μg/L (MOE, 2003). The breakthrough of permanganate in the 10 g/L column was first detected after only 0.21 g of permanganate had been supplied, which represents a breakthrough time of approximately 2 hours or 1.5 PVs. As with the 5 g/L column, the TCE concentration decreased as the effluent concentration of permanganate increased; however, the decrease of TCE and increase in the permanganate concentration of the effluent of the 10 g/L column was much more rapid. Within an hour and a half of when permanganate was first detected in the effluent, the concentration of TCE in the effluent was <1 mg/L and the permanganate concentration was >2 g/L and after an additional hour and a half, the TCE concentration was below the detection limit. The initial delay in permanganate breakthrough and slower increase in permanganate concentration in the 5 g/L column, compared to the 10 g/L column, is likely due to the greater time available for mass transfer of TCE into the aqueous phase and reaction with aquifer materials or aqueous phase TCE.

The permanganate BTCs were analyzed to determine the mass of permanganate consumed based on the mass of permanganate supplied to the columns and the mass of permanganate recovered from the effluent. Approximately 90% of the permanganate supplied to the 5 g/L column was consumed by TCE and the aquifer material within the column. The mass of permanganate consumed in the 5 g/L column was 1.14 g. Based on the stochiometry of the TCE/$KMnO_4$ reaction and the mass of Cl$^-$ recovered from the effluent, approximately 0.45 g of permanganate (or 40%) was used to reduce the TCE concentrations, the remaining 60% went to satisfying the NOD demand. The mass of permanganate consumed in the 10 g/L column was 0.59 g; of this, approximately 0.2 g of the permanganate (or 34%) was consumed by the TCE and the remaining 66% was used to satisfy the permanganate demand.

3.4.1.4 Chloride

The chloride BTCs for the 5 and 10 g/L experiments (Figures 3.3(d) and 3.4(d) respectively) show that the concentration of chloride in the effluent started at a non-zero value while Milli-Q water was flushed, and decreased steadily until permanganate reached the zone of TCE spiked material. The source of this chloride is unknown and any attempts at explanation are speculation.

The maximum concentration of chloride observed in the 5 and 10 g/L columns was 700 and 880 mg/L respectively near the end of the permanganate flush (i.e., at 70 hours in the 5 g/L column and 4.7 PVs in the 10 g/L column). Since the highest observed concentration of TCE exiting the column was ~ 160 mg/L, the observed chloride concentrations in the effluent support that increased mass transfer of TCE into the aqueous phase was accomplished (based on the stochiometry of TCE oxidation and the maximum observed concentration of TCE, 130 mg/L of chloride would be expected in the effluent if there was no increase in mass transfer).

The lower concentration observed to exit the 5 g/L column could be indicative of several processes. The concentration of TCE in the column may have reached a lower solubility due to inhibited mass transfer by flow short circuiting (i.e. non-uniform flow through column) or manganese by-product formation. Additionally, complete mineralization of TCE may not have occurred (i.e., TCE could be present in the effluent or, organic reaction by-products could bind chlorine and prevent the release of chloride ions). Yan and Schwartz (2000) investigated the reaction pathway of TCE oxidation and found that several of the intermediate by-products contained chlorine. Incomplete reaction is supported by low non-zero TCE concentrations in effluent samples from the 5 g/L column which also contained measurable concentrations of permanganate. Permanganate was first detected in the 5 g/L effluent at 29 hours and measurable amounts of TCE were detected in the effluent from 28.5 to 57 hours; after which the concentrations dropped below the MDL. An early, unaccounted for, unidentified, peak on several gas chromatograms may be indicative of chlorine-containing organic oxidation by-products. The presence of unidentified peaks on the chromatograms occurred consistently

throughout the first 25 hours of the permanganate flush, however, these peaks were much higher during the initial stages of the permanganate flush when only small concentrations of permanganate were suspected to have reached the source zone.

3.4.2 Bulk Soil Concentrations

The bulk soil manganese (Mn) and TCE concentrations for both column experiments are shown in Figure 3.5 for the 5 and 10 g/L columns.

3.4.2.1 Manganese

The Mn concentration in the soil post treatment is expressed in terms of g MnO_2/kg aquifer material following MacKinnon and Thomson (2002). As expected, the lowest concentration of manganese oxides (24.72 g/kg and 4.27 g/kg for the 5 and 10 g/L columns respectively) was observed in the first 3 cm of the column (the first section packed with uncontaminated material) and was assumed to be the product of reaction between the permanganate and the aquifer materials. Evidence of manganese oxides being produced in systems with no contamination is presented by Xu (2006). Xu (2006) reported that 15.8 g MnO_2/kg aquifer material were produced in long-term batch experiments containing EGDY aquifer material and permanganate; less than the value observed in the 5 g/L column but greater than the value observed in the 10 g/L column. The greater concentration of Mn in the 5 g/L column is likely due to sampling error that may have included material from the adjacent source. The lower concentration of Mn in the 10 g/L column was likely due to incomplete oxidation of the slow reacting OAM. The highest Mn concentration was observed in the TCE source zone located between 3 and 6 cm and is presumed to have been produced by the oxidation of aquifer materials and TCE. In the down-gradient 4 cm of the columns, the Mn concentration was higher than the up-gradient interval but lower than the source zone. Manganese observed in the last section of the columns was due to reaction between permanganate and aquifer materials, transport of manganese by-products from the source zone, and further reaction between aqueous TCE originating from the source zone and permanganate. Evidence that manganese oxides were transported from the source zone was observed by the

presence of solid precipitates in the effluent. Although these precipitates were not analyzed for composition, due their brown colour it was assumed that they were manganese oxides. Other researchers have reported finding brown precipitates in the effluent of column and 2-D studies (MacKinnon and Thomson, 2002; Schroth et al., 2001).

The concentration of Mn deposited in the 5 g/L column was much higher than the 10 g/L column. Visual evidence of precipitates deposited in the 5 and 10 g/L columns is shown in Figure 3.6 as dark bands. The dark area in each column is coincident with the TCE source area. The 5 g/L column had a thick band of manganese oxides which likely caused the plugging of the column resulting in the premature termination of the experiment. To a lesser extent, the 10 g/L column also had a band of manganese oxides; however, it is presumed that the porosity was not significantly decreased. The greater concentration of Mn in the 5 g/L column is likely due to the greater mass of permanganate supplied (since treatment lasted for several days); which resulted in more oxidation of both the spiked TCE zone and the oxidizable materials within the aquifer. Approximately 67% of the permanganate consumed within the 5 g/L column remained in the column as manganese precipitates, where as 65% remained in the 10 g/L column; the remaining fraction is assumed to have been transported out of the column.

3.4.2.2 TCE

After treatment, the bulk TCE concentration in the 5 g/L experiment was significantly reduced from the initial concentration with more than 98% of the TCE removed. As expected, higher removal was observed on the up-gradient side and lower removal occurred down-gradient side of the source zone, because the up-gradient side was exposed to higher concentrations of permanganate and has higher mass transfer. The 10 g/L column also experienced significant depletion of the source, more than 85% removal of TCE with less permanganate supplied than the 5 g/L column (0.84 g of $KMnO_4$ in the 10 g/L column compared to 1.26 g in the 5 g/L column). However, the distribution of TCE remaining in the column at the end of the experiment is confusing. The highest removal was observed in the mid section of the source zone with less removal at both the

up-gradient and down-gradient ends of the source zone. This trend could indicate short circuiting in the column, an initial heterogeneous distribution of TCE in the contaminated material, or sampling errors due to single samples taken from each of the 3 one cm-long sections of the source zone. However, the effects of possible short-circuiting or heterogeneous distribution of TCE were presumed to be minimal since there was only a 4% difference in TCE mass removal between the highest and lowest concentrations in the source zone.

3.5   *Mass Balance Considerations*

The BTC and the results of the soil extractions were used to determine the mass balance of Mn and TCE during the experiments.

3.5.1   Manganese Mass Balance

The mass balance of manganese (Table 3.1) was completed by analyzing the mass of manganese supplied to the column (as permanganate), the mass of manganese present in the effluent as permanganate, and the mass of manganese remaining in the column at the end of the experiment duration.

The mass of permanganate supplied to the column was determined by the flow rate and the concentration of permanganate in the source solution; the mass of permanganate was converted into the mass of manganese (~ 0.40 g supplied to the 5 g/L column and ~ 0.29 g to the 10 g/L column). The mass of manganese exiting the column as permanganate was determined based on the permanganate BTC and converting the mass of permanganate in the effluent to a mass of manganese (~ 0.04 g exited the 5 g/L column and ~ 0.09 g from the 10 g/L column). The mass of manganese oxides remaining in the column at the end of the experiment was determined from the bulk soil concentrations of MnO_2 which was converted to a mass of Mn (~ 0.25 g in the 5 g/L column and ~ 0.13 g in the 10 g/L column). The unaccounted for mass of manganese could have been due to un-quantified manganese oxides in the effluent, non-representative soil samples, flow rate variations, and/or experimental error.

3.5.2 TCE Mass Balance

The TCE mass balance (Table 3.2) was determined through analysis of the TCE and Cl⁻
BTCs and the bulk TCE concentration post treatment.

The initial mass of TCE in the column was determined based on the bulk concentration of
TCE in the spiked material and the thickness of the source zone within each column. The
initial mass of TCE in the columns was ~ 1.27 g and ~ 1.14 g for the 5 and 10 g/L
columns respectively. The TCE BTCs were analyzed to determine the mass of TCE
exiting the column in the effluent during flushing. Approximately 0.01 g of TCE was
accounted for in the effluent of both the 5 and 10 g/L columns. The chloride BTCs were
used to estimate the mass of TCE destroyed in the column by assuming complete
mineralization of TCE (i.e., 1 mole of TCE oxidizes to produce 3 moles of chloride). The
results indicate that ~ 0.19 g and ~ 0.08 g of TCE were oxidized in the 5 and 10 g/L
columns respectively. Fluctuations in the flow rate and outflow concentrations
(particularly during times when no data was available) could result in over or under
estimation of the mass destroyed or present in the effluent. The mass of TCE remaining
in the columns post treatment was determined from the bulk soil TCE concentrations. In
the 5 g/L column, ~ 0.01 g of TCE remained at the end of the column experiment,
whereas ~ 0.10 g of TCE remained in the 10 g/L column. The TCE mass balance does
not account for the full initial mass in the source zone. The unaccounted for mass of TCE
could be due to incorrect characterization of the initial mass of TCE present, non-
representative soil samples, flow rate variations, experimental error, and sorption of
aqueous TCE to the down-gradient aquifer materials. Based on the f_{oc} of the aquifer
material (0.003 g organic carbon/g material; Xu, 2006) and the log K_{ow} for TCE (2.29;
Merck, 2003, the full unaccounted for mass could be sorbed to the down-gradient
materials in the column, however these materials were not extracted.

Table 3.1: Manganese mass balance for the 5 and 10 g/L columns. Unaccounted for manganese is assumed to have exited the column as oxidation by-products.

	Mass of Manganese	
Pathway	5 g/L column	10 g/L column
	g	g
Supplied	0.40	0.29
Effluent	0.04	0.09
Mass in Column	0.25	0.13
Unaccounted	0.11	0.07

Table 3.2: TCE mass balance for the 5 and 10 g/L columns. Unaccounted for TCE is assumed to be sorbed to the soil in the final 4 cm of the column.

	Mass of TCE	
Pathway	5 g/L column	10 g/L column
	g	g
Pre-oxidation Mass	1.27	1.14
Post-oxidation Mass	0.01	0.10
TCE Effluent	0.01	0.01
Chloride Effluent	0.19	0.08
Unaccounted	1.06	0.95
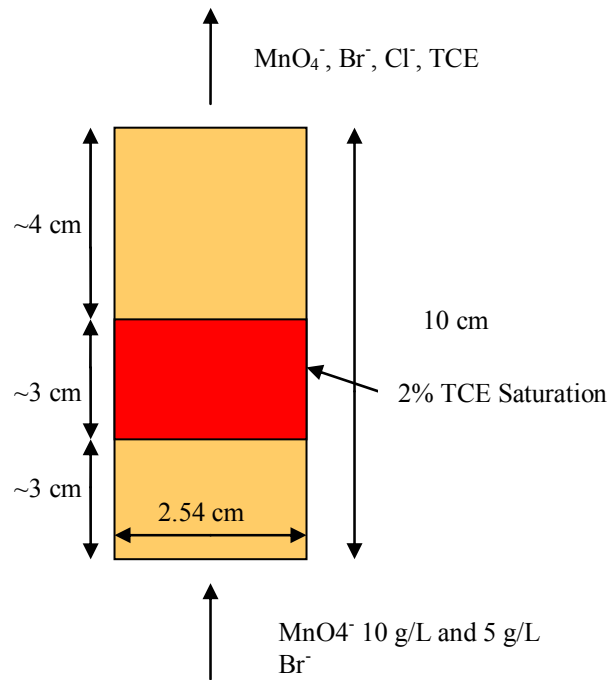
Figure 3.1: Schematic of column showing over all dimensions and location of TCE contaminated region.
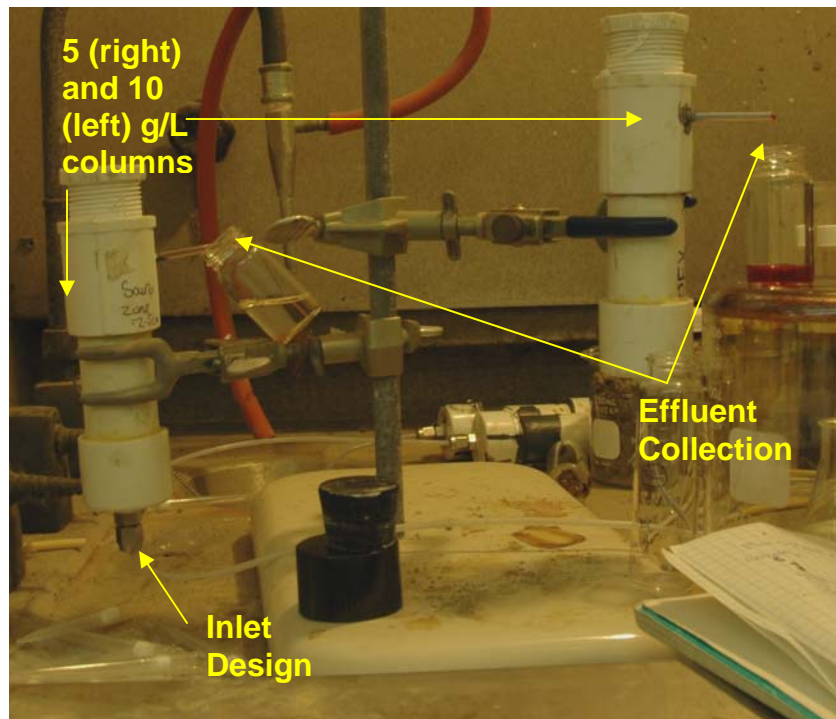
Figure 3.2: Image of the column experiment showing the 10-cm long column, the effluent collection vial, and the column set-up.
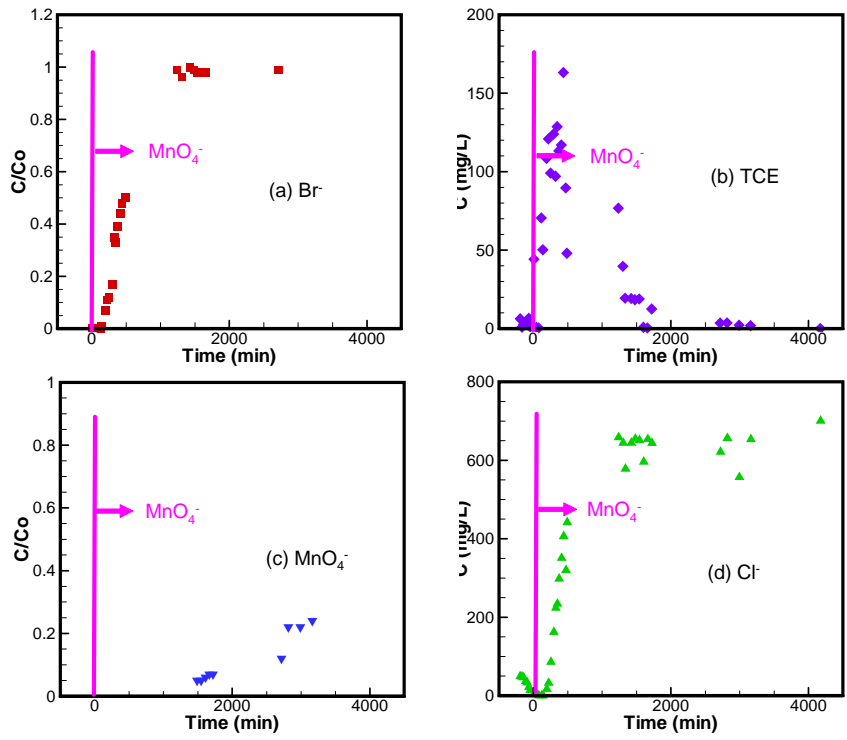
Figure 3.3: Breakthrough curves for (a) Bromide, (b) TCE, (c) Permanganate, and (d) Chloride for the column flushed with a 5 g/L solution of permanganate. Also indicated is the start of the permanganate flush.
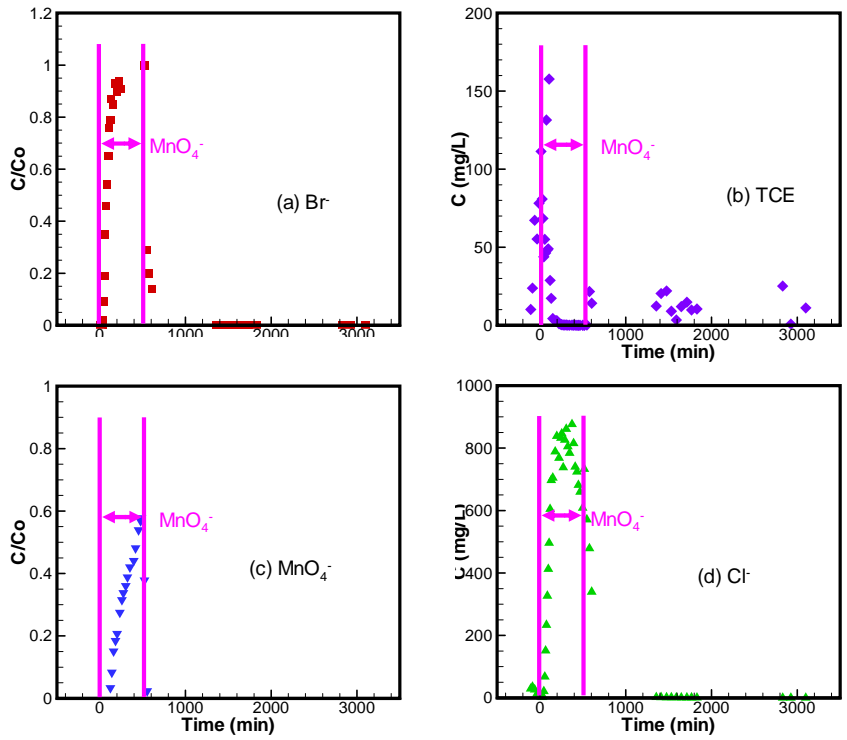
Figure 3.4: **Breakthrough curves for (a) Bromide, (b) Chloride, (c) TCE, and (d) Permanganate for the column flushed with a 10 g/L solution of permanganate. Also indicated is the start and end time of the permanganate flush.**
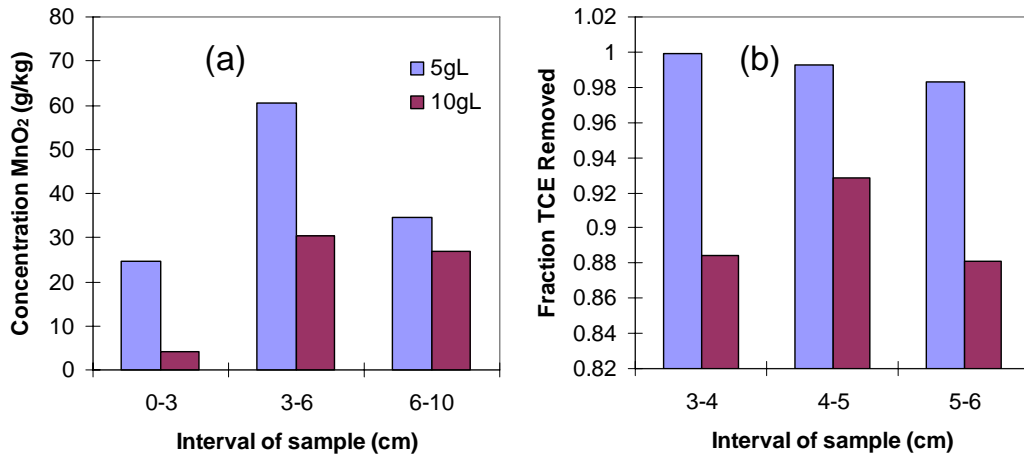
Figure 3.5: Bulk soil concentration for (a) Mn expressed as g MnO_2/kg soil and (b) TCE expressed at the fraction of TCE removed.
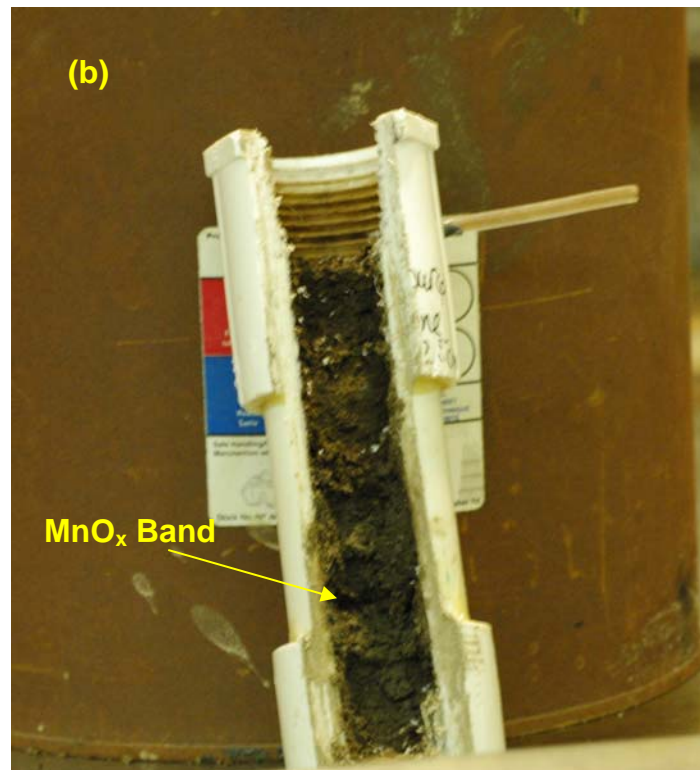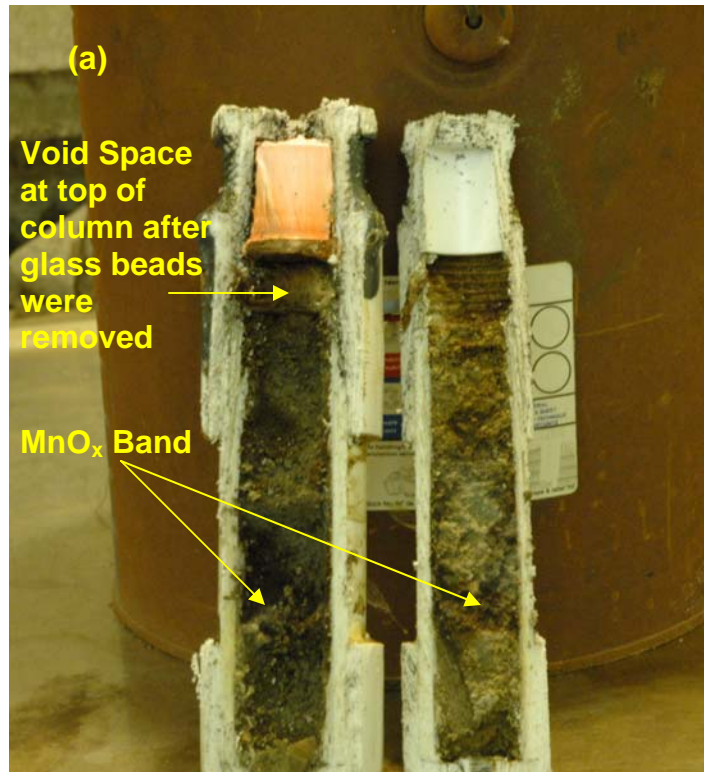
Figure 3.6: Images of Mn deposition within the (a) 5 g/L column and (b) 10 g/L column.

CHAPTER 4: TREATMENT EFFICIENCY

The NOD kinetic model developed in Chapter 2 was adapted into the 1-D reactive transport model presented in Appendix A to investigate the efficiency of permanganate treatment systems subject to NOD kinetic considerations. The model included the important physical and chemical processes of permanganate ISCO: advection, dispersion, mass transfer between the free and aqueous phase, reaction (productive reaction between the organic compound and permanganate, and non-productive reaction between the aquifer material and permanganate), and sorption. For the purpose of this study, treatment efficiency is defined as the percent of permanganate supplied to the system that was consumed by the oxidation of reduced organic compounds; therefore, a treatment efficiency of less than 100% indicates that permanganate was consumed to satisfy the NOD and/or exited the system.

4.1   Model Validation

The results from the 10 g/L column study discussed in Chapter 3 were used to validate the transport model developed in Appendix A including the NOD kinetic expressions derived in Chapter 2.   For a complete discussion on the model validation refer to Section A.5 in Appendix A.

4.2   Model Simulations

The model was used to simulate the treatment of several common non-aqueous organic compounds. The compounds modeled were chosen from an assembled list (Table 4.1) of chemicals with a wide variety in $k_i^{''}$. From this list, four were chosen for further investigation based on preliminary results: TCE, perchloroethylene (PCE), Trans dichloroethylene (DCE), and naphthalene (a prevalent component of creosote). These chemicals were chosen due to the varying chemical properties (most importantly C_s and $k_i^{''}$), the historical prevalence of these organic compounds in industry, and the persistence of these chemicals at contaminated sites (i.e., lack of complete natural attenuation). Naphthalene has a low C_s and a small $k_i^{''}$. PCE has a higher C_s and $k_i^{''}$ than naphthalene,

but is amongst the lowest when compared to the other 9 chemicals listed in Table 4.1. TCE has a C_s approximately 10 times higher than PCE and a $k_i^{''}$ 20 times higher. Trans DCE has the highest C_s and $k_i^{''}$ of the chemicals investigated in these simulations, both of which are amongst the highest of all chemicals summarized in Table 4.1 (in fact, out of the 10 chemicals listed, Trans DCE has the largest $k_i^{''}$).

The developed model was used to simulate each compound as a residual source zone contained in the EGDY or Borden aquifer material. These materials were chosen since they have vastly different NOD properties – Borden was observed to consume the least amount of permanganate (only 2.12 ± 0.57 g KMnO$_4$/kg – 14.6% fast) during the bench scale studies completed by Xu (2006) and had the smallest f_{OC} of all soils investigated, whereas, EGDY had both the highest consumption of permanganate (32.29 ± 3.55 g – 38.6% fast) and the greatest f_{OC}.

Two sets of simulations were completed for each aquifer material. The first set of simulations represents the vertical well flushing scenario in which injection and extraction wells are used to force permanganate through the source zone. The second set of simulations represents an inject-and-leave treatment system in which several injection points are used to quickly deliver permanganate uniformly and radially from the point of injection. See Section A.1 for additional details of these injection schemes.

4.2.1 Simulation Details

Table 4.2 summarizes the details of the inject-and-leave and vertical well flushing schemes. The contaminated material comprising the simulated source zones had a NAPL saturation (S_n) between 1.5 and 5% (i.e., a residual source zone) to prevent NAPL migration and limit mass transfer effects from oxidation by-products. The mass of each compound simulated was consistent across each injection scheme, however, the S_n varied due to differing densities of the organic compounds (Table 4.1).

The simulated domain for the vertical well flushing scheme had a length of 10 cm and a diameter of 2.54 cm with a mass of 0.5 g for each compound. The length of the simulated domain does not impact the results since the number of pore volumes (PVs) is used for comparison purposes. A longer domain would more realistically represent an actual injection scheme; however, it would require a longer simulation time to achieve the same results. The simulated domain for the inject-and-leave scheme was a slice of the aquifer 1 cm thick and 1 m in diameter surrounding the injection point. The simulated domain contained an organic compound mass of 400 g. For both injection schemes, the entire spatial domain contained contamination, rather than an isolated source zone, to allow for a fair comparison of the mass of permanganate used to treat the organic compound versus that used to satisfy the NOD. The vertical well flushing simulations were flushed with a 5 g/L permanganate solution at 0.25 L/day for approximately 1.15 days (corresponds to 20 PVs for the EGDY material). A much higher injection rate of 15 L/min was used in the inject-and-leave simulations to deliver permanganate (5 g/L) to the entire solution domain within 5 minutes. The permanganate injection was then terminated and the permanganate was allowed to react for 6 hours. A spatial discretization of 0.001m and a time step of 0.005 s were used for all simulations. Table 4.3 summarizes various transport and mass transfer parameters used.

4.3   *Vertical Well Flushing*

The results of the vertical flushing model simulations indicate that the reaction kinetics do change the treatment efficiency, but not to a large extent. Figure 4.1 shows the breakthrough curves (BTCs) at the extraction well for permanganate and aqueous organic compound, and the fraction of OAM and organic compound mass remaining. The BTCs are normalized to the injected permanganate concentration (5 g/L) and the maximum solubility of the chemical (see Table 4.1). The point where the fast fraction of OAM has been satisfied is indicated by a solid square symbol on the OAM mass remaining profile. Figure 4.2 shows the treatment efficiency for both the EGDY and Borden material. For all figures, the PVs flushed are not equal in the two materials because the porosity of the Borden material is ~ 1.33 times higher than the EGDY material (Table 4.3). Hence, 20

PVs of permanganate supplied to the EGDY material corresponds to the same mass of permanganate supplied in 15 PVs to the Borden material.

4.3.1 Breakthrough Curves and Consumption of OAM and the Organic Compound

The results presented in Figure 4.1 are largely controlled by the mass action law that represents the reaction between the organic compound and permanganate as given by

$$\frac{dC_i}{dt} = r = -k_i'' C_i C_{MnO_4^-} \tag{4-1}$$

where r is the reaction rate (M/L^{3}T), k_i'' is the reaction rate coefficient (L^3/MT), C_i is the concentration of the dissolved organic (M/L^3), and $C_{MnO_4^-}$ is the concentration of permanganate (M/L^3). The reaction rate is dependant on three parameters: the reaction rate coefficient, the organic compound concentration, and the permanganate concentration. Since the solubility represents the maximum aqueous concentration of an organic compound, C_s is an important factor that controls the overall reaction rate. Similar to the reaction rate law (Equation 4-1) the kinetics of the OAM reactions are dependant on the concentration of OAM and permanganate, and the reaction rate coefficient (see Chapter 2). The kinetics of the NOD reactions of the Borden and EGDY material, determined in Chapter 2, indicate that the k_{OAM}^{fast} and k_{OAM}^{slow} for EGDY and Borden are similar, however, the C_{OAM} for the two materials differs greatly. For EGDY the k_{OAM}^{fast} observed was 0.105 L/min and the initial k_{OAM}^{slow} was 0.113 L/min but it decreased rapidly. For Borden the k_{OAM}^{fast} was 0.160 L/min and the initial k_{OAM}^{slow} was 0.402 L/min (which also decreased rapidly). The differences between the profiles of the two materials in Figure 4.1 are therefore largely attributed to the different C_{OAM}^{fast} and C_{OAM}^{slow} values.

The rising limb of the organic compound BTC is the same for all chemicals investigated; all rise quickly during the first PV to a maximum concentration as the permanganate is

flushed into the system. The breakthrough of MnO_4^- in the EGDY material is slightly delayed when compared to the Borden material which is partially due to the difference in porosity which affects the PVs, but is also due to the higher NOD of the EGDY material where more permanganate is consumed by the aquifer solids, and less is available for the organic compound reaction. In the organic compound BTCs for naphthalene and PCE in both aquifer materials, there is a slight oscillation in the concentration profile that coincides with the satisfaction of the C_{OAM}^{fast} and is suspected to be due to numerical issues. In general, the BTCs for compounds with similar C_s and $k_i^{''}$ values (e.g., PCE and naphthalene, or TCE and Trans DCE) behave much the same.

For the compounds with a lower C_s and $k_i^{''}$ (e.g., PCE and naphthalene), the breakthrough concentration decreases quickly after the maximum concentration was reached coincident with permanganate breakthrough; the organic compound concentration is decreased and does not have enough time to transfer from the free phase into solution. The naphthalene concentration decreases until both it and the permanganate concentration reach near steady state values when the competition for permanganate between C_{OAM}^{slow} and naphthalene are similar. The PCE concentration however, continues to decrease and the permanganate concentration increases. In this case, instead of reaching a steady concentration, the PCE concentration profile decreases at a constant rate since the rate of PCE removal is greater than the rate of C_{OAM}^{slow} removal. The breakthrough concentration of both PCE and naphthalene reach a lower maximum value in the Borden material than the EGDY material and stays lower throughout the simulation due to the lower C_{OAM}^{fast} and C_{OAM}^{slow} of the Borden material which allows permanganate to breakthrough more quickly.

The high C_s and $k_i^{''}$ values of Trans DCE and TCE combine to create a fast rate of reaction which significantly delays the arrival of permanganate and allows the organic concentration to remain at close to 100% while a significant mass of organic compound remained in the system. There are two main differences between the TCE and Trans DCE BTCs: the concentration of TCE remains high longer due to the lower C_s and $k_i^{''}$ (organic

mass remains longer relative to Trans DCE), and the presence of TCE and permanganate appear concurrently in the extracted fluid (permanganate does not breakthrough in the Trans DCE simulations until there is no aqueous organic). For both compounds, the extraction well organic concentration decreased as the mass close to the injection well was destroyed and the available travel time for the organic compound to reach C_s through mass transfer decreased. Eventually the organic concentration was low enough that permanganate could breakthrough at the extraction well since the rate of reaction with the organic compound was low (small aqueous concentration of organic compound and permanganate). Due to the extremely high $k_i^{"}$ for Trans DCE, the organic concentration at the extraction well had to essentially be zero before any permanganate could breakthrough.

As previously discussed, the mass removed was greater for the Borden material due to a lower NOD. The mass of the organic compound remaining decreases at an approximately steady rate for all simulations except for TCE and Trans DCE where there was a marked rate change when most of the mass had been removed. In general, the timing of the C_{OAM}^{fast} satisfaction occurs later as both C_s and $k_i^{"}$ increase which produces a faster rate of organic reaction and hence more permanganate consumption by the oxidation reaction rather than the NOD reaction. However, in the Trans DCE simulation the satisfaction of C_{OAM}^{fast} coincides with the complete removal of Trans DCE mass. The profiles for OAM remaining in the two materials cross due to the slightly higher k_{OAM}^{fast} of the Borden material which results in a faster decrease in OAM mass at the start of the simulation, however, the OAM reduction in the EGDY material crosses the Borden profile before the C_{OAM}^{fast} is depleted as it accounts for a greater percent of the C_{OAM}^{total} in the EGDY material (15.5% rather than 9.7% for Borden). The profiles of OAM mass removal represent the C_{OAM}^{total} not just the reactive fractions of the OAM, however, over half of the C_{OAM}^{slow} remains at the end of every simulation.

Since most field ISCO applications would not deliver 20 PVs of permanganate (Siegrist et al., 2001), these results indicate that for organics with a low C_s and k_i'', the competition for permanganate between the organic compound and the OAM occurs when the C_{OAM}^{fast} is satisfied and only the C_{OAM}^{slow} reaction remains. However, for organics with a higher C_s and k_i'', the organic compound competes for permanganate with the C_{OAM}^{fast} which greatly reduces the rate of satisfaction and results in the C_{OAM}^{fast} remaining the dominant NOD reaction for a longer period. For example, when the C_{OAM}^{fast} is depleted, only 20-30% of the TCE mass remained, indicating that for organics with a high C_s and k_i'' the C_{OAM}^{fast} reaction dominates the NOD and should be characterized with accuracy. Likewise organic compounds with lower C_s and k_i'', the fast reactions occur quickly and competition arises between the C_{OAM}^{slow} and organic and hence the slow NOD reactions need to be characterized.

4.3.2   Treatment Efficiency

Treatment efficiency is defined here as the percent of permanganate injected used to oxidize the organic compound. The efficiency is a cumulative term so at any given time the efficiency is a factor of all that has occurred previously. The treatment efficiency indicates how well the designed injection system is at destroying the aqueous phase organic compound which drives mass transfer and results in increased mass removal (the primary goal of ISCO). An efficiency of less than 100% indicates that either permanganate was extracted or was used to satisfy the NOD.

Generally, as the C_s and k_i'' of the organic compound increase so does the efficiency, and therefore the treatment efficiency profiles were similar for both materials (Figure 4.2). However, the efficiency was greater for all organic compounds investigated for the Borden material (2-7%) due to the lower NOD which meant that more permanganate was available for reaction with the organic compound; the ultimate NOD of the EGDY material was 15 times greater than the Borden material. The relatively small difference

in the treatment efficiency (given the large difference in ultimate NOD) is due to the interactions of all the controlling factors that determine the treatment efficiency: C_s and k_i'', injection rate, rate of mass transfer, etc. NOD is only one component of the overall model. Additionally, the ultimate NOD assumes that the permanganate has unlimited time available for reaction and can only react with C_{OAM} which is not true when flushing permanganate through contaminated material.

The most important time period to investigate the treatment efficiency is during the first 5 to 10 PVs since typically, injections do not last for a long duration (Siegrist et al., 2001). During the first 5 to 10 PVs, the treatment efficiency of TCE, PCE, and naphthalene increased more rapidly in the Borden material than in the EGDY material due to the lower demand for permanganate from the C_{OAM}^{fast} fraction. During this time, the efficiency of Trans DCE started at nearly 100% but decreased more rapidly in the EGDY material also due to the high consumption of permanganate from the C_{OAM}^{fast}. The impact on treatment efficiency due to the reaction rate coefficients of C_{OAM}^{slow} and C_{OAM}^{fast} is not apparent in these figures, but as discussed in Section 4.3.1, the fast reaction kinetics seem to compete for permanganate in systems containing organic compounds with high C_s and k_i'' values (e.g., TCE and Trans DCE), whereas the slow reaction competes for permanganate with organic compounds that have low C_s and k_i'' values since the treatment efficiency continues to increase after the C_{OAM}^{fast} was removed from the system (e.g., naphthalene and PCE).

The efficiency of naphthalene removal was limited by a low C_s and k_i'' which lead to slow rates of reaction. The permanganate treatment efficiency slowly increased over the first 5 PVs volumes and reached a maximum efficiency when the competition for permanganate between naphthalene and the aquifer solids reached steady state. The maximum efficiency of naphthalene in the EGDY material was ~ 12.5% whereas the efficiency in the Borden material reached a maximum of ~ 17%.

The removal efficiency of PCE was also limited by the C_s and k_i'', however since the reaction rate was higher (Equation 4-1), the treatment efficiency was greater. As with naphthalene, the treatment efficiency increased during the first 5 PVs before reaching an approximately steady efficiency; however, unlike naphthalene, in the Borden material, the treatment efficiency decreased slightly from the maximum value corresponding to the time at which approximately 25% of the PCE mass was removed. The decrease in efficiency is due to complete removal of PCE close to the injection well, which decreases the time available for mass transfer. As with naphthalene, the treatment efficiency of PCE in the Borden material is greater (maximum ~ 23%) than in the EGDY material (~ 20%) due to less competition for permanganate from the NOD. Preliminary results indicated that if the flow through the domain was decreased, more time would be available for reaction and mass transfer to occur and would result in a higher PCE treatment efficiency. For example, if the flow rate were to decrease by one half then the maximum treatment efficiency of PCE removal from the EGDY material would increase by 140% and the mass removed would increase by 130%. The efficiency of the PCE and naphthalene systems are both limited by the rate of permanganate injection: a slower injection rate results in higher treatment efficiency since it is limited by time available for reaction and mass transfer.

The competition for permanganate is strong between TCE and the fast reacting OAM within the first PV with the mass of both reduced (Figure 4.1). Initially, the treatment efficiency of TCE rapidly increased to over 80% before it reached a maximum determined by the competition for permanganate between the C_{OAM}^{fast} and the organic compound. It took longer to reach the maximum efficiency for the EGDY material since it has a greater permanganate demand from the C_{OAM}^{fast}. After 5 PVs in the EGDY material and 2 PVs in the Borden material the efficiency reached a quasi steady state value of ~ 89% for the Borden and ~ 83% for the EGDY material. As with PCE, the treatment efficiency slowly started to decrease when mass close to the injection well was removed; however, unlike PCE, the treatment efficiency also started to decrease more rapidly corresponding to the near complete destruction of TCE and significant breakthrough of permanganate (at 15 PVs in the EGDY material and 10 PVs in the Borden material). The

69

treatment efficiency of TCE is somewhat limited by the C_{OAM}^{fast} and the injection rate; however, the treatment efficiency of the system is very high.

The efficiency curves for Trans DCE removal from for both the Borden and EGDY material are initially close to 100% indicating that the C_{OAM}^{fast} reacts more slowly than the Trans DCE. Despite the extremely fast rate of reaction for Trans DCE, the efficiency of the EGDY material quickly drops to 98% due to the high demand for permanganate from the C_{OAM}^{fast}. As the organic compound mass is destroyed near the injection well, the treatment efficiency decreases and permanganate is used to satisfy the NOD of the treated material. As expected, the treatment efficiency of the EGDY material decreases at a more rapid rate due to the higher C_{OAM}^{fast} associated with the EGDY material. The treatment efficiency steadily decreases until it reaches ~ 80% efficiency for the Borden material and ~ 75% for the EGDY material at which point only 1% of the initial Trans DCE mass remains. Even with the extremely fast reaction rate for the Trans DCE and permanganate reaction, there are still noticeable differences in the treatment efficiencies of the two materials; however, due to the high efficiency of both systems, the oxidation reaction with Trans DCE is dominant in both materials.

4.3.3   Implications

The simulation results of the vertical well flushing scheme indicate that the NOD kinetic parameters values do not have a large impact on the treatment efficiency. Despite, the ultimate NOD of the EGDY material being approximately 15 times greater than the Borden material, the treatment efficiency during the simulations was only 2-7% lower supporting the hypothesis that using the ultimate NOD as a predictive tool for determining the treatment efficiency in a given material will lead to underestimating the treatment efficiency, particularly for materials with a high ultimate NOD.

The results also indicate that the C_{OAM}^{fast} competes for permanganate with organic compounds that have high C_s and $k_i^{''}$ values, whereas the C_{OAM}^{slow} competes for

permanganate with organic compounds that have low C_s and $k_i^{''}$ values (the C_{OAM}^{fast} is satisfied prior to permanganate treating the organic). This would imply that for organics with high C_s and $k_i^{''}$, such as TCE, the kinetic parameters associated with C_{OAM}^{fast} should be characterized, whereas if the aquifer is contaminated with organic compounds having low C_s and $k_i^{''}$ values both the C_{OAM}^{fast} and C_{OAM}^{slow} need to be characterized.

Organic compounds with a high C_s and $k_i^{''}$ result in a fast rate of reaction and have a higher treatment efficiency since permanganate can be used effectively to destroy the organic compound of concern rather than transporting through the treatment zone or reacting with the OAM species. Organic compounds with a low C_s and $k_i^{''}$ have a lower treatment efficiency since permanganate must first satisfy the C_{OAM}^{fast} before it can be used to significantly deplete the organic mass.

4.4   Inject-and-Leave

The results of the inject-and-leave simulations were influenced by the same factors (mainly the C_s and $k_i^{''}$ of the organic compounds) as the vertical well flushing simulations, indicating that the NOD reaction kinetics do impact the treatment efficiency, but not to a large extent. Figure 4.3 shows the concentration profiles of permanganate and aqueous organic compound at a representative point in space 1 m from the injection point along with the fraction of organic compound and OAM mass remaining throughout the domain. Figure 4.4 illustrates the PCE concentration profiles in the EGDY material at 0.5 m from the injection point to determine the impact of distance from the injection well on the concentration profiles. Figure 4.5 shows the treatment efficiency for both the EGDY and Borden material. Unlike Figures 4.1 and 4.2, the figures representing the inject-and-leave results have time on the x-axis rather than pore volumes since after 5 minutes, the injection was discontinued.

4.4.1 Concentration Profiles and Oxidation of Organic compound and OAM

As with the vertical well flushing scheme, the model results indicate that organics with low C_s and $k_i^{''}$ (naphthalene and PCE) behave in a similar fashion. However, in this case, the profiles for TCE are also similar in shape and are controlled by the same factors with only Trans DCE deviating from the basic trends. The concentration profiles and mass remaining for Trans DCE are not included; due to the high C_s and $k_i^{''}$, Trans DCE is completely removed from the domain during the initial 5 minutes when the permanganate was supplied to the system. The findings show that the inject-and-leave scheme is more dependent on mass transfer, characterized by high concentration of the organic compounds while flushing occurs, and a fast decrease in concentration after flushing is terminated. Since the rate of flushing is faster than the vertical well flushing scheme, the Reynold's number and subsequently the mass transfer coefficient increase and the aqueous mass is replaced at close to the same rate as it is destroyed. However, after injection ceased, the removal of TCE, PCE and naphthalene behave much like they would in a batch reactor system since there was no advective transport and hence a small mass transfer rate.

For TCE, PCE, and naphthalene, the concentration of the organic compound and permanganate increased during the first 5 minutes while flushing occurred, and then dropped after flushing was terminated. The rate at which both the organic compound and permanganate concentration decreased was determined by the C_s, $k_i^{''}$, concentration of permanganate, and the NOD reaction kinetics. While a large concentration of permanganate remained, the organic concentration decreased since the rate of the reaction was greater than the rate of mass transfer (i.e., more organic was removed from the aqueous phase by reaction than could be replaced by mass transfer). Organics with higher C_s and $k_i^{''}$ depleted more quickly due to the faster rate of reaction. For all three organic compounds, after the permanganate mass reached a critical point, the concentration of the organic compound rebounded as the reaction rate became slower than the rate of mass transfer. Organics with a higher C_s and $k_i^{''}$ had a faster rate of

reaction; therefore, lower concentrations of permanganate were required before the organic concentration rebounded. The concentration of naphthalene, which had the lowest C_s and k_i'' of all four organic compounds, rebounded when approximately 40% of the permanganate remained; the concentration of TCE (higher C_s and k_i'') rebounded when less than 15% of permanganate remained.   For all three organic compounds, the magnitude of the rebound was greater in the EGDY material since less permanganate remained due the higher C_{OAM}^{slow} (the full concentration of C_{OAM}^{fast} for both materials was satisfied during the initial permanganate flushing period). The TCE concentration did not rebound in the Borden material since the concentration of permanganate at the end of the simulation remained high enough that all TCE transferred into the aqueous phase was oxidized.

To confirm that the concentration profiles at 1 m were representative of other locations within the domain, the concentration profiles for the PCE simulation were investigated at a mid-point of the domain (0.5 m). The concentration profiles were similar at 0.5 m from the injection point when compared to 1 m (Figure 4.4), with a slightly higher concentration of permanganate and lower concentration of PCE closer to the injection point. The differences in the profiles are due to a greater fraction of the OAM satisfied closer to the injection well during the initial permanganate flush which resulted in less permanganate consumed to satisfy the NOD after the injection was terminated. With less permanganate required to satisfy NOD, higher concentrations of permanganate and greater mass removal of PCE were observed. From these results, it can be assumed that regions closer to the injection point experience a greater removal of organic compound and satisfaction of the NOD; this finding corresponds to the vertical well flushing scheme.

The profiles of the removal of OAM and organic compound for naphthalene, TCE, and PCE support the finding that the destruction of organic compound is limited by the mass transfer. All three organic compounds experienced an initial fast removal rate during the initial flushing phase of the simulation, ranging from 4% mass removal of naphthalene,

which has a low C_s and k_i'', to over 85% mass removal of TCE, which has a high C_s and

k_i''. As previously stated, the C_{OAM}^{fast} was satisfied at some point during the initial flushing phase. After the initial flushing was complete, the rate of organic and OAM mass removal slowed due to a limited mass of permanganate available and the decreased rate of mass transfer in a stagnant system. There was still, however, an increased mass removal in the Borden material over the EGDY material since less permanganate is required to satisfy the C_{OAM}^{slow}. The difference in mass removal is small ($< 0.5\%$) for naphthalene, since the rate of organic mass removal was limited by the low C_s and k_i'', which were quickly overcome by the mass transfer, making the organic reaction the rate limiting step. However, the difference in TCE mass remaining at the end of the simulation was $\sim 4\%$ greater in the EGDY material than in the Borden material. The OAM mass remaining profiles, indicate that the OAM mass removal is approximately the same for each organic in a given aquifer material with less than 0.3% difference between the different organics. This finding implies that while the organic mass removal is dictated by the aquifer material simulated, the C_{OAM} satisfaction is not dependant on the on the organic compound, which is contrary to the findings for the vertical well flushing scheme due to the heavy reliance on mass transfer and fast satisfaction of the C_{OAM}^{fast}. This finding also implies that the ability of an organic compound to compete for permanganate with the C_{OAM}^{slow} is limited by the slow rate of mass transfer.

4.4.2 Treatment Efficiency

Due to the high injection rate used at the beginning on the inject-and-leave simulations, a large mass of permanganate exited the system through advection within the first 5 minutes. The unreacted permanganate leaving the system during this time was taken into consideration when determining the treatment efficiency of the inject-and-leave scheme to more accurately reflect the efficiency of the treatment system.

As with the vertical flushing scheme, the treatment efficiency for the EGDY material (4.5(a)) is less than the Borden material (4.5(b)). These results were expected due to the

greater permanganate demand of the oxidizable materials in the EGDY material. Another significant trend is that the treatment efficiency for all materials is lower than those observed in Figure 4.2 for the vertical well flushing scenario, due to the greater effects of velocity on the results. Based on the thin film model (Pankow and Cherry, 1996; Powers et al., 1994), the mass transfer coefficient is proportional to velocity and a higher velocity results in a thinner film thickness which decreases the time for diffusion across the film. Despite the lower overall efficiencies of all materials, the efficiency profiles indicate that treatment efficiency again increases with increasing C_s and $k_i^{''}$.

The treatment efficiency of naphthalene, PCE, and TCE increases slightly over time as more of the C_{OAM}^{slow} is satisfied allowing a greater mass of permanganate to react with the organic compound. For the organics with lower C_s and $k_i^{''}$ (i.e., naphthalene and PCE), the treatment efficiency increases slowly over the entire duration of the simulation since the overall reaction rate is slower and permanganate cannot be used efficiently during the initial flushing phase. However, for TCE, which has a higher C_s and $k_i^{''}$, the efficiency increases rapidly during the flushing stage as permanganate is supplied and the C_{OAM}^{fast} is satisfied. After the flushing ceases, the efficiency increases slowly since there is only a finite mass of permanganate available and a slower rate of mass transfer.

Final treatment efficiency of naphthalene was 3.7% in the Borden material and only 1.8% in the EGDY material. For PCE the efficiencies were 1.5% and 3.7% for the EGDY and Borden materials respectively. The lower treatment efficiency of PCE compared to naphthalene was not expected from the C_s and $k_i^{''}$, however, the stochiometric ratio for the PCE reaction is significantly lower (4 MnO_4^- : 3 PCE) than it is for naphthalene (16 MnO_4^- : 1 naphthalene) which explains the difference. The TCE efficiencies were 11.7% and 15.4% for the EGDY and Borden materials, which parallels the results of the vertical flushing scheme where increased C_s and $k_i^{''}$ resulted in a greater difference in treatment efficiency between the two aquifer materials.

The treatment efficiencies for permanganate ISCO of Trans DCE were 92.8% for the EGDY material and 92.1% for the Borden material. Unlike all other organic compounds, the treatment efficiency is lower in the Borden material than in the EGDY material which is due to the slightly higher k_{OAM}^{fast} for the fast reaction of the Borden material which interferes with the treatment efficiency of Trans DCE. However, the difference in treatment efficiency is very small compared to the differences with the other organic compounds. The final treatment efficiencies for both the EGDY material and the Borden material were similar (0.5-4% difference for all organics) indicating that the NOD kinetic parameters did not play a large role in the treatment efficiency.

4.4.3 Implications

The simulation results of the inject-and-leave scheme indicate that the NOD kinetic parameters values do not have a large impact on the treatment efficiency. Despite the ultimate NOD of the EGDY material being approximately 15 times greater than the Borden material, the treatment efficiency during the simulations was only 0.5-4% lower supporting the hypothesis that using the ultimate NOD as a predictive tool for determining the treatment efficiency will lead to underestimating the treatment efficiency, particularly for materials with a high ultimate NOD.

The results also indicate that the C_{OAM}^{fast} was depleted rapidly during the initial flushing phase and only compounds with a very high C_s and $k_i^{''}$ (e.g., Trans DCE) can compete effectively with C_{OAM}^{fast}. The C_{OAM}^{slow} competes for permanganate with organic compounds after the injection is ceased, however, the results indicate that the C_s and $k_i^{''}$ have little bearing on the rate of C_{OAM}^{slow} destruction implying that the oxidation reaction is limited by the transfer of the organic into the aqueous phase. Organics with very high C_s and $k_i^{''}$, such as Trans DCE, fully deplete during the initial flushing period regardless of the kinetic parameters associated with the C_{OAM}^{fast} and C_{OAM}^{slow} reactions. However, for all other organics both the C_{OAM}^{fast} and C_{OAM}^{slow} reactions should be characterized to adequately determine the mass of permanganate required since a significant mass of organic remains

after the C_{OAM}^{fast} has been satisfied due to the limits of mass transfer and limited permanganate.

4.5   *Traditional modelling approaches*

As stated in Section 1.1.2, assuming the ultimate NOD of the aquifer material as an instantaneous sink for permanganate that must be satisfied before permanganate can propagate through the system is suspected to lead to significant underestimation of the treatment efficiency, whereas not including NOD kinetics would lead to over estimation of the efficiency. To support this hypothesis, two sets of simulations were completed for the vertical flushing of the EGDY material. In the first set of simulations, the NOD was ignored so that the permanganate concentration is only reduced through oxidation of the reduced organic compounds. In the second set of simulations, the ultimate NOD of the EGDY material had to be satisfied before permanganate could propagate through the subsurface.

4.5.1   No NOD Considerations

Figure 4.6 shows the comparison of treatment efficiency between the simulations where NOD kinetics (as developed in Chapter 2) were used to simulate the consumption of OAM compared to the simulations where NOD was not included as a sink for permanganate. As expected, the treatment efficiency for all simulations was overestimated when NOD was not included in the model.

Naphthalene and PCE (low C_s and $k_i^{''}$), which had low treatment efficiencies, had a final treatment efficiency marginally higher when no C_{OAM} was included reflecting the lack of reaction between permanganate and C_{OAM}^{slow}. However, for both PCE and naphthalene there is considerable difference in the treatment efficiency of the two systems over the first 5 to 10 PVs since the treatment efficiency increases at a more rapid rate when no C_{OAM}^{fast} is present to consume large amounts of the permanganate during the initial PVs.

77

The treatment efficiency of TCE is much greater in the system in which no C_{OAM} was included. The maximum treatment efficiency was close to 100% after permanganate was supplied for 1 PV, reflecting the absence of the C_{OAM}^{fast} term. The treatment efficiency of TCE decreases at ~ 10 PVs when a significant fraction of the TCE had been removed close to the injection well, leaving less time available for reaction to occur between the front of the source and the extraction well. However, the treatment efficiency is still greater with no NOD term included for the entire simulation.

The general shape of the Trans DCE treatment efficiency profile is similar when NOD is not included compared to the NOD kinetic model. However, the treatment efficiency is greater at all times for the simulation not including NOD kinetics. When the treatment efficiency starts to decrease (indicating a significant mass of Trans DCE had been depleted from the source zone), it decreases at a slower rate than the NOD kinetic model since permanganate is not consumed by C_{OAM}^{fast}. However, as with the NOD kinetic model simulation, the entire mass of Trans DCE is eventually depleted. During the simulation not including NOD kinetics, the full mass of Trans DCE is removed from the system after 8 PV of permanganate had been supplied, however, with the NOD kinetics included, 9 PVs of permanganate were supplied before the mass was removed.

4.5.2   Ultimate NOD

The ultimate NOD is the traditional modelling approach used to handle NOD in ISCO simulations. Long-term batch tests are performed on aquifer materials to determine the mass of permanganate required to satisfy the natural demand. The value reached at the end of the tests (typically on the order of several days to weeks) is taken as the ultimate NOD of the material. To model the ultimate NOD in the vertical well flushing scheme, one reactive OAM component was used and the k_{OAM} was adjusted to a large number ensuring that the ultimate NOD for the mass of the material in the domain was satisfied prior to 50% breakthrough of permanganate in the extraction well. Figure 4.7 compares the efficiency results of the NOD kinetic model for the EGDY material with the results using the ultimate NOD model of EGDY material.

The treatment efficiency of all organic compounds is significantly underestimated when the ultimate NOD model is used. Very little permanganate is used by organic compounds with low C_s and $k_i^{''}$ (i.e., naphthalene and PCE) during the entire simulation duration since most of the permanganate mass is used instantly by the C_{OAM}. When the NOD is satisfied near the injection well, some permanganate is used to treat the organic compound, however due to the lower C_s and $k_i^{''}$ of these materials, the reaction is not instantaneous and very little organic compound mass is removed before permanganate is transported down-gradient to where the NOD has not yet been satisfied.

The treatment efficiency of TCE increases more quickly than PCE and naphthalene due to the higher C_s and $k_i^{''}$ which results in more TCE removal before permanganate transports down-gradient to material with unsatisfied C_{OAM}. However, the treatment efficiency of permanganate is much less than when the NOD kinetic model is used and no permanganate can be effectively used to decrease organic compound mass until the NOD is satisfied.

The treatment efficiency of Trans DCE (very high C_s and $k_i^{''}$) is initially high with over 80% efficiency, but quickly drops to around 50%; the initial high efficiency is due to the reaction between permanganate and the initial aqueous concentration of the organic compound. After the aqueous concentration is oxidized, the efficiency decreases significantly indicating that a greater mass of permanganate is consumed by the aquifer material than by the Trans DCE. Since the C_s and $k_i^{''}$ are high enough to compete for permanganate (due to the initial high efficiency), the treatment efficiency is limited by the mass transfer from free phase to the aqueous phase which results in the mass being depleted before permanganate can be supplied to the source. Most of the mass removal of Trans DCE is due to mass transfer since only 35% of the C_{OAM} is satisfied at the end of the simulation despite near complete removal of Trans DCE after only 10 PVs.

4.5.3 Implications

The results of the no NOD model and the ultimate NOD model stress the importance of characterizing the NOD reaction kinetics with a reasonable degree of accuracy when determining if permanganate ISCO is a viable treatment option. The C_{OAM}^{fast} is important for all organics whether they have a high or low C_s and $k_i^{"}$; whereas the C_{OAM}^{slow} is only important when the organic has low C_s and $k_i^{"}$.

Not including OAM species as a permanganate sink while investigating the aquifer material leads to over-estimation of the treatment efficiency and could result in incomplete oxidation or a more expensive clean-up strategy than predicted. The treatment efficiency was overestimated by up to 15% when the NOD reactions were ignored. For example TCE is effectively removed (less than 1% of the mass remaining) after 8.8 PVs of permanganate were flushed when NOD kinetics were not included, however, when NOD kinetics are included ~ 40% of the TCE mass remains. By not including the NOD kinetics when designing the remediation system, the mass of permanganate required and duration of flushing would be underestimated.

Using traditional modeling approaches which ensure the ultimate NOD of the material is satisfied before the permanganate front can propagate through the subsurface significantly underestimates the treatment efficiency. The treatment efficiency of three of the organic compounds investigated (with lower C_s and $k_i^{"}$ – TCE, PCE, and naphthalene) was roughly 10% of the value determined using the NOD kinetics, which would lead to cost estimates of permanganate ISCO being greatly overestimated and the treatment technique being prematurely discarded as a possible remedial strategy during the technology screening process.

Table 4.1: Chemical properties of selected organic compounds.

Contaminant	Solubility (g/m^3) [1]	Density (g/m^3) [1]	k" $(M^{-1}s^{-1})$ [2]	MolWt	K_{OC} mL H_2O/g C [3]	Stochiometry		Formula
						MnO_4^-	Contaminant	
2-Chlorophenol	2.85E+04	1.24E+06	7.43E+01	128.56	15	26	3	C_6H_5ClO
Chloroform	7.95E+03	1.49E+06	5.63E-04	119.38	31	2	3	$CHCl_3$
Dichlorvos	1.00E+04	1.42E+06	1.57E+01	220.98	N/A	6	1	$C_4H_7Cl_2O_4P$
Ethylbenzene	2.06E+02	8.67E+05	3.90E-03	106.17	1100	14	1	C_8H_{10}
MTBE	5.10E+04	7.41E+05	9.80E-05	88.15	12.3[4]	10	1	$C_5H_{12}O$
Naphthalene	3.10E+01	9.97E+05	1.10E-02	128.17	1300	16	1	$C_{10}H_8$
PCE	2.00E+02	1.62E+06	3.50E-02	165.83	277	4	3	C_2Cl_4
TCE	1.10E+03	1.46E+06	8.00E-01	131.39	126	2	1	C_2HCl_3
Trans-DCE	5.00E+03	1.27E+06	3.90E+01	96.94	59	8	3	$C_2H_2Cl_2$
Vinyl Chloride	2.25E+03	1.21E+06	2.10E+00	96.94	57	8	3	$C_2H_2Cl_2$

1) Merk, 2003
2) Waldemer and Tratnyek, 2006
3) USEPA, 1986
4) USEPA, 1993

Table 4.2: Injection scheme properties.

Injection Scheme	Mass of Contaminant (g)	NAPL Saturation (-)		Dimensions (cm)	Injection Rate (L/day)
		Chemical	EGDY/Borden		
Vertical Flushing	0.5 g	Naphthalene	3.5% / 2.5%	diameter 2.54 length 10 cm	0.250
		PCE	2.2% / 1.6%		
		TCE	2.4% / 1.7%		
		Trans DCE	2.8% / 2.0%		
Inject and Leave	400 g	Naphthalene	4.5% / 3.3%	Well diameter 1.6 cm Domain diameter 101.6 cm Domain thickness 1 cm	21600 (for 5 min)
		PCE	2.8% / 2.0%		
		TCE	3.1% / 2.2%		
		Trans DCE	3.6% / 2.6%		

Table 4.3: Transport and mass transfer parameters

Parameter	Material	
	EGDY	Borden
Porosity (-)[1]	0.28	0.39
Dispersivity (m)[1]	0.01	0.001
β_2' (mass tansfer)[2]	1	1
f_{oc} [3]	0.002	0.003

1) Calculated
2) Powers et al., 1994
3) Xu, 2006
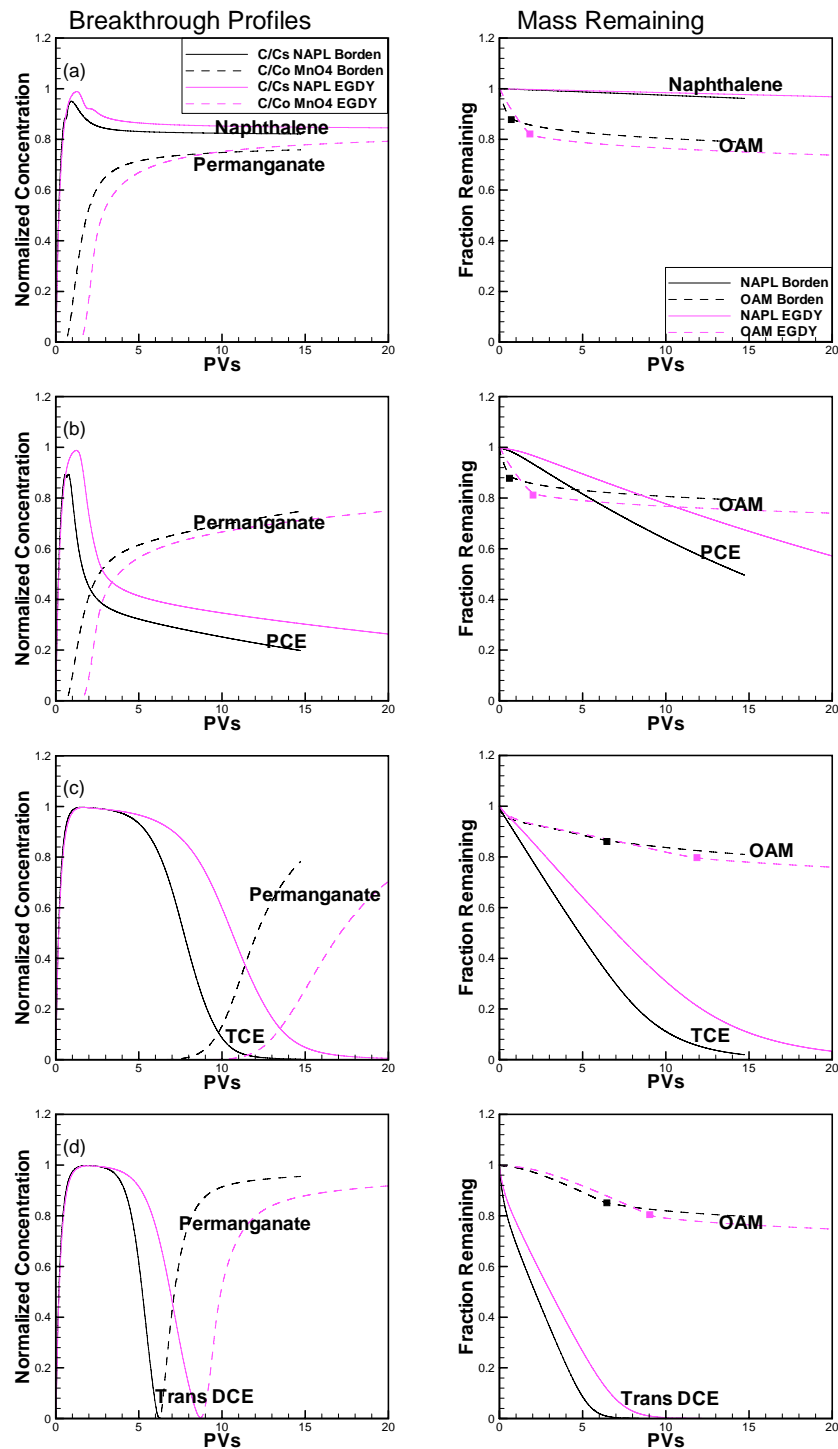
Figure 4.1: Normalized breakthrough concentration of the organic compound and permanganate, and fraction of OAM and NAPL mass remaining during the vertical flushing simulation for (a) naphthalene, (b) PCE, (c) TCE, and (d) Trans DCE.
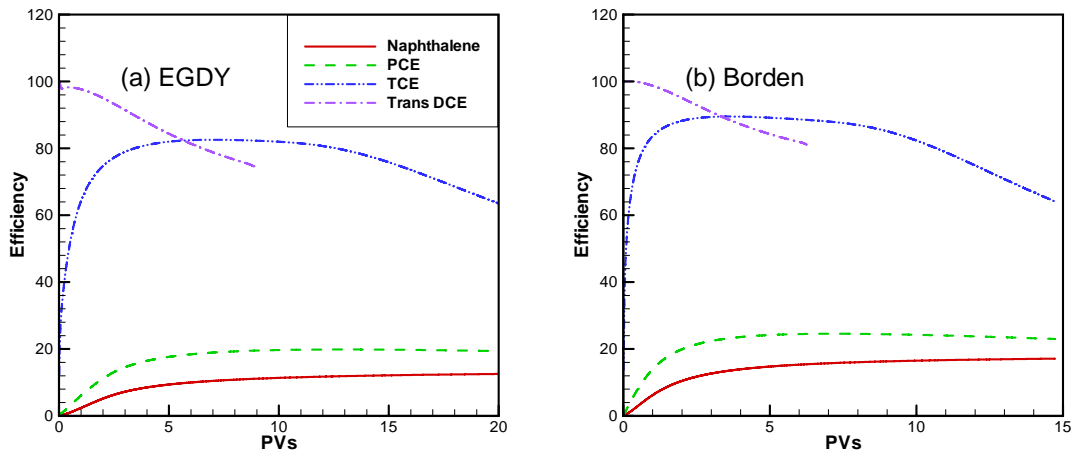
Figure 4.2: Treatment efficiency of the vertical well flushing simulations for (a) EGDY aquifer material and (b) Borden aquifer material.
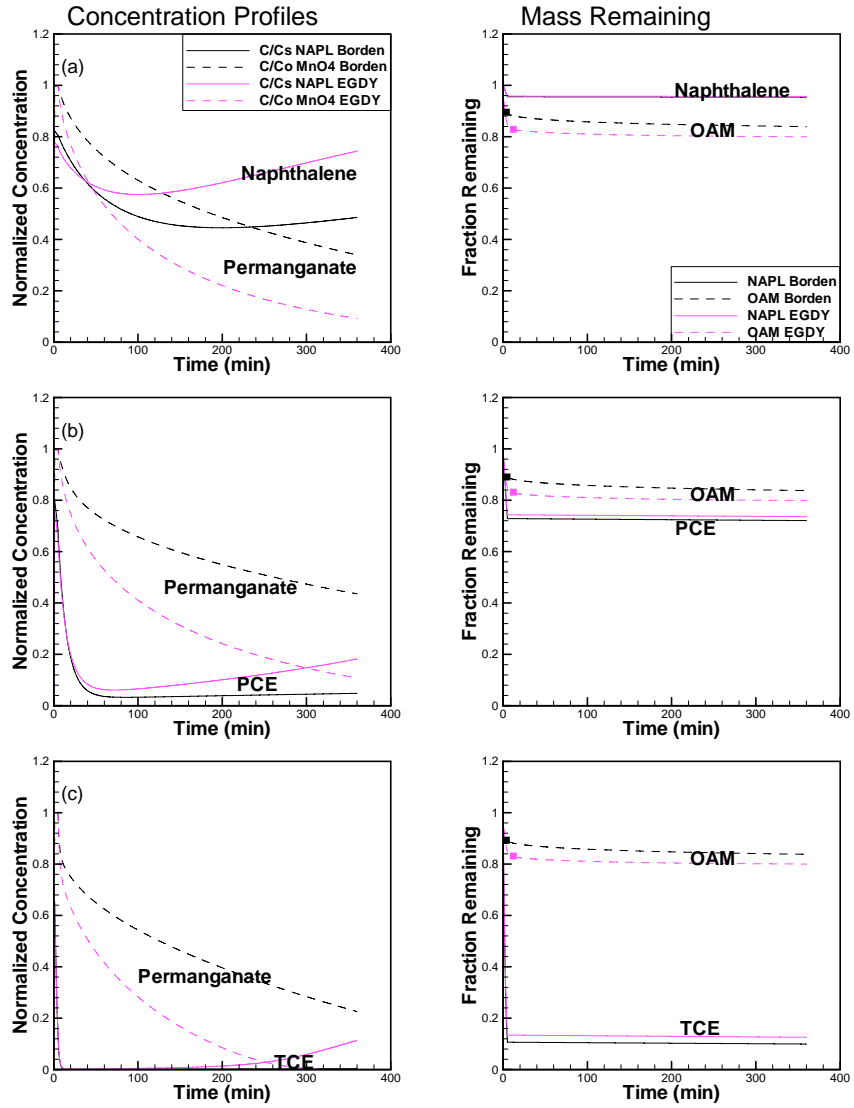
Figure 4.3: Normalized concentration of organic compound and permanganate and fraction of OAM and NAPL mass remaining during the inject-and-leave simulation for (a) naphthalene, (b) PCE, and (c) TCE.
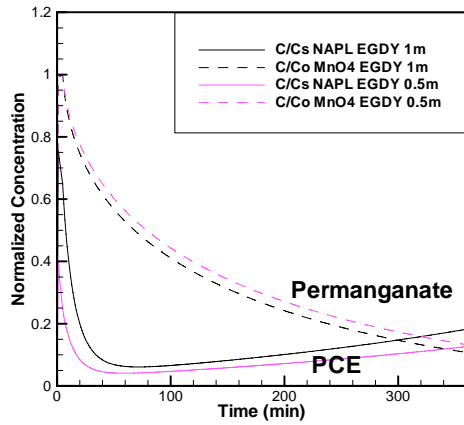
Figure 4.4: Concentration profile for PCE and permanganate in the EGDY inject-and-leave simultion a 0.5 m and 1 m from the injection point.
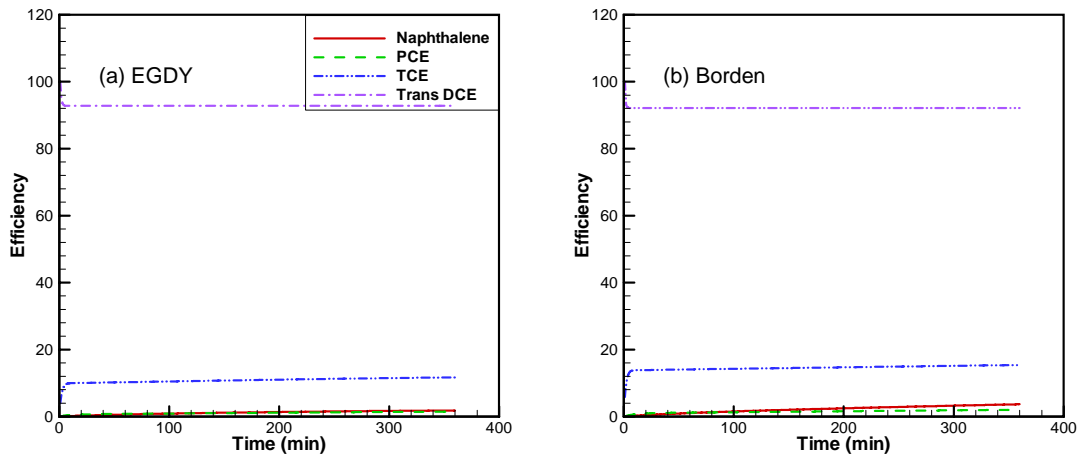
Figure 4.5: Treatment efficiency for the inject-and-leave simulations for (a) EGDY aquifer material and (b) Borden aquifer material.
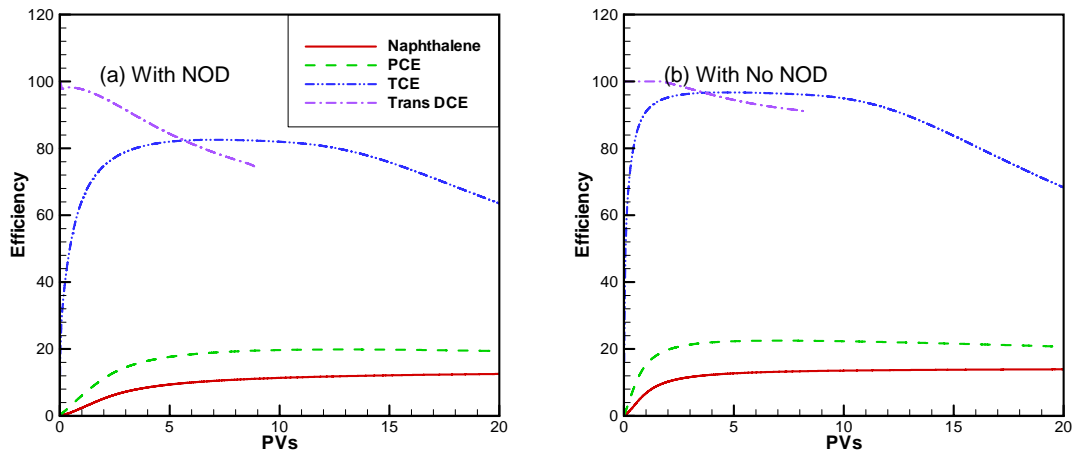
Figure 4.6: Treatment efficiency of the EGDY vertical flushing scenario compared to material with no NOD (a) with NOD considered, (b) with no NOD considerations.
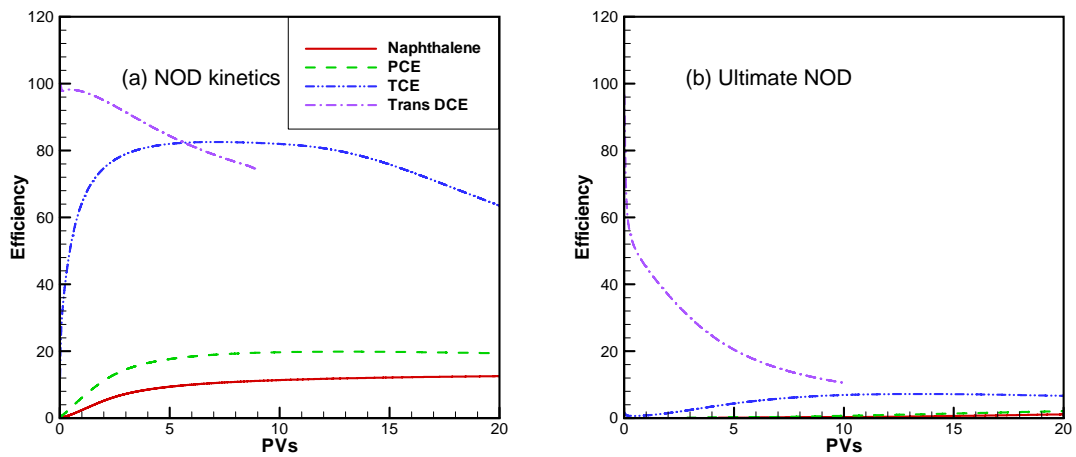
Figure 4.7: Treatment efficiency of the EGDY vertical flushing scenario using (a) NOD kinetic model and (b) Ultimate NOD model.

CHAPTER 5: CONCLUSIONS AND RECOMMENDATIONS

5.1 *Conclusions*

This investigation into the competition for permanganate between aquifer materials and organic compounds produced several conclusions related to the kinetic nature of the NOD reactions, and on the treatability of material with different NOD properties using permanganate ISCO.

5.1.1 NOD Kinetic Model

Through analysis of bench-scale experiments completed by Xu (2006), it was determined that there are two distinct reactions occurring in the NOD process: a fast reaction which results in an almost instantaneous consumption of permanganate and OAM, and a slower reaction which continued for the remainder of the experiment.

Due to insufficient data < 5 minutes, the fast reaction was assumed to follow a first-order rate law, while the slow reaction was fit to the data using the integral method. Furthermore, the slow reaction appeared to decrease as the concentration of permanganate in the excess aquifer material experiments increased. To capture this observation, it was proposed that that decreasing rate of reaction was due to passivation by manganese oxide by-product formation and was reasonably captured by a hyperbolic decay function. The mass ratio of $OAM:MnO_4$ for the slow reaction was within published ranges.

5.1.2 Column Experiment

The column experiment was completed to aid in the validation of the 1-D reactive transport model developed to simulate ISCO processes. The model contained several simplifying assumptions; however, it was able to simulate the chloride and bromide breakthrough curves obtained from the experiment with reasonable accuracy and minimal adjustment to the transport and chemical parameters. Adsorption of TCE to the aquifer

material may have accounted for some of the mass of TCE lost. The chloride breakthrough curve was used to track the fate of oxidized TCE.

5.1.3 Model Simulations and Treatment Efficiency

The validated model was used to simulate permanganate treatment of four common organic compounds (TCE, PCE, Trans DCE, and naphthalene) present as residual source zones in two aquifer materials (EGDY and CFB Borden) using two common oxidant injection schemes (vertical well flushing and inject-and-leave). The results were analyzed to determine the treatment efficiency of different organic compounds in the aquifer materials and the impact of NOD kinetics on the treatment efficiency.

Treatment efficiency was defined as the percent of total permanganate supplied used to treat the organic compound of concern. For all simulations performed, CFB Borden aquifer material showed higher treatment efficiency due to a lower demand for permanganate from the aquifer material (ultimate NOD of EDGY was ~ 15 times larger than Borden material).

The treatment efficiency of the organic compound increased as the C_s and $k_i^{''}$ increased. Compounds with lower C_s and $k_i^{''}$ (e.g., naphthalene and PCE) are limited by the organic reaction rate, and competition for permanganate occurs between the organic compound and the C_{OAM}^{slow}. Compounds with a higher C_s and $k_i^{''}$ (e.g., TCE and Trans DCE), which have higher treatment efficiencies, are limited by permanganate consumption of the C_{OAM}^{fast} which reduces the permanganate mass available for reaction with the organic compound.

Treatment of organic compounds having low C_s and $k_i^{''}$ (e.g., naphthalene or PCE) requires that the kinetics of C_{OAM}^{fast} and C_{OAM}^{slow} both be characterized since both exert a strong demand for permanganate in both vertical flushing well and inject-and-leave schemes. With organic compounds having moderate C_s and $k_i^{''}$ (e.g. TCE) the OAM

species that require kinetic characterization depends on the injection scheme used; while using the vertical well flushing scheme, only the C_{OAM}^{fast} requires characterization, whereas using the inject-and-leave scheme both the C_{OAM}^{fast} and C_{OAM}^{slow} require characterization. For organic compounds with high C_s and $k_i^{''}$ (e.g. Trans DCE) only the C_{OAM}^{fast} requires characterization since the organic and C_{OAM}^{fast} are depleted at the same time and the C_{OAM}^{slow} does not play a significant role in permanganate consumption while free phase organic and C_{OAM}^{fast} remain.

The EGDY material in the vertical well simulations was used to investigate the impacts on the treatment efficiency when an ultimate consumption approach was used to simulate NOD rather than the kinetic model approach. The results indicated that the ultimate NOD approach significantly underestimated the treatment efficiency, whereas ignoring the NOD sink resulted in over estimation of the treatment efficiency when compared to the kinetic model. Both approaches stress the importance of being able to characterize NOD kinetics.

5.2   Recommendations

With a kinetic model for NOD in place, most of the important processes of ISCO treatment are now well understood. At this point it is recommended that these processes be developed into a 3-dimensional reactive transport model to aid in the understanding of the fate of permanganate in the subsurface during treatment and be able to model the interaction of several injection wells. A 3-dimensional model would also be able to model a greater number of injection schemes.

Modelling efforts could also be made to determine the most efficient injection well design (flow rate, concentration, etc) to minimize the mass of permanganate supplied to treat each compound. For compounds with a slow reaction rate, this would involve a slower rate of injection allowing more reaction time, and for organics with a high solubility this would involve a faster injection rate which would result is less permanganate being used for satisfaction of the NOD.

CHAPTER 6: REFERENCES

Allen-King, R. M., Grathwohl, P., & Ball, W.P. 2002. "New modeling paradigms for the sorption of hydrophobic organic chemicals to heterogeneous carbonaceous matter in soils, sediments, and rocks." Advances in Water Resources **25**: 985-1016.

APHA 1998. A. E. Greenberg & R.R. Trussell, (Eds). Standard Methods for the Examination of Water and Wastewater, 20th Ed. Washington D.C., American Public Health Association, American Water Works Association, and Water Environment Federation.

Appelo, C. A. J. & Postma, D. 1996. Geochemistry, Groundwater and Pollution. Rotterdam, A.A. Balkema Publishers.

ASTM 2003. ASTM D6520-00, Standard Practice for the Solid Phase Micro Extraction (SPME) of Water and its Headspace for the Analysis of Volatile and Semi-Volatile Organic Compounds. ASTM Annual Book of Standards. West Conshohocken, PA, ASTM International. **11.02, Water (II)**.

Barcelona, M. J. & Holm, T.R. 1991. "Oxidation-reduction capacities of soil." Environmental Science and Technology **25**(9): 1565-1572.

Barry, D.A., Miller, C.T., & Culligan-Hensley, P.J. 1996. "Temporal discretization errors in non-iterative split-operator approaches to solving chemical reaction/groundwater transport models." Journal of Contaminant Hydrology **22**: 1-17.

Bear, J. 1972. Dynamics of Fluids in Porous Media. New York, N.Y., American Elsevier Publishing Company.

Blair, G. J., Lefroy, R.D.B., & Lisel, L. 1995. "Soil carbon fractions based on their degree of oxidation and the development of carbon management index for aquicultural systems." Australian Journal of Aquacultural Research **46**: 1459-1466.

Brown, D.G. & Gupta, L. submitted. "Reduced mass transfer of BTEX and naphthalene from coal tar into water following oxidation with potassium permanganate." Chemosphere

Carrayrou, J., Mose, R., & Behra, P. 2004. "Operator-splitting procedures from reactive transport and comparison of mass balance errors." Journal of Contaminant Hydrology **68**: 239-268.

CFR 1986. CFR Title 40, Part 136: Guidelines Establishing Test Procedures for the Analysis of Pollutants. USEPA, National Archives and Records Administration.

Chao, T. T. 1972. "Selective dissolution of manganese oxides from soils and sediments with acidified hydroxylamine hydrochloride." Soil Science Society of America Journal **36**: 764-768.

Christensen, T. H., Bjerg, P.L, Banwart, S.A., Jakobsen, R., Heron, G., & Albrechtsen, H.J. 2000. "Characterization of redox conditions in groundwater contaminant plumes." Journal of Contaminant Hydrology **45**: 165-241.

Conrad, S. H., Glass, R.J., & Peplinski, W.J. 2002. "Bench-scale visualization of DNAPL remediation processes in analog heterogeneous aquifers: surfactant floods and in situ oxidation using permanganate." Journal of Contaminant Hydrology **58**: 13-49.

Crimi, M. L. & Siegrist, R.L. 2004. "Impact of reaction conditions on MnO_2 genesis during permanganate oxidation." Journal of Environmental Engineering **130**(05): 562 - 572.

Evanko, C. A., & Dzombak, D.A. 1998. "Influence of structural features on sorption on NOM-analogue organic acids to goethite." Environmental Science and Technology **32**(19): 2846-2855.

Folger, S. 1999. <u>Elements of Chemical Reaction Engineering 3rd Edition</u>. Upper Saddle River, New Jersey, Prentice Hall PTR.

Forsey, S. P. 2004. In situ chemical oxidation of creosote/coal tar residuals: Experimental and numerical investigation. <u>Earth Sciences</u>. Waterloo, University of Waterloo. **Ph.D.**

Frind, E. O. 1988. "Solution of the Advection-Dispersion Equation with Free Exit Boundary." <u>Journal of Numerical Methods for Partial Differential Equations</u> **4**: 301-313.

Frind, E. O., Molson, J.W., & Schimer, M. 1999. "Dissolution and mass transfer of multiple organics under field conditions: The Borden emplaced source." <u>Water Resources Research</u> **35**(3): 683-694.

Gustafsson, O., Bucheli, T.D., Kukulska, S., Andersson, M., Largeau, C., Rouzaud, J.N., Reddy, C.M., & Eglington, T.I. 2001. "Evaluation of a protocol for the quantification of black carbon in sediments." <u>Global Biogeochemical Cycles</u> **15**(4): 881-890.

Hartog, N. 2003. Reactivity of organic matter and other reductants in aquifer sediments. Netherlands, University Utrecht. **Ph.D.**

Hartog, N., Griffioen, J., & van der Weijden, D.H. 2002. "Distribution and reactivity of O2-reducing components in sediments from a layered aquifer." <u>Environmental Science and Technology</u> **36**(11): 2338-2344.

Heron, G., Christensen, T.H., & Tjell, J.C. 1994. "Oxidation capacity of aquifer sediments." <u>Environmental Science and Technology</u> **28**(1): 153-158.

Hood, E. D. 2000. Permanganate flushing of DNAPL source zones: experimental and numerical investigation. <u>Department of Civil Engineering</u>. Waterloo, University of Waterloo. **Ph.D.**

Hood, E. D., & Thomson, N.R. 2000. <u>Numerical simulation of in situ chemical oxidation</u>. Remediation of Chlorinated and Recalcitrant Compounds, Monterey, California, Batelle Press.

Hood, E.D., Thomson, N.R., Grossi, D., & Farquhar, G.J. 2000. "Experimental determination of the kinetic rate law for the oxidation of perchloroethylene by potassium permanganate." <u>Chemosphere</u> **40**: 1383-1388.

Huang, K. C., Hoag, G.E., Chheda, P., Woody, B.A., Dobbs, G.M. 2002. "Chemical oxidation with potassium permanganate in a porous medium." <u>Advances in Environmental Research</u> **7**: 217-229.

Huang, K. C., Hoag, G.E., Chheda, P., Woody, B.A., Dobbs, G.M. 2001. "Oxidation of chlorinated ethenes by potassium permanganate: a kinetic study." <u>Journal of Hazardous Materials</u> **87**: 155-169.

Huang, K. C., Hoag, G.E., Chheda, P., Woody, B.A., Dobbs, G.M. 1999. "Kinetic study of oxidation of trichloroethylene by potassium permanganate." <u>Environmental Engineering Science</u> **16**(4): 265-275.

Hunkler, D., Aravena, R., Parker, B.L., Cherry, J.A., & Diao, X. 2003. "Monitoring oxidation of chlorinated ethenes by permanganate in groundwater using stable isotopes: Laboratory and field studies." <u>Environmental Science and Technology</u> **37**(4): 798-804.

ITRC 2005. Technical and Regulatory Guidance for In Situ Chemical Oxidation of Contaminated Soil and Groundwater, 2nd edition. Washington, D.C., Interstate Technology & Regulatory Council, In Situ Chemical Oxidation Team.

Imhoff, P. T., Jaffe, P.R., & Pinder, G.F. 1993. "An experimental study of complete dissolution of a nonaqueous phase liquid in saturated porous media." <u>Water Resources Research</u> **30**(2): 301-320.

Korom, S. F., M.J. McFarland, R.C. Sims (1996). "Reduced sediments: a factor in the design of subsurface oxidant delivery systems." <u>Ground Water Monitoring and Remediation</u> **Winter 1996**(100-105).

Lamarche, C. 2002. In situ chemical oxidation of an emplaced creosote source. <u>Civil Engineering</u>. Waterloo, University of Waterloo. **MASc.**

Lee, W., & Batchelor, B. 2003. "Reductive capacity of natural reductants." <u>Environmental Science and Technology</u> **37**(3): 535-541.

Levenspiel, O. 1999. <u>Chemical Reaction Engineering, Third Edition</u>. New York, N.Y., John Wiley & Sons, Inc.

Li, X. D., & Schwartz, F.W. 2004. "DNAPL remediation with in situ chemical oxidation using potassium permanganate. Part I. Mineralogy on Mn oxide and its dissolution in organic acids." <u>Journal of Contaminant Hydrology</u> **68**: 39-53.

Li, X. D., & Schwartz, F.W. 2000. <u>Efficiency problems related to permanganate oxidation schemes</u>. Remediation of Chlorinated and Recalcitrant Compounds, Monterey, California, Batelle Press.

MacKinnon, L. K., & Thomson, N.R. 2002. "Laboratory-scale in situ chemical oxidation of a perchloroethylene pool using permanganate." <u>Journal of Contaminant Hydrology</u> **56**: 49-74.

McCourt, J. L. 2005. Impacts of MnO2 solids on mass transfer from pooled TCE following ISCO with permanganate. <u>Department of Civil Engineering</u>. Waterloo, University of Waterloo. **MASc**.

Merck 2003. <u>The Merck Index</u>. Whitehouse Station, New Jersey, Merck and Company Limited.

Miller, C. T., Poirier-McNeil, M., & Mayer, A.S. 1990. "Dissolution of Trapped Nonaqueous Phase Liquids: Mass Transfer Characteristics." Water Resources Research **26**(11): 2783-2796.

MOE 2003. Technical Support Document for Ontario Drinking Water Standards, Objectives, and Guidelines. Ministry of the Environment, Government of Ontario, Toronto, ON.

Mumford, K. 2002. Investigation of natural oxidant demand reactions in a sandy aquifer material. Civil Engineering. Waterloo, University of Waterloo. **MASc.**

Mumford, K. G., Lamarche, C.S., Thomson, N.R. 2004. "Natural oxidant demand of aquifer materials using the push-pull technique." Journal of Environmental Engineering **130**(10): 1139-1146.

Mumford, K. G., Thomson, N.R., & Allen-King, R.M. 2005. "Bench-scale investigation of permanganate natural oxidant demand kinetics." Environmental Science and Technology **39**(8): 2835-2840.

Mumford, K. G., Thomson, N.R., & Allen-King, R.M. 2002. Investigation the kinetic nature of natural oxidant demand during ISCO. Remediation of Chlorinated and Recalcitrant Compounds, Monterey, California, Batelle Press.

Neamana, A., Wallerb, B., Mouéléc, F., Trolarda, F., & Bourriéa. G. 2004. "Improved methods for selective dissolution of manganese oxides from soils and rocks." European Journal of Soil Science **55**(1): 47 – 54.

Pankow, J. F. & Cherry, J.A. 1996. Dense Chlorinated Solvents and other DNAPLS in Groundwater. Waterloo, Ontario, Waterloo Press.

Pedersen, J. K., Berg, P.L., Cheristensen, T.H. 1991. "Correlation of nitrate profiles with groundwater and sediment characteristics in a shallow sandy aquifer." Journal of Hydrology **124**: 263-277.

Poulson, S. R. & Naraoka, H. 2002. "Carbon isotope fractionation dating permanganate oxidation of chlorinated ethylenes (cDCE, TCE, PCE)." Environmental Science and Technology **36**(15): 3270-3274.

Powell, R. M., Callaway, R.W., Michalowski, J.T., Vandegrift, S.A., & White, M.V. 1998. "Comparison methods to determine oxygen demand for bioremediation of a fuel contaminated aquifer." International Journal of Environmental Analytical Chemistry **34**: 253-263.

Powers, S. E., Abriola, L.M., & Weber, W.J. 1994. "An experimental investigation of nonaqueous phase liquid dissolution in saturated subsurface systems: Transient mass transfer rates." Water Resources Research **20**(2): 321-332.

Reitsma, S., & Dai, Q.L. 2001. "Reaction-enhanced mass transfer and transport from non-aqueous phase liquid source zones." Journal of Contaminant Hydrology **49**: 49-66.

Reitsma, S., & Randhawa, J. 2002. Experimental investigation of manganese dioxide plugging of porous media. Remediation of Chlorinated and Recalcitrant Compounds, Monterey, California, Batelle Press.

Sawhney, B. L., Pignatello, J.J., & Steinberg, S.M. 1988. "Determination of 1,2-dibromoethane (EDB) in field soils: implications for volatile organic compounds." Journal of Environmental Quality **17**(1): 149-152.

Schnarr, M., Truax, C., Farquhar, G., Hood, E. Gonnulu, T., & Stickney, B. 1998. "Laboratory and controlled field experiments using potassium permanganate to remediate trichloroethylene and perchloroethylene DNAPLs in porous media." Journal of Contaminant Hydrology **29**: 205-224.

Schnoor, J. L. 1996. Environmental Modelling: Fate and Transport of Pollutants in Water, Air, and Soil. New York, NY., John Wiley & Sons, Inc.

Schroth, M. H., Oostrom, M., Wietsma, T.W., & Istok, J.D. 2001. "In situ oxidation of trichloroethene by permanganate: effects on porous medium hydraulic properties." Journal of Contaminant Hydrology **50**: 79-98.

Siegrist, R. L., Urynowicz, M.A., Crimi, M.L., & Lowe, K.S. 2002. "Genesis and effects of particles produced during in situ chemical oxidation using permanganate." Journal of Environmental Engineering **128**(11): 1068-1076.

Siegrist, R. L., Urynowicz, M.A., West, O.R., Crimi, M.L., Lowe, K.S. 2001. Principals and Practices of In Situ Chemical Oxidation Using Permanganate. Columbus, Ohio, Batelle Press.

Sposito, G. 1989. The Chemistry of Soil. New York, N.Y., Oxford University Press.

Stewart, R. 1965. Oxidation in Organic Chemistry: Oxidation by Permanganate. New York, Academic Press Inc.

Swift 1996. Organic matter characterization (Chapter 35). Methods of Soil Analysis, Part 3 Chemical Methods. Madison, WI., Soil Science Society of America and American Society of Agronomy**:** 1019-1069.

Thomson, N. R. 1995. 3D3PT Manual. Waterloo, ON, Department of Civil Engineering, University of Waterloo.

Tunnicliffe, B. S. & Thomson, N.R. 2004. "Mass removal of chlorinated ethenes from rough-walled fractures using permanganate." Journal of Contaminant Hydrology **75**: 91-114.

Urynowicz, M.A. & Siegrist, R.L. 2005. "Interphase mass transfer during chemical oxidation of TCE DNAPL in aqueous system." <u>Journal of Contaminant Hydrology</u> **80**: 93-106

USEPA 2006. Engineering Issue: In Situ Chemical Oxidation, Environmental Protection Agency, Washington D.C.

USEPA 1993. Technical Information Review. Methyl tertiary Butyl Ether, Environmental Protection Agency, Washington D.C.

USEPA 1986. Superfund Public Health Evaluation Manual, Environmental Protection Agency, Washington D.C.

Waldemer, R. H. & Tratnyek, P.G. 2006. "Kinetics of contaminant degradation by permanganate." <u>Environmental Science and Technology</u> **40**(3): 1055-1061.

Weber, W. J. 1972. <u>Physicochemical Processes for Water Quality Control</u>. New York, N.Y., Wiley -Interscience - John Wiley & Sons, Inc.

Weber, W. J. J. & DiGiano, F.A. 1996. <u>Process Dynamics in Environmental Systems</u>. New York, N.Y., John Wiley & Sons, Inc.

Xu, X. 2006. Interaction of Chemical Oxidants with Aquifer Materials. <u>Civil and Environmental Engineering</u>. Waterloo, University of Waterloo. **Ph.D**.

Xu, X., & Thomson, N.R. 2007. "Estimation of the maximum consumption of permanganate by aquifer solids using a modified chemical oxygen demand test." <u>Journal of Environmental Engineering</u> **in press**.

Xu, X., Thomson, N.R., MacKinnon, L.K., & Hood, E.D. 2004. <u>Oxidant Stability and Mobility: Controlling Factors and Estimation Methods</u>. Fourth International Conference

for the Remediation of Chlorinated and Recalcitrant Compounds, Monterey, Ca., Batelle Press.

Yan, Y. E. & Schwartz, F.W. 2000. "Kinetics and mechanisms for TCE oxidation." Environmental Science and Technology **34**(12): 2535-2541.

Yan, Y. E. & Schwartz, F.W. 1999. "Oxidative degradation and kinetics of chlorinated ethylenes by potassium permanganate." Journal of Contaminant Hydrology **37**: 343-365.

Zhang, H. & Schwartz, F.W. 2000. "Simulation the in situ oxidative treatment of chlorinated ethylenes by potassium permanganate." Water Resources Research **36**(10): 3031-3042.

APPENDIX A: REACTIVE TRANSPORT MODEL DEVELOPMENT

A one-dimensional reactive transport model was developed to analyze the impact of the NOD reaction kinetics on treatment efficiency. This appendix overviews the requirements of the conceptual model, develops a mathematical representation, and outlines the numerical solution method. The developed model is validated with the laboratory results discussed in Chapter 3.

A.1   *Conceptual Model Requirements*

Permanganate is usually delivered to the source zone using either an inject-and-leave or an active flushing system. An inject-and-leave system (Figure A.1) quickly introduces permanganate into the source zone from a single well or drive-point and the oxidant is radially distributed. In this scheme, there is several injection points spaced throughout the source zone based on a calculated radius of influence. As the name implies, inject-and-leave systems do not recover un-reacted oxidant from of the subsurface. An active well flushing system (Figure A.2) operates on a different principal. Injection and extraction wells are used to force permanganate through the subsurface, at a rate higher than the ambient groundwater flow, to ensure the permanganate migrates in the desired direction. Extraction wells also have the benefit of removing excess permanganate from the subsurface and recovering oxidation by-products. Several injection and extraction wells are used to ensure permanganate is delivered to the entire source zone.

ISCO targets aqueous phase contaminants, reducing the concentration through oxidation of the organic contaminant. The rate of contaminant mass transfer from the free phase to the aqueous phase is relative to the concentration gradient (i.e. the difference between the maximum effective solubility and the aqueous concentration of a contaminant). The concentration of an aqueous organic contaminant decreases through oxidation, causing the concentration gradient at the pore scale to increase and results in more NAPL transferring into solution. The overall effect of ISCO is an increased rate of mass transfer over the ambient groundwater flow conditions and results in a faster depletion of the source zone mass.

Assuming that the aquifer is homogenous, both of the typical injection schemes can be represented by a one-dimensional model. In the inject-and-leave scenario, the height of the model domain is assumed to remain constant and equal to a thin slice of the screened portion of the injection well. Permanganate propagates uniformly and radially from the injection point throughout the radius of influence of the well (Figure A.3). The active well flushing scheme can also be represented by a one-dimensional model by choosing to model a single flow channel or flow path from the injection well to the extraction well (Figure A.4). In this case it is assumed that the flow path has uniform aquifer properties and uniform flow.

As permanganate is transported through the subsurface, three possible pathways can be taken by the permanganate as illustrated in the pore scale conceptual model presented by Mumford et al., 2005 (Figure A.5). Permanganate can react with the aqueous phase target contaminant within the pore or it can be consumed by the reduced species associated with the aquifer material. Permanganate that does not react with either the contaminant or reduced aquifer species is propagated to the next pore space. The fraction of permanganate consumed is determined by the reaction kinetics of the organic contaminant and reduced aquifer species and the transport properties (i.e. advection and dispersion). This conceptual model was adapted, using a representative elemental volume (REV), to produce a mathematical representation simulating the in *situ* treatment of a residual source zone for both injection schemes.

Attempts to model permanganate treatment of saturated zone contamination have been performed by Zhang and Schwartz (2000) and Hood (2000). Zhang and Schwartz (2000) developed a 3D model (ISCO3D) to simulate ISCO including the processes of transport, mass transfer, sorption, and oxidation. Zhang and Schwartz, however, incorrectly assumed that NOD was not kinetic in nature; which meant that NOD had to be satisfied before permanganate could propagate through the subsurface. Hood (2000) altered a reactive transport model created by Thomson (1995), 3D3PT, to include the processes of *in situ* chemical oxidation. The alterations from Hood (2000) included: the transport of a non-specific oxidant and reaction by-products, the reaction between the oxidant and

aqueous phase contaminant, the simple reaction between oxidant and organic carbon, and updating flow field based on change in NAPL saturation. However, the simple kinetic reaction between organic carbon and permanganate did not accurately model the complex NOD kinetics. Models created by Zhang and Schwartz (2000) and Hood (2000) were both early attempts to model the subsurface processes of ISCO; however, we now know that both models presented overly simple NOD reactions and new efforts are required to obtain more representative model results.

A.2 *Mathematical Representation*

To model either of the one-dimensional systems described in Section A.1, a mathematical model was developed to simulate dissolution, transport, sorption, oxidation of multi-component NAPL contaminants, and NOD reaction kinetics.

A.2.1 Assumptions

The following assumptions were used in the development of this reactive transport model:

1. The ambient hydraulic gradient was assumed to be negligible compared to the gradient imposed by permanganate injection, thus, the flow rate is determined by the injection rate;

2. The porous medium was assumed to be homogenous with respect to porosity, grain size, and reduced species distribution, hence flow through the media was uniform;

3. The fraction of organic carbon (f_{OC}) was assumed to be directly proportional to the concentration of oxidizable materials within the aquifer solids for sorption purposes.

4. The pH was assumed to remain constant at near neutral due to the high buffering capacity of most aquifer materials; and

5. The impact of ionic strength was negligible.

A.2.2   Modeled Species

In the aqueous phase the organic contaminant (C_{org}), permanganate (C_{MnO4}-), and chloride (C_{Cl}-) were modeled. Chloride is included to simulate either a conservative tracer or a reaction by-product. For the free phase, the mass of the contaminants (M_{org}) was assumed to be non-mobile and depleted through mass transfer. In the solid phase, the amount of fast (C_{OAM}^{fast}) and slow (C_{OAM}^{slow}) reacting OAM and the sorbed mass of contaminant (C_{sorb}) is included (i.e. as the aquifer material is oxidized the bulk concentration of oxidizable materials decreases).

A.2.3   Governing Equations

The one-dimensional model was created using the mathematical representation of several important physical and chemical processes in the source zone and uncontaminated materials.

A.2.3.1 Contaminant Transport and Mass Depletion

The transport of all aqueous species can be expressed by the one-dimensional reactive transport equation (Bear, 1972)

$$\frac{\partial(\theta_T S_w C_i)}{\partial t} = \frac{\partial}{\partial t}\left(\theta_T S_W D_i \frac{\partial C_i}{\partial x}\right) - \frac{\partial}{\partial x}(qC_i) \pm \gamma_i^T - \lambda_i^S , \tag{A-1}$$

with,

$$\theta_T S_W D_i = \alpha q_T + \theta_T S_W \tau D_{0,i} , \tag{A-2}$$

$$\tau = \frac{(\theta_T S_W)^{7/3}}{\theta_T^2} , \text{ and } \tag{A-3}$$

$$\gamma_i^T = \gamma_i^M + \gamma_i^R \tag{A-4}$$

where C_i is the aqueous concentration of species i (M/L^3), species i can be an organic contaminant, permanganate, or chloride, θ_T is the total porosity of the medium (dimensionless), S_w is the water saturation (dimensionless), D_i is the hydrodynamic dispersion of species i (L^2/T), γ_i^T is the total kinetic source/sink term for the aqueous species (i.e., mass transfer γ_i^M, and reaction γ_i^R) (M/L^{3}T), λ_i^S is the equilibrium sorption source/sink term (M/L^{3}T), α is the dispersivity (L), q_T is the aqueous flux (L/T), τ is the tortuosity of the medium (dimensionless), and $D_{0,i}$ is the free solution molecular diffusion of species i (L^2/T).

The rate of mass removal of the NAPL from the free phase can be expressed as

$$\frac{\partial M_{org,i}}{\partial t} = -\gamma_{org,i}^M \tag{A-5}$$

where $\gamma_{org,i}^M$ is the mass transfer sink term for the free phase of the organic species i (M/L^{3}T).

A.2.3.2 NAPL Mass Transfer

The mass transfer from the residual free phase to the aqueous phase can be captured by the single film theory (e.g., Powers et al., 1994) and expressed as

$$\gamma_{org}^M = \theta_T S_W k_{m,org} \left(C_{org}^S - C_{org} \right) \tag{A-6}$$

with the mass transfer coefficient is defined as

$$k_{m,org} = \frac{Sh D_{0,org}}{d_{50}^2} \tag{A-7}$$

where $k_{m,org}$ is the lumped mass transfer coefficient of the organic (1/T), C_{org}^{S} is the maximum solubility of the organic (M/L^3), Sh is the Sherwood number (dimensionless), and d_{50} is the median particle diameter of the aquifer material (L).

The Sherwood number is a ratio of total interfacial mass transferred relative to the mass transferred by diffusion (Weber and DiGiano, 1996). The Sherwood number is based on intrinsic properties and cannot be measured (Frind et al., 1999); thus various empirical relationships have been derived linking the Sherwood number to easily measured parameters (e.g., Powers et al., 1994; Imhoff et al.,1993; Miller et al., 1990). Zhang and Schwartz (2000) unified expressions derived by others into the following general form

$$Sh = \alpha' \, Re^{\beta_1'} \, S_n^{\beta_2'} \tag{A-8}$$

where α', β_1', and β_2' are empirical dimensionless fitting parameters, Re is the Reynolds number (dimensionless), and S_n is the NAPL saturation (dimensionless). This model used the fitting parameters outlined by Powers et al. (1994) with

$$\alpha' = \frac{4.13 \delta^{0.673} U^{0.369}}{S_{N_O}^{\beta_2'}} \tag{A-9}$$

where δ is the normalized grain size, U is the uniformity coefficient, and S_{No} is the initial NAPL saturation; β_1' is 0.598 and β_2' is between 0.5 and 1.0. The normalized grain size is defined by the median grain size (d_{50}) normalized to a medium sized grain of sand (0.05 cm) (Powers et al., 2004). The Reynolds number characterizes the fluid flow through the pore space and is expressed as

$$Re = \frac{\upsilon \rho_w d_{50}}{\mu_W} \tag{A-10}$$

where υ is the pore water velocity (M/T), ρ_w is the density of water (M/L^3), and μ_w is the dynamic viscosity of water (M/LT).

A.2.3.3 Sorption

Sorption is an important process, particularly when the fraction of organic carbon in an aquifer is large. Aqueous phase organic contaminants sorb to the organic fraction of aquifer material causing the advancement of the plume to be retarded. The process of sorption can be modelled as an instantaneous equilibrium process (Pankow and Cherry, 1996). When proper NOD kinetics are considered, the fraction of organic material in the aquifer decreases as it is oxidized, which releases contaminants from the sorbed phase.

$$C_{sorb,i} = \frac{C_{org,i}}{\rho_B k_d}, \text{ and} \tag{A-11}$$

$$\lambda_i^S = \rho_B \frac{d(k_d C_{sorb,i})}{dt}, \text{ with} \tag{A-12}$$

$$k_d = f_{OC} K_{OC}, \text{ and} \tag{A-13}$$

$$f_{OC} = R_{f_{oc}/OAM} C_{OAM} \tag{A-14}$$

where λ_i^S is the sorption equilibrium source/sink (M/L^{3}T), k_d is the sorption or distribution coefficient (dimensionless), f_{OC} is the fraction of organic carbon (dimensionless), K_{OC} is the organic carbon normalized sorption coefficient (dimensionless), and $R_{foc/OAM}$ is the initial ratio between the f_{OC} and C_{OAM}.

A.2.3.4 Organic Contaminant and Permanganate Reaction

The organic reaction term is a large sink for permanganate and aqueous phase contaminants during successful applications of ISCO. The oxidation reaction between the contaminant and permanganate can be expressed by parallel second-order reactions (Waldemer and Tratnyek, 2006)

$$\gamma_{org,i}^{R-ORG} = -\theta_T S_W k_{org,i}^{MnO_4^-} C_{org,i} C_{MnO_4^-} \tag{A-14}$$

and

$$\gamma_{MnO_4^-}^{R-ORG,i} = -\theta_T S_W k_{MnO_4^-}^{org,i} C_{org,i} C_{MnO_4^-} \tag{A-15}$$

with the reaction rate coefficients related by,

$$k_i^{''} = a_i k_{org,i} MolWt_{MnO_4^-} = b_i k_{MnO_4^-}^{org,i} MolWt_{org,i} \tag{A-16}$$

where $\gamma_{org,i}^{R-ORG}$ is the aqueous organic sink term (M/L^{3}T) of species i due to reaction,

$\gamma_{MnO_4^-}^{R-ORG,i}$ is the sink term for permanganate due to reaction with the contaminant i, $k_{org,\,i}$ is

the second-order rate constant for the oxidation of organic contaminant i due to

permanganate(L^3/MT), and $k_{MnO_4^-}^{org,i}$ is the second-order rate constant for the consumption

of permanganate due to contaminant i, $C_{org,i}$ is the concentration of contaminant i, $C_{MnO_4^-}$

is the concentration of the permanganate (M/L^{3}T), $k_i^{''}$ is the general second-order

reaction rate coefficient expressed in moles (M/L^{3}T), a_i is the stochiometric coefficient

for permanganate, $MolWt_{MnO_4^-}$ is the molecular weight of permanganate, b_i is the

stochiometric coefficient for contaminant i, and $MolWt_{org,i}$ is the molecular weight of

contaminant i.

A.2.3.5 NOD Model

The mathematical model for the NOD reactions occurring in the subsurface was
developed in Chapter 2 of this thesis.

$$C_{OAM} = C_{OAM}^{fast} + C_{OAM}^{slow} + C_{OAM}^{non-reactive} \tag{A-17}$$

$$\gamma_{OAM}^{R-fast} = -k_{OAM}^{fast} C_{OAM}^{fast} C_{MnO_4^-} \tag{A-18}$$

$$\gamma_{OAM}^{R-slow} = -k_{OAM}^{slow} C_{OAM}^{slow} C_{MnO_4^-} \tag{A-19}$$

and,

$$\gamma_{MnO_4^-}^{R-OAM} = -k_{MnO_4^-}^{fast} C_{OAM}^{fast} C_{MnO_4^-} - k_{MnO_4^-}^{slow} C_{OAM}^{slow} C_{MnO_4^-} \tag{A-20}$$

Where C_{OAM} is the concentration of the OAM, C_{OAM}^{fast} is the portion of the OAM attributed to the fast reaction (M/L^3), C_{OAM}^{slow} is the portion of the OAM attributed to the slow reaction (M/L^3), $C_{OAM}^{non-reactive}$ is the portion of the OAM that does not react with permanganate (M/L^3), γ_{OAM}^{R-fast} is the sink term for the fast reacting OAM due to reaction with permanganate (M/L^{3}T), γ_{OAM}^{R-slow} is the sink term for the slow reacting OAM due to reaction with permanganate (M/L^{3}T), $\gamma_{MnO_4^-}^{R-OAM}$ is the sink term for the permanganate due to NOD (M/L^{3}T), k_{OAM}^{fast} and k_{OAM}^{slow} are the fast and slow reaction rate coefficients respectively for the degradation of the OAM (L^3/MT), and $k_{MnO_4^-}^{fast}$ and $k_{MnO_4^-}^{slow}$ are the fast and slow reaction rate coefficients respectively for the consumption of permanganate (L^3/MT).

The slow reaction rate of the OAM is not constant and is affected by passivation of soil particles due to the formation of MnO$_2$ precipitates following a modified hyperbolic decay function.

$$k_{MnnO_4^-}^{slow} = \frac{a}{1 + b\left(MnO_2^{formed}\right)^c} \tag{A-21}$$

Where *a, b,* and *c* are fitting parameters for the decay function and MnO$_2$^{formed} is the mass of permanganate consumed per mass of aquifer material.

A.3   Boundary and Initial Conditions

The inlet boundary was set to a Type 1 or Dirchlet boundary condition (concentration specified), since the concentration of all aqueous species is known at this location. The outlet boundary was set to a Type 4 or free exit boundary (Frind, 1988). The initial concentrations of the aqueous species within the domain were assumed to be background conditions. The initial aqueous concentration of contaminants was assumed to be equal to the solubility limit due to mass transfer from the source zone.

A.4   Solution Method

Operator splitting is a common method employed to solve the reactive transport equation because it significantly reduces the computation time required and can achieve excellent results (Carrayrou et al., 2004). The method involves the decoupling of the processes of transport and reaction and solving them separately. For the purpose of this research the Strang-splitting SNI scheme was used due to it high accuracy and ease of implementation when modelling the reactive transport equation (Carrayrou et al., 2004; Barry et al., 1996). The Strang operator splitting approach involves solving the equations over 2Δt, alternating transport over one time step, batch reaction over two time steps, and transport over one additional time step (Carrayrou et al., 2004).

To facilitate the solution of the governing equations the one-dimensional spatial domain was discretized into a finite number of control volumes. The governing processes were integrated over each control volume and propagated through time using the Strang-splitting operator approach. The non-reactive advection-dispersion equation was solved over Δt, using a Thomas solver, while mass transfer, sorption, and reaction terms were solved over 2Δt, using a Runge-Kutta approach.

A.5   Model Validation

The model was validated using the laboratory results of the 10 g/L column experiment (Chapter 3). The column was 10 cm long and had a diameter of 2.54 cm. It contained a source zone of trichloroethylene (TCE) contamination located between 3 and 5.5 cm. The column was flushed with permanganate for 8 hours before switching the inlet solution to Milli-Q water and flushing for approximately 44 additional hours. The effluent was analyzed to determine the concentration of oxidation by-product chloride, conservative tracer bromide, permanganate, and TCE.

The breakthrough curves for bromide and chloride were used for model validation. Bromide was used to determine the porosity and validate the dispersivity determined through analysis of Xu's (2006) experiments. Chloride was used to trace the TCE in the

column, accounting for both the oxidation and mass transfer of TCE. TCE was not used for model validation do to the large fluctuations observed in the TCE breakthrough data. Permanganate was also not used for model validation due to the presence of TCE and permanganate together in the effluent; the model overestimated the consumption of permanganate in the column which may be attributed to the incomplete oxidation of TCE noted in Chapter 3.

The porosity was determined based on the breakthrough of the bromide tracer curve as discussed in Chapter 3. Once the porosity was determined the flushing of the conservative tracer through the column was modelled to validate the dispersivity of the material. The porosity was determined to be 0.28 and the dispersivity was determined to be 0.01 m. The resulting BTC showed that the dispersivity was similar to that previously determined (0.008 m) when modelling the EDGY NOD column experiment completed by Xu (Figure A.6).

The experiment was simulated and the resulting chloride breakthrough curve was compared to the experimental results to validate that the processes of oxidation and mass transfer were adequately accounted for by the model. Accurate simulation of these processes is essential to ensure the quality of the model results when it is used to investigate the competition for permanganate between contaminants and NOD. Only the general trend in the chloride concentration was considered due to the moderate fluctuations in the concentration.

Table A.1 summarizes all the physical and chemical properties that were used in the model validation. The reaction rate coefficient was set to 0.443 $M^{-1}s^{-1}$ as reported by Waldemer and Tratnyek (2006) for unbuffered solutions. The solubility of TCE was adjusted from 1100 mg/L (maximum solubility reported in the literature; Merck, 2003 to 700 mg/L to reflect the maximum concentration observed when Milli-Q water was exposed to pure phase TCE for several days. Other researchers have reported maximum concentrations less than the maximum solubility reported by Merck (2003. Tunnicliffe and Thomson (2004) reported a maximum TCE concentration of 110 mg/L in a fracture experiment with a TCE and PCE source zone (Raoult's law does not account for the

lower than expected maximum concentration). McCourt (2005) reported a maximum TCE concentration of 120 mg/L in reactor vials containing TCE and in glass beads.

With these chemical properties (and others summarized in Table A.1), the model was used to simulate the chloride breakthrough curve successfully (Figure A.7). One trend that the model failed to capture was the slight decrease in chloride concentration prior to the completion of the permanganate flush. It was assumed that the decrease in concentration was due to mass transfer effects from manganese by-product formation. However, since the model used in future study will have lower NAPL saturations, it is assumed that these effects on mass transfer will be negligible. Conrad et al. (2002) noted large impacts on mass transfer for pooled source zones, but not for residuals sources and indicates that this assumption is justifiable. They noted large impacts on the mass transfer for pooled source zones, but not for residual sources. The sorption process did not play a large role in the chloride BTC, due to the fast reaction rate between permanganate and TCE.

The chloride BTC from the column experiment indicates that 0.08 g of TCE reacted in the column which would account for in 0.199 g of $KMnO_4$ reacted (model predicted 0.250 g of $KMnO_4$ would be consumed by the contaminant). Further the model predicted that 0.487 g of $KMnO_4$ would react with the OAM, and the remaining mass of reacted permanganate in the column experiments was 0.575 g. Both of the model numbers closely correspond to the actually masses of permanganate consumed indicated by the experimental results.

A.6   *Numerical Code*

The mathematical model was adapted into a computer model using FORTRAN90. The code is available in Appendix C of this thesis.

Table A.1: Chemical and physical properties used during model validation. Source of each value is also stated as fit, calculated, literature, or assumed.

| Chemical/Physical	Porperty	Value	Source
Chemical	Solubility	700 mg/L	Model Fit - approximate laboratory value
	Density	1.46 g/mL	Literature - Merck, 2001
	k"	0.443 $M^{-1}s^{-1}$	Literature - Waldemer and Tratnyek, 2006
	MolWt	131.4	Literature - Merck, 2001
	Log k_{ow}	2.29	Literature - Merck, 2001
	Stochiometric Coefficent MnO_4^-	2	Calculated
	Stochiometric Coefficient TCE	1	Calculated
Physical	Porosity	0.28	Calculated
	Dispersivity	0.01 m	Model Fit
	Flow Rate	0.174 mL/min	Observed
	β_2' (empirical mass transfer value)	1	Assumed (range of 0.5-1.0)
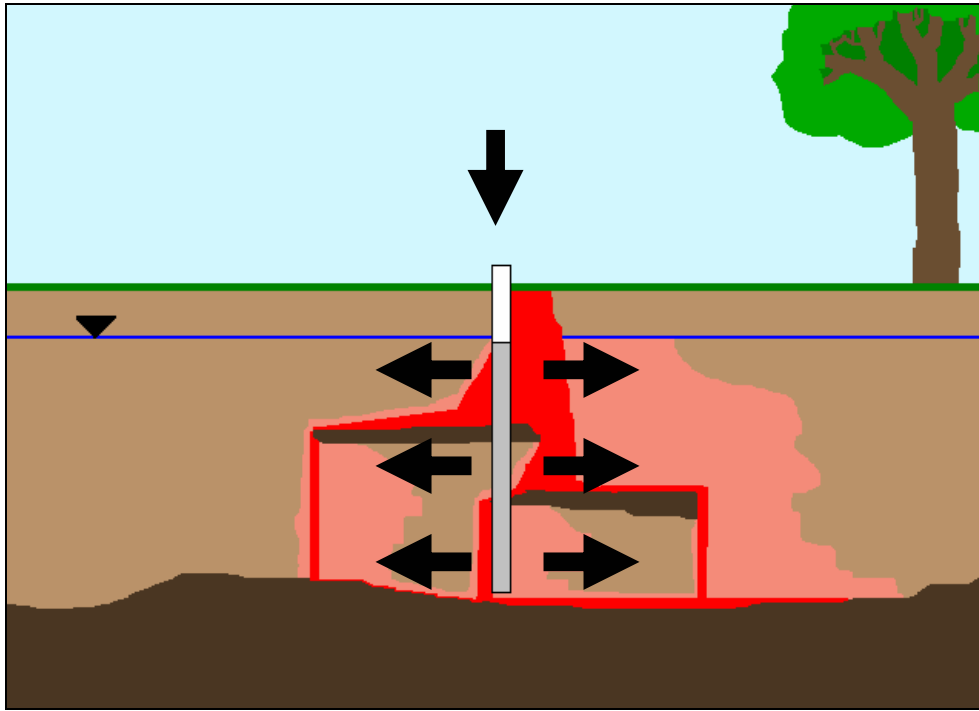
Figure A.1: Inject-and-leave injection scheme.
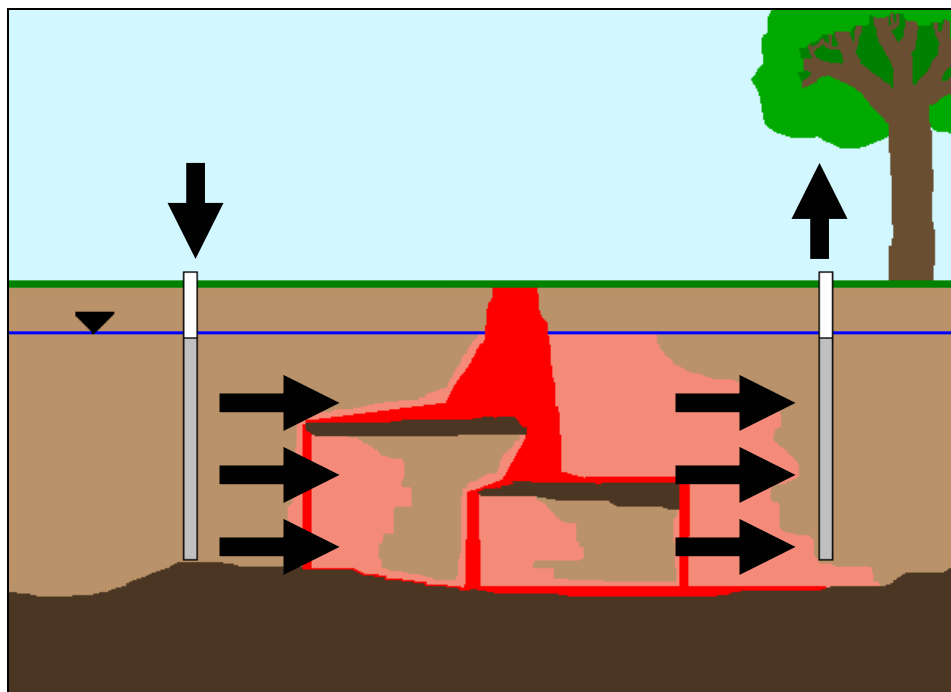
Figure A.2: Well flushing injection scheme.
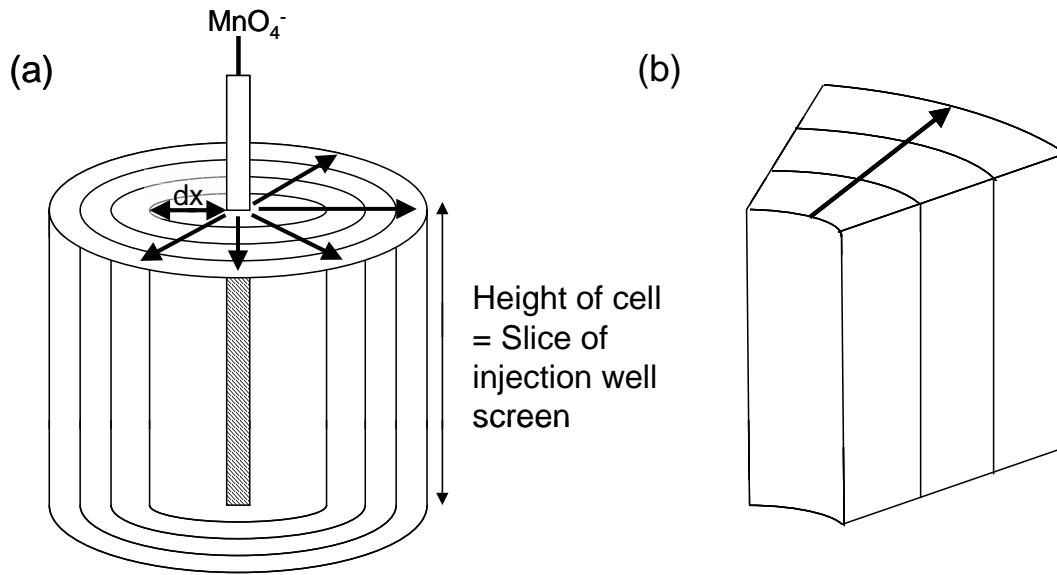
Figure A.3: Inject-and-leave scheme as a 1-D domain (a) the full extent of the radial flow from the injection point and (b) a section of the full domain to illustrate the discretization.

(a)

Injection Well
MnO_4^-

Extraction Well
Unreacted MnO_4^-,
Oxidation by-products

dx

(b)
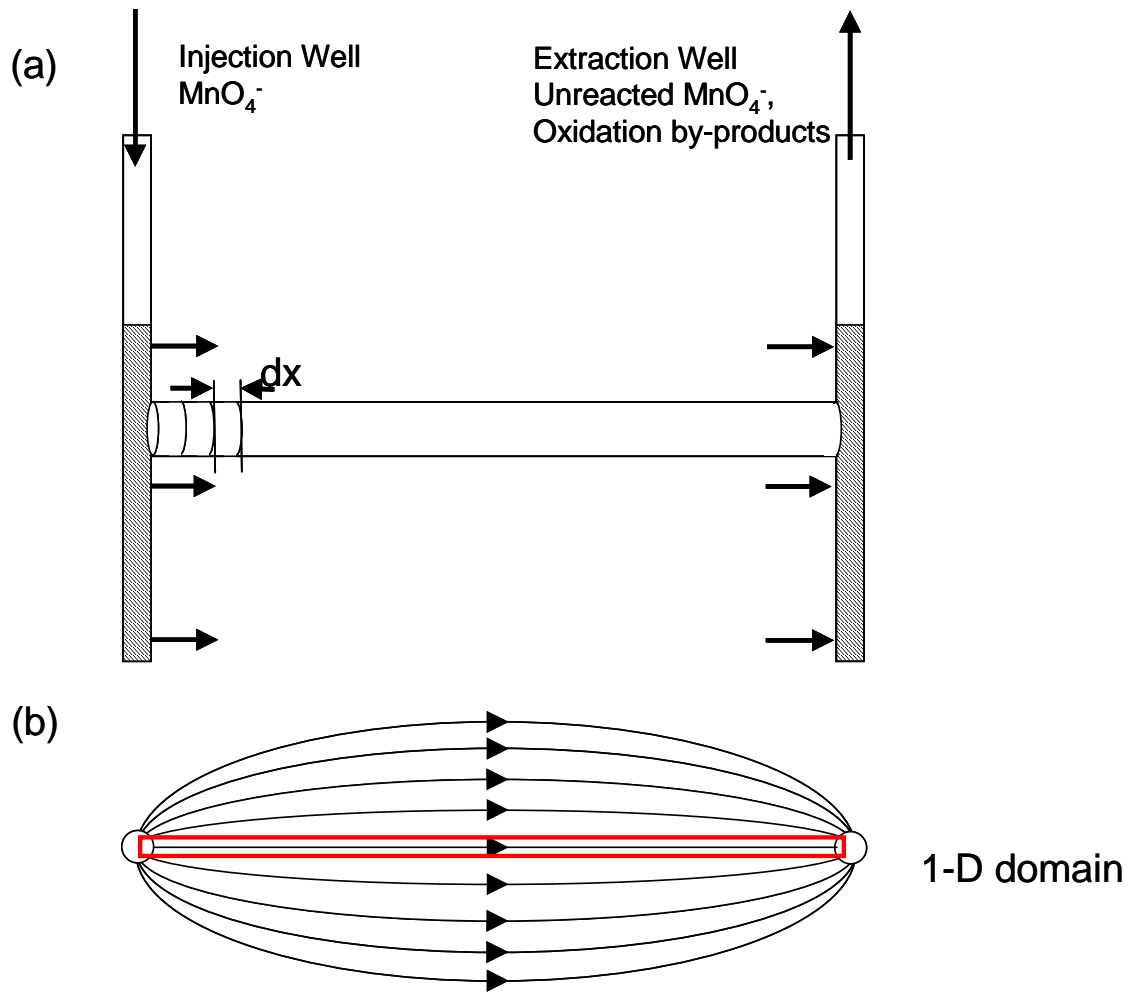
1-D domain

**Figure A.4: Active well flushing scheme as a 1-D domain (a) cross sectional view –
modeled flow path illustrated as column connected the injection and extraction well
– and (b) plan view – modeled flow path enclosed in rectangle.**
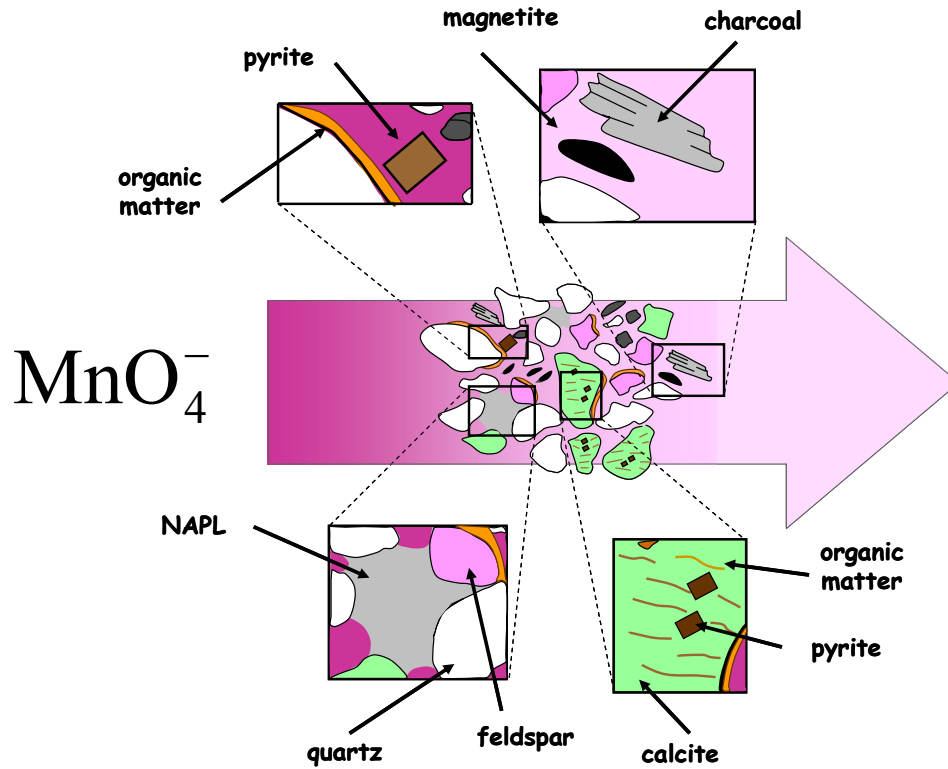
Figure A.5: Conceptual model of pore scale permanganate oxidation including non-productive consumption of permanganate by aquifer species (Mumford et al., 2005).
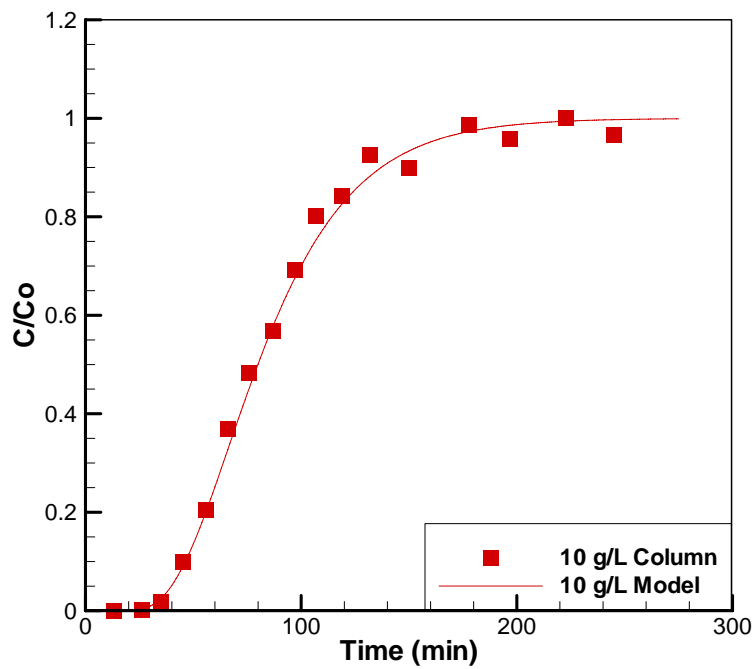
Figure A.6: Observed and simulated bromide breakthrough curve.

Figure A.7: Observed and simulated chloride breakthrough curve.

APPENDIX B: THEORETICAL COLUMN EXPERIMENT CALCULATIONS

	log Kow	
TCE	2.29	
Kow	194.9845	concentration in octanol/concentration in water
Solubility	1100	mg/L
Koc	122.8402	mass sorbed/mass of OC / water concentration
foc	0.003	mass of OC/mass soil g/g

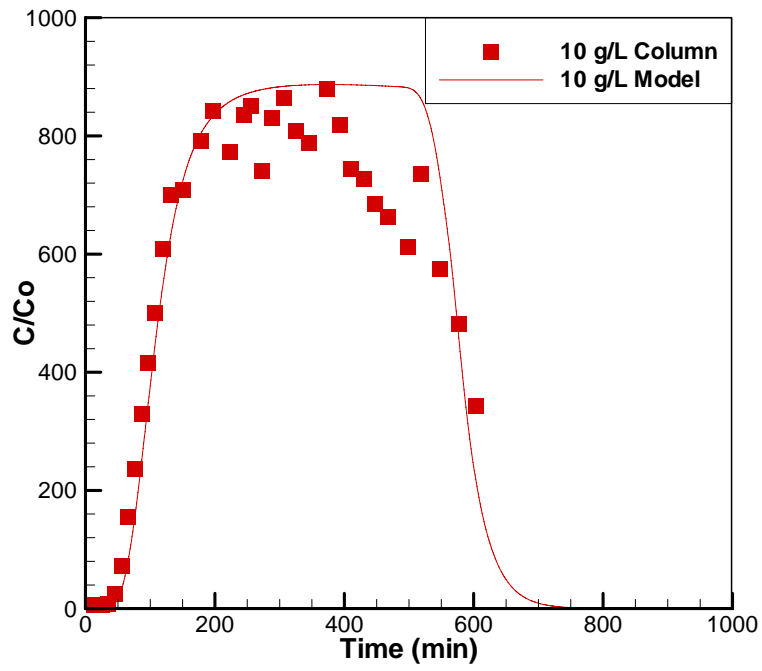| Kp=foc*Koc	Kp	0.3685206	mass sorbed/mass soil * 1/(Water Concentration)
Cs=Cw*Kp	Cs	0.4053727	mass sorbed/mass soil g/g

pore volume	length	4 cm		
	diameter	2.54 cm		
	Volume	20.268299 mL		6.08049 mL
	Porosity	0.28	porosity	0.33
	Pore volume	5.6751238 mL	Pore Volume	2.006562
	Dissolved Mass of TCE	0.0062426 g		
	Volume of Soil	14.593175 mL	Volume of Soil	4.073928
	Mass of Soil	39.693437 g	Mass of Soil	11.08108
	Mass of TCE adsorbed	16.090635 g	Mass TCE adsorbed	4.491969 g
				3.076691 mL

0.277653 mL/g

Mass of Soil	60 g	32.92362	10.86479

100% ML TCE	16.65915	0.217296	16.87645
50% ML TCE	8.329576	0.217296	8.546872
10% ML TCE	**1.665915**	**0.217296**	**1.883211** chosen from batch experiment visual inspection

2.749488 g TCE
60 g soil   Actual Sn   20.4%
7 g DI Water

APPENDIX C: NUMERICAL CODE

```
!    Last change:  LJ   24 Apr 2007   10:58 am


!Reactive Transport
!Laura Jones, November 2005

!********* Copied straight from Kevin's Code
!!*Note: to convert from radial to linear scenario:
!      1. Switch velocity calculation subroutines in the transport subroutine
!      2. Set rwell=0, position of inflow boundary face
!      3. Change r position vectors rw and re to equal rp
!      4. Change the definition of q to be Qwell/hwell where
!         hwell is now the area on which Qwell is exerted
!      5. Change volume calculation from pi*h*(re**2-rw**2) to h*dr
!      6. Set grid spacing (dr) to not be a function of rwell
!!*Note: X is the contaminant being oxidized

program RTMultiComp

implicit none

REAL (KIND=8) :: rwell, QWell, CKMnO4Well, CClWell, hwell              !Well
Characteristics
REAL (KIND=8) :: dr, rmax, dt, theta                          !Solution characteristics
REAL (KIND=8) :: napltop, naplbottom                          !Column Properties
REAL (KIND=8) :: pi, rhow, muw                          !Constants
REAL (KIND=8) :: n, rhob, d50, d10, d60, U, foc, focRatio                          !Soil
Properties
REAL (KIND=8) :: q, qKMnO4, qCl                          !Well Fluxes
REAL (KIND=8) :: Tor, DMolwKMnO4, DMolwNAPL, DMolwCl
!Diffusion in water
REAL (KIND=8) :: DMolKMnO4, DMolNAPL, DMolCl, alphaR
!Diffusion and dispersivity in porous media
REAL (KIND=8) :: TotMoles
REAL (KIND=8) :: KMnO4toOAMf, KMnO4toOAMs, kCl
REAL (KIND=8) :: CTCEold, delTCE
REAL (KIND=8) :: alphas, betas, alphaf, betaf                          !Reaction orders for
the OAM reactions
REAL (KIND=8) :: betap1, betap2
REAL (KIND=8) :: COAMsInit, COAMfInit, COAMAtT
Real (KIND=8) :: DCOD, PCOD, fracslow, kOAMsp, kOAMfp, kOAMssp, kOAMs,
kOAMf, kOAMss, beta
REAL (KIND=8) :: k1, k2, k3, k4
REAL (KIND=8) :: FromNAPL, MassMnO4, MasstoNAPL, C
```

```fortran
REAL (KIND=8) :: MnO2blc
REAL (KIND=8) :: e, f, g
REAL (KIND=8) :: VolContam



REAL (KIND=8), DIMENSION(:), ALLOCATABLE :: MassInit, MassAtT, Solubility,
Density, k, Molwt, CoefMnO4, CoefNAPL, Koc          !NAPL Properties
REAL (KIND=8), DIMENSION(:), ALLOCATABLE :: CNAPLWell, qNAPL
REAL (KIND=8), DIMENSION(:), ALLOCATABLE :: kNAPL, kNAPLp
REAL (KIND=8), DIMENSION(:), ALLOCATABLE :: kOAMSlow, MnO2,
kMnO4slow

REAL (KIND=8), DIMENSION(:), ALLOCATABLE :: CKMnO4, CCl, CKMnO4old,
COAMs, COAMf, COAMsold, COAMfold, Csorbed, Csorbedold
REAL (KIND=8), DIMENSION(:), ALLOCATABLE :: TotMass, RhoAvg
REAL (KIND=8), DIMENSION(:), ALLOCATABLE :: Reynolds, Sh, alphap
REAL (KIND=8), DIMENSION(:), ALLOCATABLE :: Sw
!Saturations - Water and NAPL

REAL (KIND=8), DIMENSION (:,:), ALLOCATABLE :: Mass, Moles, MoleFrac,
MassFrac, CSat
REAL (KIND=8), DIMENSION (:,:), ALLOCATABLE :: km, Sn, SnInit
REAL (KIND=8), DIMENSION (:,:), ALLOCATABLE :: CNAPL, CNAPLold

!Solution arrays
REAL (KIND=8), DIMENSION(:), ALLOCATABLE :: rp, re, rw, Vol
real (KIND=8), DIMENSION (:), ALLOCATABLE :: vw,vp,ve
real (KIND=8), DIMENSION (:), ALLOCATABLE :: Dw1,De1,aW1,aP1,aE1 !for
MnO4
real (KIND=8), DIMENSION (:), ALLOCATABLE :: Dw2,De2,aW2,aP2,aE2 !for
NAPL
real (KIND=8), DIMENSION (:), ALLOCATABLE :: Dw3,De3,aW3,aP3,aE3 !for Cl
real (KIND=8), DIMENSION (:,:), ALLOCATABLE :: A1,A2,A3
REAL (KIND=8), DIMENSION (:), ALLOCATABLE :: B1,B2,B3

INTEGER :: t, i, NAPLComp, loop, nblc, napltopblc, naplbottomblc, RunMode,
drwellratio, it, itmax, flag
INTEGER, DIMENSION(:), ALLOCATABLE :: tmax

OPEN (Unit = 11, file = "NAPLProperties.txt")
OPEN (Unit = 12, file = "RunMode.txt")
OPEN (Unit = 13, file = "SoilProperties.txt")
OPEN (UNIT = 14, File = "OAMProperties.txt")
OPEN (UNIT = 15, File = "efg.txt")
```

```fortran
read (11, *) NAPLComp          !Number of Components in NAPL

read (12, *) RunMode          !Column (1) vs. Radial (2)

read (15, *) e, f, g

IF (RunMode == 1) THEN
  rwell = 0.d0                 !position of Inflow Boundary (m)
  rmax = 0.1d0                 !domain extent (m)
  dr = 0.001d0                 !grid spacing (m)
  napltop = 0.00d0
  naplbottom = 0.1d0
  napltopblc = napltop/dr + 1.d0
  naplbottomblc = naplbottom/dr
ELSEIF (RunMode == 2) then
  rwell = 0.016                !injection well radius (m)
  rmax = 1.016d0               !domain extent (m)
! drwellratio = 0.1            !ratio between well radius and grid spacing (-)
  dr = 0.001        !grid spacing (m)
  napltop = rwell
  naplbottom = rmax
  napltopblc = napltop/dr + 1.d0 - rwell/dr
  naplbottomblc = naplbottom/dr - rwell/dr
else
  PRINT *, "Invalid run mode option"
  GOTO 100
END IF

nblc = (rmax - rwell)/dr + 1
napltopblc = napltop/dr - 15.d0
naplbottomblc = naplbottom/dr - 15.d0

ALLOCATE (MassInit(NAPLComp), Solubility(NAPLComp), Density(NAPLComp),
kNAPL(NAPLComp), kNAPLp(NAPLComp), k(NAPLComp))
ALLOCATE (MassAtT(NAPLComp))
ALLOCATE (Molwt(NAPLComp), CoefMnO4(NAPLComp),
CoefNAPL(NAPLComp), Koc(NAPLComp))
ALLOCATE (CNAPLWell(NAPLComp), qNAPL(NAPLComp))
ALLOCATE (tmax(NAPLComp))

ALLOCATE (CKMnO4(nblc), CCl(nblc), CKMnO4old(nblc), COAMs(nblc),
COAMf(nblc), COAMsold(nblc), COAMfold(nblc))
ALLOCATE (Csorbed(nblc), CsorbedOld(nblc))
ALLOCATE (kOAMSlow(nblc), MnO2(nblc), kMnO4slow(nblc))
ALLOCATE (TotMass(nblc), RhoAvg(nblc))
ALLOCATE (Reynolds(nblc), Sh(nblc), alphap(nblc))
```

```
ALLOCATE (rp(nblc), re(nblc), rw(nblc), Vol(nblc))
ALLOCATE (Sw(nblc))

ALLOCATE (Mass(NAPLComp, nblc), Moles(NAPLComp, nblc),
MoleFrac(NAPLComp, nblc), MassFrac(NAPLComp, nblc), CSat(NAPLComp, nblc))
ALLOCATE (km(NAPLComp, nblc), Sn(NAPLComp,nblc), Sninit(NAPLComp, nblc))
ALLOCATE (CNAPL(NAPLComp, nblc), CNAPLold(NAPLComp, nblc))

ALLOCATE (vw(nblc),vp(nblc),ve(nblc))
ALLOCATE (Dw1(nblc),De1(nblc),Dw2(nblc),De2(nblc),Dw3(nblc),De3(nblc))
ALLOCATE (aW1(nblc),aP1(nblc),aE1(nblc))
ALLOCATE (aW2(nblc),aP2(nblc),aE2(nblc))
ALLOCATE (aW3(nblc),aP3(nblc),aE3(nblc))
ALLOCATE (A1(nblc,3),B1(nblc),A2(nblc,3),B2(nblc),A3(nblc,3),B3(nblc))


READ (11, *) (MassInit(loop), loop = 1, NAPLComp)
READ (11, *) (Solubility(loop), loop = 1, NAPLComp)
READ (11, *) (Density(loop), loop = 1, NAPLComp)
READ (11, *) (k(loop), loop = 1, NAPLComp)
READ (11, *) (MolWt(loop), loop = 1, NAPLComp)
READ (11, *) (CoefMnO4(loop), loop = 1, NAPLComp)
READ (11, *) (CoefNAPL(loop), loop = 1, NAPLComp)
read (11, *) (tmax(loop), loop = 1, NAPLComp)
read (11, *) (Koc(loop), loop = 1, NAPLComp)

pi = 3.14159
rhow = 0.9991*1000.*1000.        !Density of water (g/m3)
muw = 1.307                !viscosity of water (g/m.s)

!Reading in Soil Properties of the Column
READ (13, *) n, d50, d10, d60, foc
rhob = (1-n)*2.72*1000.*1000.     !bulk soil density (g/m3)
U = d60/d10

!Well injection Properties
if (Runmode==1) then
  QWell = 0.174/1000./1000./60.          !volumetric flow rate - darcy flux = ~120 cm/day
(m3/s)
ELSEIF (Runmode==2) then
  QWell = 15000./1000./1000./60.          !volumetric flow rate - darcy flux = ~120
cm/day (m3/s)
end if
CKMnO4Well = 5.d0*1000.              !injection concentration of KMnO4 (g/m3)
CClWell = 0.d0                !injection concentrations of Chloride (or other
conservative tracer)
```

```
CNAPLWell = 0.d0                      !Injection concentrations of NAPLs - Likely 0, if
changes will need to read in

!Well Properties
if (RunMode == 1) then
  hwell = pi*(1.*2.54/2./100.)**2       !Cross-sectional area of column (m2)
  q = QWell/hwell
  Vol = hwell*dr                  !Volume of blocks (m3)
ELSEIF (RunMode == 2) then
  hwell = 0.01d0                  !Screen height (m)
  q = QWell/2./pi/rwell/hwell
  do i = 1, nblc
    Vol(i) = hwell* ((i*dr)**2*pi - ((i-1)*dr)**2*pi)    !Volume of blocks (m3)
  end do
end if
qKMnO4 = CKMnO4Well*q
qNAPL = CNAPLWell*q
qCl = CClWell*q


dt = 0.005d0                    !time step (s)
theta = 0.5                     !time weighting scheme - Crank Nicholson

Mass = 0.d0
VolContam = 0.d0
do i = napltopblc, naplbottomblc
  VolContam = VolContam + Vol(i)
end do
do loop = 1, NAPLComp
  do i = napltopblc, naplbottomblc
    Mass(loop, i) = MassInit(loop)*Vol(i)/VolContam
  end do
end do


Tor = n**(7./3.)/n**2              !Tortuosity (-)
DMolwKMnO4 = 1.632e-5/100/100           !molecular diffusion coefficient in water for
KMnO4 (m2/s) - from breakthrouhg
DMolwNAPL = 6.80e-6/100./100.           !molecular diffusion coefficient in water for
NAPLs (m2/s) - from mumford
DMolwCl = 2.032e-5/100/100 .          !molecular diffusion coefficient in water for Cl
(m2/s) - from breakthrough

DmolKMnO4 = DmolwKMnO4*Tor          !effective molecular diffission coefficient
for KMnO4 (m2/s)
DmolNAPL = DmolwNAPL*Tor            !effective molecular diffussion coefficient for
NAPLs (m2/s)
```

```
DmolCl = DmolwCl*Tor                        !effective molecular diffusion coefficient for
Cl (m2/s)
alphar = 0.0006              !dispersivity (m)


CSat = 0.d0
do i = napltopblc, naplbottomblc
  do loop = 1, NAPLComp
    CSat(loop, i) = Solubility(loop)
  end do
end do


RhoAvg = 0.d0
Sn = 0.d0
do i = napltopblc, naplbottomblc
  do loop = 1, NAPLComp
    Sn(loop, i) = Mass(loop, i)/(Density(loop)*n*Vol(i))
  end do
end do


!Mass Transfer Variables
betap1 = 0.598
betap2 = 1.
alphap = 0.
!PRINT *, alphap
!pause

!OAM Properties - Need to figure out
READ (Unit = 14, *) DCOD, PCOD, fracslow, kOAMsp, kOAMfp, kOAMs, kOAMf,
beta
COAMsInit = (DCOD-(1-fracslow)*DCOD)*rhob/1000.          !in g/m3
COAMfInit = (1-fracslow)*DCOD*rhob/1000.        !in g/m3
focRatio = foc/(COAMsInit+COAMfInit)

!Reaction Stuff
do loop = 1, NAPLComp
  kNAPL(loop) = k(loop)/1000/MolWt(loop)*CoefMnO4(loop)
  kNAPLp(loop) = k(loop)/1000/158*CoefNAPL(loop)
end do
kCl=0.045/1000/35/1000*2/3

!Radial face position
do i=1, nblc
  rp(i) = rwell + (i-1./2.)*dr
```

```fortran
  if (RunMode == 1) then
    re(i) = rp(i)
    rw(i) = rp(i)
  ELSEIF (RunMode == 2) then
    rw(i) = rwell + (i-1)*dr
    re(i) = rwell + (i)*dr
  end if
end do

!Initializing column concentrations
CKMnO4 = 0.d0

CNAPL = Csat

CCl = 0.d0
Csorbed=0.d0

OPEN(21, FILE = "Coutsola13.dat")
OPEN(22, FILE = "FracRemovedsola13.dat")
OPEN(23, FILE = "MnO4.dat")

do loop = 1, NAPLComp
  CKMnO4Well = 5.d0*1000.              !injection concentration of KMnO4 (g/m3)
  CKMnO4 = 0.d0
  CCl = 0.d0
  Csorbed=0.d0
  IF (Runmode==2) then
    QWell = 150000./1000./1000./60.         !volumetric flow rate - darcy flux = ~120
cm/day (m3/s)
  end if

  WRITE(21, *) 'Contaminant= ',loop
  WRITE(21, "(a)") 'Titles="Concentration of outflow"'
  WRITE(21, "(a)") ' "t" "CNAPL out (g/L)" "CKMnO4 out (g/L)", "CCl out (g/L)"'
  WRITE(22, *) 'Contaminant= ',loop
  WRITE(22, "(a)") 'Title="Fraction of Mass Removed"'
  WRITE(22, "(a)") ' "t" "FracMass " "FracOAM"'
  WRITE(23, *) 'Contaminant= ',loop
  WRITE(23, "(a)") 'Titles="Treatment efficiency"'
  WRITE(23, "(a)") ' "PV" "Efficiency"'

  COAMs = COAMsInit
  COAMf = COAMfInit
  CKMnO4 = 0.d0
  MnO2 = 0.d0
  CCl = 0.d0
```

```fortran
  Sw = 1 - Sn(loop, :)

 PRINT *, Sn(loop, napltopblc)
 Sninit = Sn

 MasstoNAPL = 0.d0

 do t = 0, tmax(loop)/(2.*dt)

   if (t .gt. 5*60/(2.*dt)) then
    QWell = 0.d0
    q = QWell/2./pi/rwell/hwell
   else
    MassMnO4 = QWell*CKMnO4well*(t*2.*dt)
   end if

   qKMnO4 = q*CKMnO4well

   !Transport of KMnO4
   call Transport(Qwell, hwell, Sw*n, nblc, vw, vp, ve, rw, rp, re, Dw1, De1, alphar,
DmolKMnO4,&
   &aW1, aP1, aE1, dr, A1, B1, CKMnO4, theta, dt, qKMnO4/Sw(1)/n, RunMode)
   !Transport of NAPL
   call Transport(Qwell, hwell, Sw*n, nblc, vw, vp, ve, rw, rp, re, Dw2, De2, alphar,
DmolNAPL,&
   &aW2, aP2, aE2, dr, A2, B2, CNAPL(loop, :), theta, dt, qNAPL(loop)/Sw(1)/n,
RunMode)
   !Transport of Tracer
   call Transport(Qwell, hwell, Sw*n, nblc, vw, vp, ve, rw, rp, re, Dw3, De3, alphar,
DmolCl,&
   &aw3, ap3, ae3, dr, A3, B3, CCl, theta, dt, qCl/Sw(1)/n, RunMode)

 !  C=0.d0
 !  do i=1, nblc
 !    C=C+CKMnO4(i)*Vol(i)
 !  end do

   !Mass Transfer Parameters
   Reynolds = vp*rhow*d50/muw
   do i=napltopblc, naplbottomblc
    alphap(i) = 1.0*4.13*(d50/0.0005)**0.673*U**0.369/SnInit(loop, i)**betap2
   end do
   Sh=alphap*Reynolds**betap1*Sn(loop,:)**betap2
   km=0
   km(loop, 1:nblc) = Sh*DmolwNAPL/d50**2       !Mass Transfer Coefficient (1/s)
 !  km=km/2000
```

```fortran
    !Update Mass
    MassAtT = 0
    COAMAtT = 0
    do i = 1, nblc
      k1 = km(loop, i)*(CSat(loop, i)-CNAPL(loop, i))
      k2 = km(loop, i)*(CSat(loop, i)-(CNAPL(loop, i)+k1*0.5*dt*2.))
      k3 = km(loop, i)*(CSat(loop, i)-(CNAPL(loop, i)+k2*0.5*dt*2.))
      k4 = km(loop, i)*(CSat(loop, i)-(CNAPL(loop, i)+k3*dt*2.))
      if (Mass(loop, i)<1./6.*(k1+2.*k2+2.*k3+k4)*2.*dt*Vol(i)*Sw(i)*n) then
        CNAPL(loop, i) = CNAPL(loop, i) + Mass(loop, i)
        Mass(loop, i) = 0
      else
        Mass(loop, i) = Mass(loop, i) - 1./6.*(k1+2.*k2+2.*k3+k4)*2.*dt*Vol(i)*Sw(i)*n
!       if (i>napltopblc .and. t>1) then
!         PRINT *, CNAPL(loop, i)
!       endif
        CNAPL(loop, i) = CNAPL(loop, i) + 1./6.*(k1+2.*k2+2.*k3+k4)*2.*dt
!       if (i>napltopblc .and. t>1) then
!         PRINT *, CNAPL(loop, i)
!         pause
!       endif
      endif
      MassAtT(loop) = MassAtT(loop) + Mass(loop, i)
    end do

    !Reaction Terms - Solved using Runge Kutta

    kOAMSlow = e/(1+f*(MnO2)**g)/60./1000.
    kMnO4slow = kOAMslow/beta/n
    CsorbedOld = Csorbed
!   MasstoNAPL =0.d0
    do i = 1, nblc
      CTCEold = CNAPL(loop, i)
      call reaction(kMnO4slow(i), kOAMfp, kOAMSlow(i), kOAMf, CKMnO4(i),
    CNAPL(loop, i), COAMs(i), COAMf(i), 1, &          !For Multi component NAPL, 1=
    NAPLComp
      &2*dt, kNAPL(loop), kNAPLp(loop), FromNAPL, MnO2blc)
      delTCE = CTCEold - CNAPL(loop, i)
      CCl(i) = CCl(i) + delTCE*0.8099          !converting reacted TCE to chloride
      foc=(COAMs(i)+COAMf(i))*focRatio
      Csorbed(i) = CNAPL(loop, i)/(foc*Koc(loop)*rhob)
      CNAPL(loop, i) = CNAPL(loop, i) - rhob*foc*Koc(loop)*(Csorbed(i)-
    CsorbedOld(i))
      COAMAtT = COAMAtT + COAMf(i)*1./nblc + COAMs(i)*1./nblc
      MasstoNAPL = MasstoNAPL + FromNAPL*Vol(i)*n
```

```fortran
      MnO2(i) = MnO2(i) + MnO2blc*Vol(i)*n/(Vol(i)*(1-n)*rhob)
    end do


    !Update Densities and Saturations
    do i = napltopblc, naplbottomblc
      Sn(loop,i) = Mass(loop,i)/(Density(loop)*n*Vol(i))
    end do
    Sw = 1 - Sn(loop, :)


    !2nd Transport of KMnO4
    call Transport(Qwell, hwell, Sw*n, nblc, vw, vp, ve, rw, rp, re, Dw1, De1, alphar, DmolKMnO4,&
      &aW1, aP1, aE1, dr, A1, B1, CKMnO4, theta, dt, qKMnO4/Sw(1)/n, RunMode)
    !2nd Transport of NAPL
    call Transport(Qwell, hwell, Sw*n, nblc, vw, vp, ve, rw, rp, re, Dw2, De2, alphar, DmolNAPL,&
      &aW2, aP2, aE2, dr, A2, B2, CNAPL(loop, :), theta, dt, qNAPL(loop)/Sw(1)/n, RunMode)
    !2nd Transport of Tracer
    call Transport(Qwell, hwell, Sw*n, nblc, vw, vp, ve, rw, rp, re, Dw3, De3, alphar, DmolCl,&
      &aw3, ap3, ae3, dr, A3, B3, CCl, theta, dt, qCl/Sw(1)/n, RunMode)


!   if (t*2.0*dt/60>40) then
!     PRINT *, MassAtT(loop)
!     pause
!   end if
!   PRINT *, t*2.0*dt/60, CKMnO4(1)/1000., COAMf(1), COAMs(1), CNAPL(loop, 1)
!   pause
    if (RunMode==1) then
      if (MOD(t, 30/dt)==0) then
        WRITE (21,*) t*2.0*dt*Qwell/(hwell*rmax*n), CNAPL(loop, nblc)/1000., CKMnO4(nblc)/1000., CCl(nblc)
        WRITE (22,*) t*2.0*dt*Qwell/(hwell*rmax*n), MassAtT(loop)/MassInit(loop), COAMAtT/(COAMsInit+COAMfInit)
        PRINT *, t*2.0*dt/60, CKMnO4(nblc)/1000., COAMf(nblc), COAMs(nblc)
        if (t>0) then
          WRITE (23,*) t*2.0*dt*Qwell/(hwell*rmax*n), -1.*MasstoNAPL/MassMnO4*100
!         PRINT *,t*2.0*dt*Qwell/(hwell*rmax*n), -1.*MasstoNAPL/MassMnO4*100
        end if
      end if
    ELSEIF (RunMode==2) then
      if (MOD(t, 30/dt)==0) then
        WRITE (21,*) t*2.0*dt/60, CNAPL(loop, nblc)/1000., CKMnO4(nblc)/1000., CCl(nblc)
```

```fortran
      WRITE (22,*) t*2.0*dt/60, MassAtT(loop)/MassInit(loop),
COAMAtT/(COAMsInit+COAMfInit)
      PRINT *, t*2.0*dt/60, CKMnO4(nblc)/1000., COAMf(nblc), COAMs(nblc)
      if (t>0) then
        WRITE (23,*) t*2.0*dt/60, -1.*MasstoNAPL/MassMnO4*100
!       PRINT *,t*2.0*dt*Qwell/(hwell*rmax*n), -1.*MasstoNAPL/MassMnO4*100
      end if
     end if
    end if
  end do

end do

100 continue

CLOSE (Unit = 11)
CLOSE (Unit = 12)
CLOSE (Unit = 13)
CLOSE (Unit = 14)
CLOSE (Unit = 15)
CLOSE (Unit = 21)
CLOSE (Unit = 22)
CLOSE (Unit = 23)


end program

!---SUBROUTINES
!---Transport subroutine
subroutine Transport(Q, h, por, big, v1, v2, v3, r1, r2, r3, D1, D3, alpha, D,&
 &a1, a2, a3, delta, A, B, C, theta, deltat, flux, RunMode)

  implicit none
  real (KIND=8) :: Q, h
  integer :: big, RunMode
  real (KIND=8) :: v1(big), v2(big), v3(big), por(big)
  real (KIND=8) :: r1(big), r2(big), r3(big)
  real (KIND=8) :: D1(big), D3(big)
  real (KIND=8) :: alpha, D
  real (KIND=8) :: a1(big), a2(big), a3(big)
  real (KIND=8) :: delta
  real (KIND=8) :: A(big,3), B(big), C(big)
  real (KIND=8) :: theta, deltat, flux

  !---Velocities at faces and centroids (m/s)
  if (RunMode==1) then              !Linear solution
```

```fortran
   call velocitycalc_lin(v1, v2, v3, Q, h, por, big)
ELSEIF (RunMode == 2) then          !Radial solution
  call velocitycalc(v1, v2, v3, r1, r2, r3, Q, h, por, big)
end if

!---Dispersion constants for KMnO4 and aqueous TCE (m2/s)
call Dispcalc(D3, D1, v3, v1, alpha, D, big)

!---Matrix coefficients for KMnO4
call acalcup(a1, a2, a3, v1, v3, D1, D3, r1, r2, r3, delta, big)
call acalcup_type3(a1(1), a2(1), a3(1), v3(1), D3(1), r2(1), r3(1), delta)
call acalcup_type4(a1(big), a2(big), a3(big), v1(big), v3(big)&
&, D1(big), D3(big), r1(big), r2(big), r3(big), delta)

!---Advective Diffusive Transport for dt
call makeA(A, theta, a1, a2, a3, deltat, big)
call makeB_Type34(B, C, theta, a1, a2, a3, deltat, flux, big, r1(1), r2(1), delta)

!---Solve for Aqueous Concentrations
call thomas(A, C, B, big, big)


end subroutine

!---Reaction Subroutine

subroutine reaction(kOAMsp, kOAMfp, kOAMs, kOAMf, CKMnO4, CNAPL, COAMs, COAMf, NAPLComp, &
&dt, kNAPL, kNAPLp, FromNAPL, MnO2)

 implicit none
 INTEGER:: NAPLComp, i
 REAL (KIND=8)::dt
 REAL (KIND=8)::kOAMs, kOAMsp, kOAMf, kOAMfp
 REAL (KIND=8)::CKMnO4, CKMnO4old, COAMs, COAMsold, COAMf, COAMfold
 REAL (KIND=8)::CNAPL(NAPLComp), CNAPLold(NAPLComp),
kNAPL(NAPLComp), kNAPLp(NAPLComp), CSat(NAPLComp), km(NAPLComp)
 REAL (KIND=8)::kn1(NAPLComp), kn2(NAPLComp), kn3(NAPLComp),
kn4(NAPLComp)

 !Runge Kutta parameters s=OAMs, f=OAMf, m=permanganate
 REAL (KIND=8):: ks1, ks2, ks3, ks4, kf1, kf2, kf3, kf4,  km1, km2, km3, km4
 Real (KIND=8):: P1, P2, P3, P4, FromNAPL, MnO2

 !Updating Old concentrations
 CKMnO4old = CKMnO4
```

```
CNAPLold = CNAPL
COAMsold = COAMs
COAMfold = COAMf

P1 = 0.d0
P2 = 0.d0
P3 = 0.d0
P4 = 0.d0

!Runge Kutta stuff
ks1 = -kOAMsp*CKMnO4*COAMs
kf1 = -kOAMfp*CKMnO4*COAMf
km1 = -kOAMf*CKMnO4*COAMf - kOAMs*CKMnO4*COAMs
do i = 1, NAPLComp
  kn1(i) = -kNAPLp(i)*CKMnO4*CNAPL(i)
  P1 = - kNAPL(i)*CKMnO4*CNAPL(i)
  km1 = km1 - kNAPL(i)*CKMnO4*CNAPL(i)
end do

ks2 = -kOAMsp*(CKMnO4+km1*0.5*dt)*(COAMs+ks1*0.5*dt)
kf2 = -kOAMfp*(CKMnO4+km1*0.5*dt)*(COAMf+kf1*0.5*dt)
km2 = -kOAMf*(CKMnO4+km1*0.5*dt)*(COAMf+kf1*0.5*dt) -
kOAMs*(CKMnO4+km1*0.5*dt)*(COAMs+ks1*0.5*dt)
do i = 1, NAPLComp
  kn2(i) = -kNAPLp(i)*(CKMnO4+km1*0.5*dt)*(CNAPL(i)+kn1(i)*0.5*dt)
  P2 = - kNAPL(i)*(CKMnO4+km1*0.5*dt)*(CNAPL(i)+kn1(i)*0.5*dt)
  km2 = km2 - kNAPL(i)*(CKMnO4+km1*0.5*dt)*(CNAPL(i)+kn1(i)*0.5*dt)
end do

ks3 = -kOAMsp*(CKMnO4+km2*0.5*dt)*(COAMs+ks2*0.5*dt)
kf3 = -kOAMfp*(CKMnO4+km2*0.5*dt)*(COAMf+kf2*0.5*dt)
km3 = -kOAMf*(CKMnO4+km2*0.5*dt)*(COAMf+kf2*0.5*dt) -
kOAMs*(CKMnO4+km2*0.5*dt)*(COAMs+ks2*0.5*dt)
do i = 1, NAPLComp
  kn3(i) = -kNAPLp(i)*(CKMnO4+km2*0.5*dt)*(CNAPL(i)+kn2(i)*0.5*dt)
  P3 = - kNAPL(i)*(CKMnO4+km2*0.5*dt)*(CNAPL(i)+kn2(i)*0.5*dt)
  km3 = km3 - kNAPL(i)*(CKMnO4+km2*0.5*dt)*(CNAPL(i)+kn2(i)*0.5*dt)
end do

ks4 = -kOAMsp*(CKMnO4+km3*dt)*(COAMs+ks3*dt)
kf4 = -kOAMfp*(CKMnO4+km3*dt)*(COAMf+kf3*dt)
km4 = -kOAMf*(CKMnO4+km3*dt)*(COAMf+kf3*dt) -
kOAMs*(CKMnO4+km3*dt)*(COAMs+ks3*dt)
do i = 1, NAPLComp
  kn4(i) = -kNAPLp(i)*(CKMnO4+km3*dt)*(CNAPL(i)+kn3(i)*dt)
  P4 = - kNAPL(i)*(CKMnO4+km3*dt)*(CNAPL(i)+kn3(i)*dt)
```

```fortran
    km4 = km4 - kNAPL(i)*(CKMnO4+km3*dt)*(CNAPL(i)+kn3(i)*dt)
  end do

  FromNAPL = 1./6.*(P1+2.*P2+2.*P3+P4)*dt
  MnO2 = -1./6.*(km1+2.*km2+2.*km3+km4)*dt + 1./6.*(P1+2.*P2+2.*P3+P4)*dt
  CKMnO4 = CKMnO4old + 1./6.*(km1+2.*km2+2.*km3+km4)*dt
  do i = 1, NAPLComp
    CNAPL(i) = CNAPLold(i) + 1./6.*(kn1(i)+2.*kn2(i)+2.*kn3(i)+kn4(i))*dt
  end do

  COAMs = COAMsold + 1./6.*(ks1+2.*ks2+2.*ks3+ks4)*dt
  COAMf = COAMfold + 1./6.*(kf1+2.*kf2+2.*kf3+kf4)*dt

end subroutine




!---Calculation of velocities for radial solution!!!
subroutine velocitycalc(v1, v2, v3, r1, r2, r3, Q, h, por, big)
  implicit none
  integer :: big
  real (KIND=8) :: v1(big), v2(big), v3(big), r1(big), r2(big), r3(big), por(big)
  real (KIND=8) :: Q, h, pi


  pi=3.14159

  v1 = Q/2.0/pi/h/por/r1
  v2 = Q/2.0/pi/h/por/r2
  v3 = Q/2.0/pi/h/por/r3
end subroutine

!---Calculation of Dispersion constants
subroutine Dispcalc(D1, D2, v1, v2, alpha, D, big)
  implicit none
  integer :: big
  real (KIND=8) :: D1(big), D2(big), v1(big), v2(big)
  real (KIND=8) :: alpha, D


  D1 = alpha*v1 + D
  D2 = alpha*v2 + D

end subroutine

!---Calculation of matrix coefficients for upstream scheme
```

```fortran
subroutine acalcup(a1, a2, a3, v1, v3, D1, D3, r1, r2, r3, delta, big)
  implicit none
  integer :: big
  real (KIND=8) :: a1(big), a2(big), a3(big)
  real (KIND=8) :: v1(big), v3(big), D1(big), D3(big)
  real (KIND=8) :: r1(big), r2(big), r3(big)
  real (KIND=8) :: delta


  a1 = (v1*r1/delta + D1*r1/delta**2)/r2
  a2 = (-D1*r1/delta**2-v3*r3/delta - D3*r3/delta**2)/r2
  a3 = (D3*r3/delta**2)/r2
end subroutine

!---Calculation of matrix coefficients for Type 3 inflow, upstream scheme
subroutine acalcup_type3(a1, a2, a3, v3, D3, r2, r3, delta)
  implicit none
  real (KIND=8) :: a1, a2, a3, v3, D3, r2, r3, delta

  a1 = 0
  a2 = (-v3*r3/delta - D3*r3/delta**2)/r2
  a3 = (D3*r3/delta**2)/r2
end subroutine

!---Calculation of matrix coefficients for Type 4 outflow, updtream scheme
subroutine acalcup_type4(a1, a2, a3, v1, v3, D1, D3, r1, r2, r3, delta)
  implicit none
  real (KIND=8) :: a1, a2, a3, v1, v3, D1, D3, r1, r2, r3, delta

  a1 = (v1*r1/delta + D1*r1/delta**2-D3*r3/delta**2)/r2
  a2 = (-D1*r1/delta**2 - v3*r3/delta + D3*r3/delta**2)/r2
  a3 = 0
end subroutine

!---Assemble stiffness function matrix
subroutine makeA(A, theta, a1, a2, a3, deltat, big)
  implicit none
  integer :: big
  real (KIND=8) :: A(big, 3)
  real (KIND=8) :: a1(big), a2(big), a3(big)
  real (KIND=8) :: deltat, theta


  A(:, 1) = -theta*a1
  A(:, 2) = -theta*a2 + 1/deltat
  A(:, 3) = -theta*a3
```

```fortran
  A(1, 1) = 0
  A(big, 3) = 0
end subroutine

!---Assemble forcing function matrix for Type 3 inflow and Type 4 outflow
subroutine makeB_Type34(B, C, theta, a1, a2, a3, deltat, flux, big, r1, r2, delta)
  implicit none
  integer :: big
  real (KIND=8) :: B(big), C(big), a1(big), a2(big), a3(big)
  real (KIND=8) :: deltat, theta, flux, r1, r2, delta


  B(2: big-1) = (1 - theta)*(a1(2: big-1)*C(1: big-2) + a2(2: big-1)*C(2: big-1)&
  &+ a3(2: big-1)*C(3: big)) + C(2: big-1)/deltat
  B(1) = (1 - theta)*(a2(1)*C(1)+a3(1)*C(2)) + flux*r1/delta/r2 + C(1)/deltat        !for
Type 3 inflow
  B(big) = (1 - theta)*(a1(big)*C(big - 1) + a2(big)*C(big)) + C(big)/deltat           !for
Type 4 outflow
end subroutine

!---Matrix solver
subroutine thomas (aa, uu, ff, nn, mndf)

        implicit real (KIND=8)(a-h, o-z)
        dimension aa(mndf, 3), uu(mndf), ff(mndf)

!       decompose a
        do 10 i = 2, nn
          aa(i, 1) = aa(i, 1)/aa(i-1, 2)
 10       aa(i, 2) = aa(i, 2) - aa(i, 1)*aa(i-1, 3)

!       forward substitution
        uu(1) = ff(1)
        do 20 i = 2, nn
 20       uu(i) = ff(i) - aa(i, 1)*uu(i-1)

!       backward substitution
        uu(nn) = uu(nn)/aa(nn, 2)
        do 30 k = 2, nn
          i = nn - k + 1
 30       uu(i) = (uu(i) - aa(i,3)*uu(i+1))/aa(i,2)

        return
        end

!---Calculation of velocities for linear scenario
```

```fortran
subroutine velocitycalc_lin(v1, v2, v3, Q, h ,por, big)
  implicit none
  integer :: big
  real (KIND=8) :: v1(big), v2(big), v3(big), por(big)
  real (KIND=8) :: Q, h


  v1 = Q/h/por                    !If linear, why are we bothering with V1, V2, and V3???
  v2 = Q/h/por
  v3 = Q/h/por
end subroutine

subroutine decomp(N, A, B)

  implicit none
  INTEGER :: N, I, J, K
  REAL (KIND=8) :: Ratio
  REAL (kind=8), DIMENSION (:) :: B(N)
  REAL (KIND=8), DIMENSION (:,:) :: A(N, N)

  DO I = 1, N
    do J = I+1, N
      if (A(I, I) == 0) then
        Ratio = 0.d0
      else
        Ratio = A(J, I)/A(I, I)
      end if
      do K = I+1, N
        A(J, K) = A(J, K) - A(I, K)*Ratio
      end do
      B(J) = B(J) - B(I)*Ratio
    end do
  END DO

end subroutine

subroutine bsub(N, A, X, B)

  implicit none
  INTEGER :: N, I, J
  REAL (KIND=8) :: SumAB
  REAL (KIND=8), DIMENSION (:) :: X(N), B(N)
  REAL (KIND=8), DIMENSION (:,:) :: A(N, N)

  DO I = N, 1, -1
    SumAB = B(I)
```

```
  do J = I+1, N
    SumAB = SumAB-A(I, J)*X(J)
  end do
 if (A(I, I) == 0) then
   X(I) = 0
 else
   X(I) = SumAB/A(I, I)
 end if

 END DO
end subroutine
```